13:19:21 OCA PAD INITIATION - PROJECT HEADER INFORMATION 10/12/94

Active

Project #: E-20-W32 Cost share #: Rev #: 0
Center # : 10/24-6-R8323-0A0 Center shr #: OCA file #: 90
Work type : RES
Contract#: TASK ORDER 44 Mod #: Document : DO
Prime #: Contract entity: GTRC

Subprojects ? : N CFDA:
Main project #: PE #:

Project unit: CIVIL ENGR Unit code: 02.010.116
Project director(s):
RIX G J CIVIL ENGR (404)894-2292
JACOBS L J CIVIL ENGR (404)-

Sponsor/division names: GA DEPT OF TRANSPORTATION /
Sponsor/division codes: 300 / 035

Award period: 940901 to 951031 (performance) 951031 (reports)

Sponsor amount	New this change	Total to date
Contract value	55,539.00	55,539.00
Funded	55,539.00	55,539.00
Cost sharing amount		0.00

Does subcontracting plan apply ?: N

Title: NONDESTRUCTIVE ASSESSMENT OF PILE TIP ELEVATION

PROJECT ADMINISTRATION DATA

OCA contact: Brian J. Lindberg 894-4820

Sponsor technical contact

LAMAR CAYLOR
(404)363-7569

GA DEPARTMENT OF TRANSPORTATION
OFFICE OF MATERIALS AND RESEARCH
15 KENNEDY DRIVE
FOREST PARK, GA 30050-2599

Sponsor issuing office

LAMAR CAYLOR
(404)363-7569

GA DEPARTMENT OF TRANSPORTATION
OFFICE OF MATERIALS AND RESEARCH
15 KENNEDY DRIVE
FOREST PARK, GA 30050-2599

Security class (U,C,S,TS) : U ONR resident rep. is ACO (Y/N): N
Defense priority rating : N/A N/A supplemental sheet
Equipment title vests with: Sponsor X GIT
HOWEVER, NONE PROPOSED OR ANTICIPATED.
Administrative comments -
INITIATION OF PROJECT E-20-W32. TASK ORDER UNDER THE TERMS & CONDITIONS OF BOA #90.

E-20-632

DRAFT

School of Civil and Environmental Engineering

Nondestructive Assessment of Pile Tip Elevations Using Flexural Waves

Glenn J. Rix, Ph.D.

Laurence J. Jacobs, Ph.D.

Patrick B. Rhodes

Raymond Q. Raparelli

**Georgia Department of Transportation
Project No. 9406**

September 1995

Report No. GIT-CEE/GEO-95-5

Georgia Institute of Technology

Georgia Institute of Technology
Georgia Institute of Technology
Georgia Institute of Technology
Georgia Institute of Technology
Georgia Institute of Technology
Georgia Institute of Technology
Georgia Institute of Technology
Georgia Institute of Technology
Georgia Institute of Technology
Georgia Institute of Technology
Georgia Institute of Technology
Georgia Institute of Technology
Georgia Institute of Technology
Georgia Institute of Technology
Georgia Institute of Technology
Georgia Institute of Technology
Georgia Institute of Technology
Georgia Institute of Technology
Georgia Institute of Technology
Georgia Institute of Technology
Georgia Institute of Technology
Georgia Institute of Technology
Georgia Institute of Technology
Georgia Institute of Technology
Georgia Institute of Technology
Georgia Institute of Technology
Georgia Institute of Technology
Georgia Institute of Technology
Georgia Institute of Technology
Georgia Institute of Technology
Georgia Institute of Technology
Georgia Institute of Technology
Georgia Institute of Technology
Georgia Institute of Technology
Georgia Institute of Technology
Georgia Institute of Technology
Georgia Institute of Technology
Georgia Institute of Technology
Georgia Institute of Technology
Georgia Institute of Technology
Georgia Institute of Technology
Georgia Institute of Technology
Georgia Institute of Technology
Georgia Institute of Technology
Georgia Institute of Technolog

GEORGIA INSTITUTE OF TECHNOLOGY
OFFICE OF CONTRACT ADMINISTRATION

NOTICE OF PROJECT CLOSEOUT

Closeout Notice Date 01/05/96

Project No. E-20-W32_____ Center No. 10/24-6-R8323-0A0_

Project Director RIX G J_____ School/Lab CIVIL ENGR_____

Sponsor GA DEPT OF TRANSPORTATION/_____

Contract/Grant No. TASK ORDER 44_____ Contract Entity GTRC

Prime Contract No. _____

Title NONDESTRUCTIVE ASSESSMENT OF PILE TIP ELEVATION_____

Effective Completion Date 951031 (Performance) 951031 (Reports)

Closeout Actions Required:	Y/N	Date Submitted
Final Invoice or Copy of Final Invoice	Y	_____
Final Report of Inventions and/or Subcontracts	Y	_____
Government Property Inventory & Related Certificate	Y	_____
Classified Material Certificate	N	_____
Release and Assignment	N	_____
Other _____	N	_____

Comments_____

Subproject Under Main Project No. _____

Continues Project No. _____

istribution Required:

Project Director	Y
Administrative Network Representative	Y
GTRI Accounting/Grants and Contracts	Y
Procurement/Supply Services	Y
Research Property Managment	Y
Research Security Services	N
Reports Coordinator (OCA)	Y
GTRC	Y
Project File	Y
Other _____	N
_____	N

E: Final Patent Questionnaire sent to PDPI.

Table of Contents

TABLE OF CONTENTS i

LIST OF TABLES iii

LIST OF FIGURES iv

1 INTRODUCTION 1

PURPOSE 1
METHOD 1
REPORT ORGANIZATION 2

2 REVIEW OF EXISTING NONDESTRUCTIVE TEST METHODS 3

NDT OVERVIEW 3
SONIC ECHO 3
IMPULSE RESPONSE 4
APPLICATION OF NDT METHODS TO UNKNOWN FOUNDATIONS 6
Flexural Wave Tests 6

3 NUMERICAL MODELING 12

ANALYTICAL DERIVATION 12
FINITE ELEMENT ANALYSIS 15
COMPARISON OF ANALYTICAL AND NUMERICAL RESULTS 18

4 TESTS ON SMALL-SCALE PILES 21

SMALL-SCALE PILE FACILITY 21
Test Pile Sections 24
TESTS ON FIXED-FREE PILES 26
Test Equipment and Configuration 27
Test Method 27
Test Results 30
Comparison of Experimental, Analytical, and Numerical Results on Fixed-Free Piles 38
TESTS ON EMBEDDED PILES 3
Sand Fill 4
Sand Placement 4
Test Configuration and Equipment .....
Test Results .....
Comparison of Experimental and Numerical Results on Embedded Piles .....
Sensitivity Study .....

5 TESTS ON FULL-SCALE PILES **49**

BRIDGE SITE 49
TEST SETUP 50
TEST METHOD 50
TEST RESULTS 53

6 SUMMARY **58**

7 REFERENCES **60**

List of Tables

TABLE 3.1 COMPARISON OF ANALYTICAL AND NUMERICAL SOLUTIONS 20

TABLE 4.1 COMPARISON OF EXPERIMENTAL, ANALYTICAL, AND NUMERICAL RESULTS ON FIXED-FREE PILES WITH FIXED END CONDITION 38

TABLE 4.2 COMPARISON OF EXPERIMENTAL, ANALYTICAL, AND NUMERICAL RESULTS ON FIXED-FREE PILES WITH PINNED END CONDITION 39

List of Figures

FIGURE 2.1 TEST CONFIGURATION USED FOR NONDESTRUCTIVE TESTS 4

FIGURE 2.2 ACCELERATION TIME HISTORY OBSERVED AT THE TOP OF DRILLED SHAFT 5

FIGURE 2.3 MOBILITY FREQUENCY RESPONSE FUNCTION 5

FIGURE 2.4 PARALLEL SEISMIC METHOD 7

FIGURE 2.5 TEST CONFIGURATION FOR FLEXURAL WAVE TEST DEVELOPED BY DOUGLAS AND HOLT (1993) 8

FIGURE 2.6 DETERMINATION OF BENDING WAVE VELOCITY USING SHORT KERNEL METHOD 9

FIGURE 2.7 DETERMINATION OF PILE LENGTH USING SHORT KERNEL METHOD 10

FIGURE 3.1 BEAM ELEMENT 12

FIGURE 3.2 ILLUSTRATION OF NODAL FORCES AND DISPLACEMENTS USING SIMPLE, ELASTIC SPRING 16

FIGURE 3.3 SUMMARY OF CLOSED-FORM CALCULATIONS 19

FIGURE 4.1 EXPERIMENTAL FACILITY FOR TESTING SMALL-SCALE PILES 21

FIGURE 4.2 END VIEW OF EXPERIMENTAL FACILITY FOR TESTING SMALL-SCALE PILES 22

FIGURE 4.3 PLAN VIEW OF EXPERIMENTAL FACILITY FOR TESTING SMALL-SCALE PILES 23

FIGURE 4.4 RIGHT ELEVATION VIEW OF SMALL-SCALE PILE TEST FACILITY 25

FIGURE 4.5 LEFT ELEVATION VIEW OF SMALL-SCALE PILE TEST FACILITY 26

FIGURE 4.6 TEST CONFIGURATION USED FOR TESTING PILE A WITH FREE END CONDITION 28

FIGURE 4.7 DEFINITION OF X-X AND Y-Y DIRECTIONS 29

FIGURE 4.8 FREQUENCY RESPONSE FUNCTION (R_{11}) FOR PILE A WITH FREE END CONDITION 31

FIGURE 4.9 FREQUENCY RESPONSE FUNCTION (R_{23}) FOR PILE A WITH FREE END CONDITION 32

FIGURE 4.10 MODE SHAPES OF A FIXED-FREE PILE 33

FIGURE 4.11 COMPARISON OF FREQUENCY RESPONSE FUNCTIONS FOR PILE A WITH FREE END CONDITION 34

FIGURE 4.12 WATERFALL PLOTS FOR PILE A WITH FREE END CONDITION 35

FIGURE 4.13 GRAIN SIZE DISTRIBUTION FOR CHATTAHOOCHEE RIVER SAND 40

FIGURE 4.14 TEST CONFIGURATION USED FOR EMBEDDED PILES 42

FIGURE 4.15 FREQUENCY RESPONSE FUNCTION (R_{11}) FOR PILE A WITH EMBEDDED END CONDITION 43

FIGURE 4.16 WATERFALL PLOTS FOR PILE A WITH EMBEDDED END CONDITION 44

FIGURE 4.17 COMPARISON OF FREQUENCY RESPONSE FUNCTIONS FOR EMBEDDED PILES 44

FIGURE 4.18 COMPARISON OF EXPERIMENTAL AND NUMERICAL FREQUENCY RESPONSE FUNCTIONS FOR PILE A 46

FIGURE 4.19 COMPARISON OF EXPERIMENTAL AND NUMERICAL FREQUENCY RESPONSE FUNCTIONS FOR PILE E 47

FIGURE 4.20 INFLUENCE OF EMBEDMENT DEPTH ON NATURAL FREQUENCIES OF VIBRATION 48

FIGURE 5.1 BRIDGE AT MERCK ROAD OVER CAMP CREEK 49

FIGURE 5.2 FIELD TEST CONFIGURATION FOR BENT 3 - PILE 2 51

FIGURE 5.3 FIELD TEST CONFIGURATION FOR BENT 4 - PILE 2 52

FIGURE 5.4 PHOTOGRAPH OF FIELD TEST 53

FIGURE 5.5 TYPICAL FREQUENCY RESPONSE FUNCTION FOR BENT 3 - PILE 2 54

FIGURE 5.6 WATERFALL PLOTS FOR BENT 3 - PILE 2 55

FIGURE 5.7 TYPICAL FREQUENCY RESPONSE FUNCTION FOR BENT 4 - PILE 2 57

1 Introduction

For approximately 6000 of Georgia's 14,500 bridges, pile tip elevations are unknown because design and construction records no longer exist (Gratton, personal communication). This lack of information is critical because it is difficult to determine the capacity of these piles - particularly in the presence of scour. The unknown bridge foundation problem is an important problem for federal and state agencies and has been the focus of several studies (Olson et al., 1995; Douglas and Holt, 1993) The unknown bridge foundation problem is one in which either the type and depth of foundation is unknown, or the type of foundation is known but the depth is unknown.

Although soil borings and other intrusive tests are capable of determining pile tip elevations, the time and cost of performing these tests on a large number of bridges is prohibitive. Nondestructive tests are an effective alternative for assessing pile tip elevations. The principle employed in these nondestructive tests is to generate stress waves by impacting the pile on an exposed surface. These stress waves then propagate downward along the pile and are reflected at the tip. The arrival of the reflected wave is monitored by sensors attached to the pile.

Purpose

This study focuses on bridges which are supported by exposed pile foundations that have unknown lengths. The purpose of this study is to evaluate the nondestructive use of flexural waves to determine the length of these bridge pile foundations. Many nondestructive test methods rely on the use of longitudinal waves excited axially down a pile. This type of testing is not feasible since the bridge superstructure prevents access to the top of a pile. Although the theory behind flexural wave testing is more complicated than that of the traditional longitudinal wave testing, flexural or bending waves can be excited laterally on the side of the pile with no physical interference from the bridge superstructure. The pile in most cases can be modeled as a long slender member since its ratio of length to section depth ratio is large. The propagation of the flexural waves within the beam is a function of its length, mass density, moment of inertia, elastic modulus and end conditions. When dealing with bridge piles the primary unknown is the embedment length since all of the other variables can be assumed or measured.

Method

This research used numerical modeling, tests on small-scale piles, and tests on full-scale bridges to develop a method to determine unknown bridge pile lengths based on flexural waves. The numerical model examined embedded piles to determine how embedment length influences pile response parameters such as natural frequency and mode shape. Tests were performed on 10 small-scale bridge piles that were

embedded in a 12 ft x 9 ft x 5 ft deep pit. Measurements were made of pile response to flexural waves induced in each pile. The measurements on small-scale piles were complemented with measurements performed on a full-scale bridge selected by the Georgia Department of Transportation. This experimental data on small and full-scale piles was then compared to numerical solutions of pile response. The experimental and numerical results were analyzed to develop an interpretive scheme which permitted the length of the piles to be determined from flexural wave testing.

Report Organization

Chapter 2 reviews the development of nondestructive test methods to assess the integrity of cast-in-place foundations. Results of recent efforts to adapt these nondestructive test methods to the unknown foundation problem are also reviewed. Chapter 3 presents the theory of flexural wave propagation in long, slender members. Examples of closed-form solutions are presented for simple boundary conditions. Fundamentals of finite element numerical analyses are also presented to model more complex and realistic boundary conditions such as those of an embedded pile. Tests on the small-scale piles are presented and discussed in Chapter 4. Chapter 5 presents test data measured on a full-scale bridge in southeast Atlanta. A summary of the research study is presented in Chapter 6.

Review of Existing Nondestructive Test Methods

Overview

estructive tests (NDT) of piles were first developed as a technique to determine the integrity of cast-
.ce pile foundations (Paquet, 1968; Davis and Dunn, 1974). These tests are frequently used to check
fects arising from drilling, casing, slurry, or concreting problems (O'Neill 1992) that could adversely
the performance of the foundation. Most existing noninvasive NDT technologies used for integrity
g are based on the theory of one-dimensional wave propagation in a long slender member. In this
t a pile is considered to be a long slender member. Access to the top of the pile is required for many
se integrity testing procedures. Typically the top of the pile is struck with an impact force and the pile
ıse to this impact is also measured at the top of the pile. The length of the pile or the depth to any
is a function of the amount of time it takes a longitudinal wave (or bar wave), induced by the impact
to propagate down and back up the pile. In addition to identifying reflections from voids, the
ıdinal wave velocity can be used to assess concrete quality (Malhotra, 1976).

Two commonly used noninvasive testing techniques are the Sonic Echo and the Impulse Response
ds. Both methods share the same basic equipment configuration and test procedure in the field. This
uration is shown in Fig. 2.1. A transient force is applied to the top of the shaft by an instrumented 12
dge hammer. The force applied to the shaft is measured by a dynamic force transducer in the face of
ımmer. The response of the pile to the impact is measured by a piezoelectric accelerometer attached to
ıft with mounting wax. Both force and acceleration are recorded by a Fast Fourier Transform (FFT)
er capable of processing data in either the time or frequency domain. The two methods differ in the
ıat the force and acceleration time histories are processed. The following sections summarize the
ls of interpretation and present typical results for each test method.

Echo

ɔtually, the sonic echo method is the simplest of the two methods. The end of the shaft and any
that exist along its length cause reflections of the seismic waves as they propagate downward
ı the shaft. By observing the time required for these reflections to return to the top of the shaft, the
ɔ the reflector can be determined:

$$z = \frac{v_c \bullet \Delta t}{2} \qquad (2.1)$$

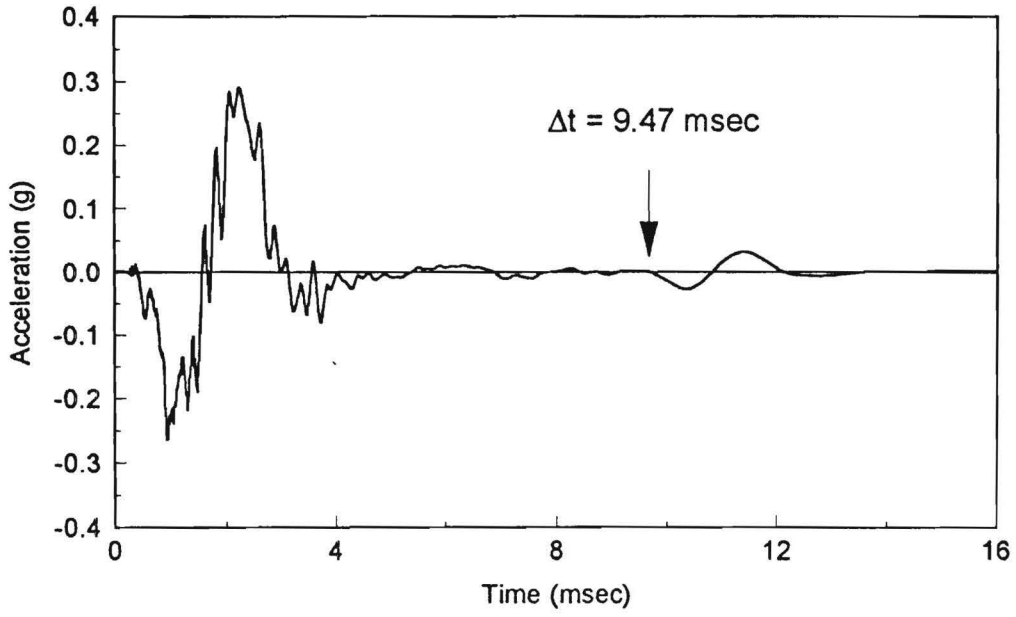

Figure 2.2 Acceleration Time History Observed At The Top Of Drilled Shaft

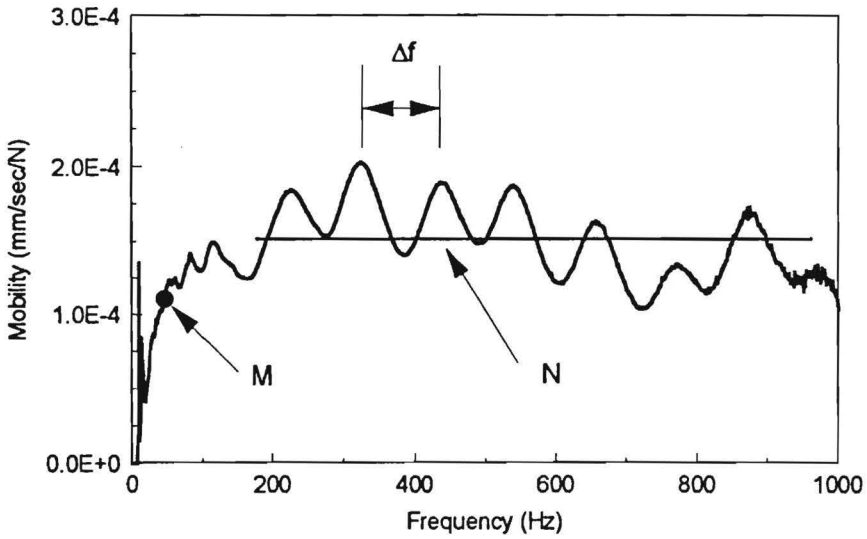

Figure 2.3 Mobility Frequency Response Function

$$\text{Mobility} = \frac{\dot{U}(f)}{P(f)} \tag{2.2}$$

where $\dot{U}$ is the particle velocity spectrum and P is the force spectrum. The particle velocity spectrum is obtained by integrating the particle acceleration spectrum The mobility is a complex-valued quantity, but typically only the magnitude is plotted. A typical plot showing the pile response in terms of the mobility is shown in Figure 2.3.

In the frequency domain the length of the pile or depth to any defects is calculated by the equation:

$$L = \frac{V_c}{2\Delta f} \tag{2.3}$$

where Δf is the change in frequencies between the adjacent peaks on the mobility vs. frequency plot. One of the advantages of this approach is that it is sometimes easier to identify peaks on the mobility vs. frequency plot than to identify reflections in the time domain. Using the value of Δf in Figure 2.3 and a V_c of 12,130 ft/sec, which was measured on concrete test cylinders, the length of the pile in the example is 56.4 ft according to Equation 2.3. The calculated length agrees well with the actual length of 55.5 ft.

Application of NDT Methods to Unknown Foundations

In recent years NDT techniques have been applied to help address the unknown bridge foundation problem. Olson et al (1995) presented a comprehensive review of all NDT techniques used to determine the depth of unknown foundations. They determined that one of the most reliable techniques is an invasive technique known as the parallel seismic method. The test configuration for the parallel seismic method is presented in Figure 2.4. In the parallel seismic method a receiver is placed in a cased, water filled borehole, drilled adjacent to the pile. The arrival of the wave is recorded by the receiver at different depths in the borehole. The length of the pile is determined from a plot of travel time vs. borehole receiver depth. The main disadvantage is that this test requires a borehole.

Flexural Wave Tests

Douglas and Holt (1993) and Holt and Douglas (1994) have developed a method to determine the length of piles using flexural waves. An illustration of the test configuration is shown in Figure 2.5. The pile is struck laterally to induce flexural waves propagating up and down within the pile. The propagation of these flexural waves is dispersive (i.e., the velocity is a function of frequency or wavelength). At low frequencies (wavelength >> pile diameter), the velocity associated with flexural waves is low. As the frequency increases, the velocity of propagation increases and approaches the Rayleigh wave velocity of the pile material.

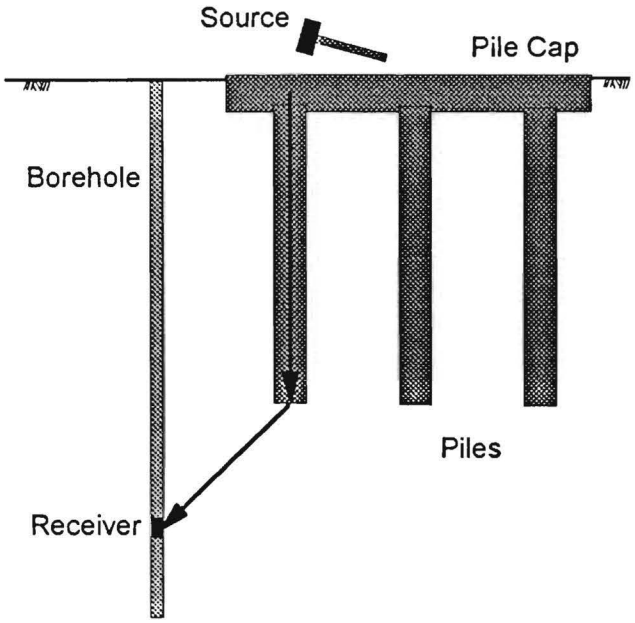

Figure 2.4 Parallel Seismic Method

The propagation of the waves in the pile is monitored by two receivers mounted horizontally on the side of the pile. Douglas and Holt (1993) used the "Short Kernel Method" (SKM) to analyze the propagation of dispersive flexural waves in timber piles. Olson et al. (1995) reviewed the short kernel method and summarized it as follows:

> "The method is similar to narrow band cross-correlation procedures between the input (the hammer blow) and the output (receiver response(s)). However, instead of measuring the hammer blow, a periodic function of 1 or more cycles is used as the 'Kernel Seed,' and a number of seeds for frequencies ranging from 500 to 4000 Hz may be cross-correlated with the receiver responses. The SKM correlation procedure amplifies bending wave energy responses with the selected seed frequency and in a way bandpass filters the response data since frequencies higher and lower than the seed frequency are filtered out. Two receivers are used in order to measure the bending wave velocity (distance divided by elapsed time between the bending wave arrival peaks) between them as determined from the peak responses in the cross-correlated data of the two receivers. The use of two receivers also allows one to determine whether the reflections of the bending wave energy are traveling back up the pile after reflection from the pile bottom, or if the bending wave energy is traveling back down the pile after reflection from the pile top or beam. This is identical to the procedures used in Sonic Echo tests when 2 receivers are used. The dispersion of the bending wave velocity is thus accounted for by calculating the bending wave velocity for each kernel seed frequency."

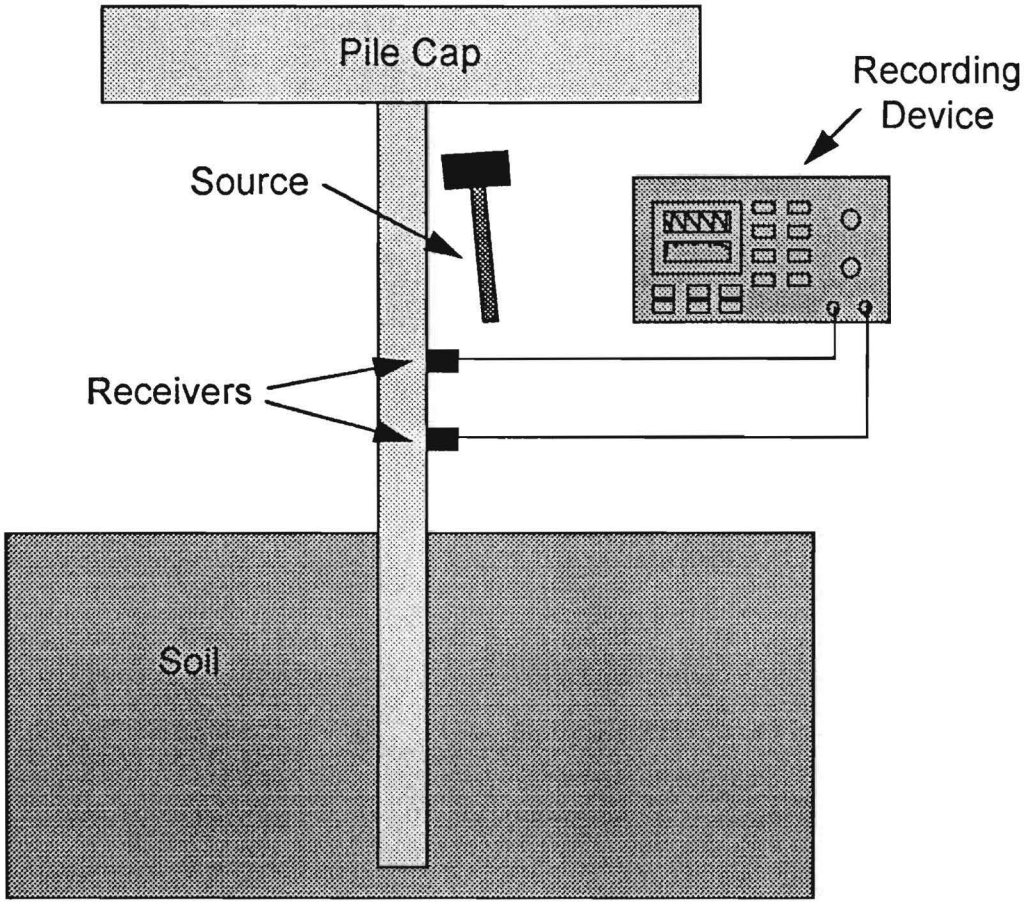

Figure 2.5 Test Configuration for Flexural Wave Test Developed by Douglas and Holt (1993)

Figures 2.6 and 2.7 illustrate the application of the Short Kernel method to a timber pile test performed by Olson et al. (1995). Figure 2.6 shows the response at each of the two accelerometers after application of the short kernel method with a kernel seed consisting of one cycle of 500 Hz. From the response, a bending wave velocity of 2480 ft/sec is calculated using the propagation delay (1.41 msec) between the two receivers. Figure 2.7 illustrates the calculation of the pile length by identifying reflected arrivals from the pile bottom. The calculated length is 27.3 ft which agrees well with the actual length of 28 ft.

Olson et al (1995) concluded that a limitation of the Short Kernel Method was that it is necessary to identify the propagation path(s) of flexural waves so as to correctly identify the propagation path of the waves reflected from the pile bottom. They concluded that identifying the correct path can be difficult for piles with several reflecting boundaries including the pile top, groundline, changes in pile geometry, etc. Olson et al. also found that using the direction of initial particle motion as an indicator to choose the correct propagation path can be misleading.

Velocity Calculation:

$\Delta t = 1.41$ ms

R1-R2 = 42 inches = 3.5 ft

Bending Wave Velocity = R1-R2 / Δt = 2,480 ft/sec

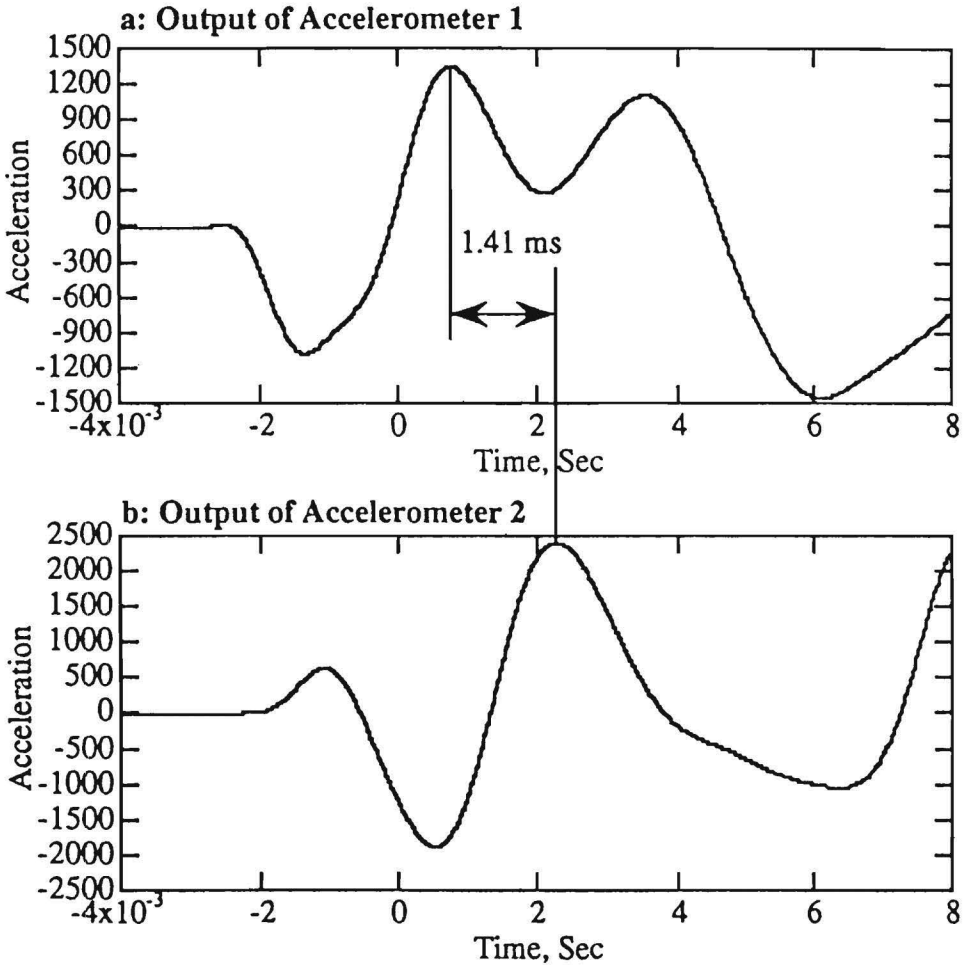

Figure 2.6 Determination of Bending Wave Velocity Using Short Kernel Method

Length Calculation:
$\Delta t = 22$ ms
V = 2,480 ft/sec
Length of Pile = V x Δt / 2 = 2,480 x 22 x 10^{-3} /2 = 27.3 ft

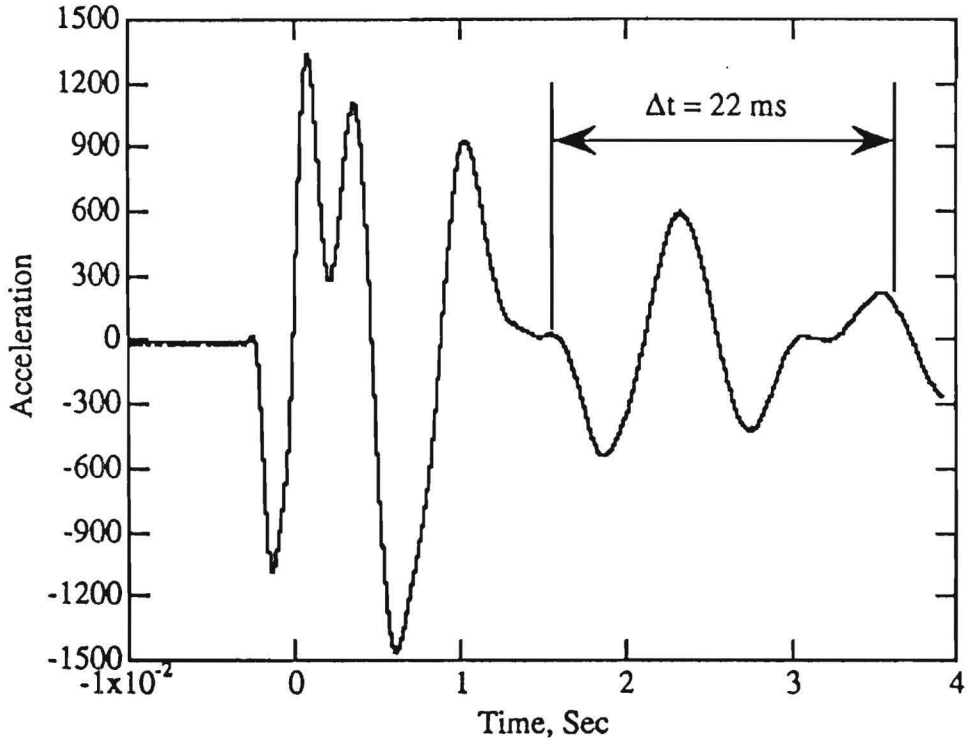

Figure 2.7 Determination of Pile Length Using Short Kernel Method

Yu and Roesset (1995) also considered frequency domain (transfer function) interpretation of bending wave test results. The interpretation is similar to the Impulse Response method described earlier which relies on longitudinal waves. The pile length is determined from the spacing between peaks, Δf, in the frequency response function between the input (hammer blow) and output (receiver response):

$$L = \frac{V_{limit}}{2\Delta f} \tag{2.4}$$

where the limiting flexural wave velocity approaches the Rayleigh wave velocity of the pile material. Since flexural waves are dispersive as described above, it is necessary to use the peaks of higher order modes (say 8th mode and higher) to determined the spacing between frequencies. For these higher modes, Δf approaches a constant value. Lower modes can be used if the appropriate value of V (accounting for dispersion) is used in Eq. 2.4.

3 Numerical Modeling

A series of analytical and numerical models were developed to study the response of long, slender members such as beams or piles to flexural waves. Closed-form solutions are developed for a cantilever beam to illustrate the basic characteristics of the response. A finite element numerical solution is derived to allow more complex pile geometry and boundary conditions such as those encountered on actual bridge foundations to be modeled.

Analytical Derivation

Closed-form analytical solutions can be obtained for long, slender members with simple geometries and boundary conditions. One such analytical solution is based on Euler's beam equation. It is derived by considering an elemental length of beam, dx, and the internal shear forces and moments acting on it. This element is shown in Figure 3.1.

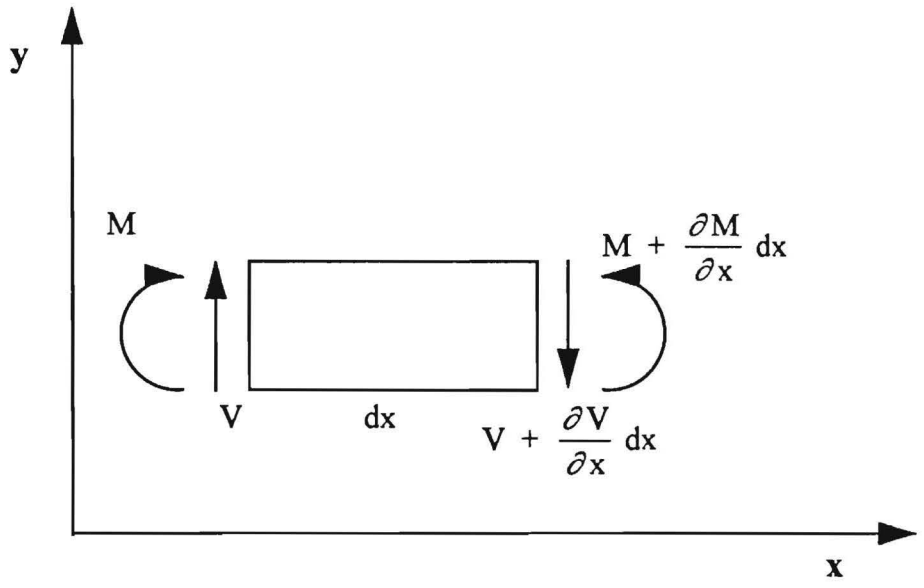

Figure 3.1 Beam Element

Euler's theory yields the following relationships:

$$y = \text{deflection} \tag{3.1}$$

$$\frac{\partial y}{\partial x} = \text{slope} \tag{3.2}$$

$$EI\frac{\partial^2 y}{\partial x^2} = M \tag{3.3}$$

$$EI\frac{\partial^3 y}{\partial x^3} = V \tag{3.4}$$

$$EI\frac{\partial^4 y}{\partial x} = w(x) \tag{3.5}$$

where

$$V' = V + \frac{\partial V}{\partial x}dx \tag{3.6}$$

and

$$M' = M + \frac{\partial M}{\partial x}dx \tag{3.7}$$

Letting the mass per unit length of the beam be γ, and the acceleration of the element be $\delta^2 y/\delta t^2$, Euler's beam equation is written as:

$$\frac{EI}{\gamma}\frac{\partial^4 y}{\partial x^4} + \frac{\partial^2 y}{\partial t^2} = 0 \tag{3.8}$$

The general solution for the partial differential equation is:

$$y(x) = C_1 \sinh(\lambda x) + C_2 \cosh(\lambda x) + C_3 \sin(\lambda x) + C_4 \cos(\lambda x) \tag{3.9}$$

In order to solve for the fixed-free condition, the appropriate boundary conditions must be defined. At the end, $x = 0$, the condition is fixed, such that there is no displacement, and the slope of the beam is zero. This yields the following equations describing this boundary:

$$y(0) = 0$$

$$\frac{\partial y(0)}{\partial x} = 0 \tag{3.10}$$

At the free end, there can not be any moment or shear forces, therefore, the boundary conditions are as follows:

$$\frac{\partial^2 y(L)}{\partial x^2} = 0$$

$$\frac{\partial^3 y(L)}{\partial x^3} = 0 \tag{3.11}$$

The next step in this solution is to take three derivatives of Eq, 3.9, since each is defined by the boundary condition constraints above.

$$\frac{\partial y}{\partial x} = \lambda(C_1 \cos(\lambda x) + C_2 \sinh(\lambda x) + C_3 \cos(\lambda x) - C_4 \sin(\lambda x))$$

$$\frac{\partial^2 y}{\partial x^2} = \lambda^2(C_1 \sinh(\lambda x) + C_2 \cosh(\lambda x) - C_3 \sin(\lambda x) - C_4 \cos(\lambda x)) \tag{3.12}$$

$$\frac{\partial^3 y}{\partial x^3} = \lambda^3(C_1 \cosh(\lambda x) + C_2 \sinh(\lambda x) - C_3 \cos(\lambda x) - C_4 \sin(\lambda x))$$

Substituting values of x leads to the following matrix formulation:

$$\begin{bmatrix} 0 & 1 & 0 & 1 \\ \lambda & 0 & \lambda & 0 \\ \lambda^2 \sinh(\lambda L) & \lambda^2 \cosh(\lambda L) & -\lambda^2 \sin(\lambda L) & -\lambda^2 \cos(\lambda L) \\ \lambda^3 \cos(\lambda L) & \lambda^3 \sinh(\lambda L) & -\lambda^3 \cos(\lambda L) & \lambda^3 \sin(\lambda L) \end{bmatrix} \begin{Bmatrix} C_1 \\ C_2 \\ C_3 \\ C_4 \end{Bmatrix} = \begin{Bmatrix} 0 \\ 0 \\ 0 \\ 0 \end{Bmatrix} \tag{3.13}$$

Leading to the characteristic equation:

$$\cos(\lambda L)\cosh(\lambda L) + 1 = 0 \tag{3.14}$$

Assuming simple harmonic motion, the natural frequencies of the fixed-free beam are given in radians/second as follows:

$$\omega_i = \frac{(\lambda L_i)^2}{L^2}\sqrt{\frac{EI}{\gamma}} \tag{3.15}$$

where

λL_i = ith root of Eq. 3.14

L = length of beam

E = Young's Modulus

I = moment of inertia

γ = mass per unit length

The roots of Eq. 3.14 can be easily solved by rearranging the equation into the form:

$$\cos(\lambda L) = -\frac{1}{\cosh(\lambda L)} \tag{3.16}$$

Then the roots of Eq. 3.16 can easily be found using a program such as Mathcad, graphing each side of the equation as a separate function. Estimates of the roots can be made from this plot for however many natural frequencies are of interest, then the root function can be used to find the exact values of λL, using the initial guess as the starting value in an iterative solver. The values calculated above can then be substituted into Eq. 3.15 along with the known properties, and the natural frequencies can be obtained. This procedure can be followed for any other boundary condition, such as pinned-pinned, fixed-fixed, etc. It is simply a matter of applying the correct boundary conditions to the derivatives of Eq. 3.12.

Finite Element Analysis

Finite element analysis has become a very valuable tool for structural analysis. It became a viable method for analysis with the advent of the electronic digital computer. Traditionally, engineers have used the fact that a structure may first be considered by examining the behavior of individual structural elements, then combining them together such that equilibrium of forces and compatibility of displacements are satisfied.

In the finite element method, a structure is idealized as a number of elements connected only at node points. Any geometry can be modeled in this manner, along with any type of loading. Various types of elements are available for analysis, however, only bar elements are treated here.

The finite element method is based on the stiffness method where:

$$\{F^e\} = [K^e]\{\delta^e\} \tag{3.17}$$

where

F^e = nodal load vector

δ^e = nodal displacement vector

K^e = element stiffness matrix

The element stiffness matrix is developed by knowing the number of degrees of freedom at each node of the element, and then relating the force and displacement with unit values. A simple elastic spring shows this relationship. Figure 3.2 shows a spring, with F_1 and u_1 being the force and displacement at the first node, and F_2 and u_2 being the same at the second node. The relationship is as follows:

$$\begin{Bmatrix} F_1 \\ F_2 \end{Bmatrix} = \begin{bmatrix} k_{11} & k_{12} \\ k_{21} & k_{22} \end{bmatrix} \begin{Bmatrix} u_1 \\ u_2 \end{Bmatrix} \tag{3.18}$$

Figure 3.2 Illustration of Nodal Forces and Displacements Using Simple, Elastic Spring

The axial stiffness of the spring is known, but the individual terms in the stiffness matrix must be determined. These terms are determined by allowing each node to deform an amount u while fixing the other, and then relating the nodal forces to this deformation.

Deform node 1 and keep node 2 fixed:

$$F_{11} = ku_1$$

$$F_{11} + F_{21} = 0$$

$$F_{21} = -ku_1 \tag{3.19}$$

Deform node 2 and keep node 1 fixed:

$$F_{22} = ku_2$$

$$F_{12} + F_{22} = 0$$

$$F_{12} = -ku_2 \tag{3.20}$$

The total forces at the nodes are:

$$F_1 = F_{11} + F_{12}$$

$$F_2 = F_{21} + F_{22} \tag{3.21}$$

$$F_1 = ku_1 - ku_2$$

$$F_2 = -ku_1 + ku_2 \tag{3.22}$$

This can be written in matrix form as follows:

$$\begin{Bmatrix} F_1 \\ F_2 \end{Bmatrix} = \begin{bmatrix} k & -k \\ -k & k \end{bmatrix} \begin{Bmatrix} u_1 \\ u_2 \end{Bmatrix} \tag{3.23}$$

Giving the stiffness matrix for the single spring element:

$$\left[K^e\right] = \begin{bmatrix} k & -k \\ -k & k \end{bmatrix} \tag{3.24}$$

As can be seen here, the stiffness matrix is symmetric. This is due to the phenomenon explained by the reciprocal theorem, and is taken advantage of by finite elements codes to reduce the amount of memory

used by only needing to store an upper or lower triangle of the matrix. Knowing the element stiffness matrix, the deflection due to any applied load, or the loading due to any deflection consistent with the degrees of freedom of the nodes can be determined.

The procedure outlined above simply shows some of the concepts of the stiffness analysis which lead up to the heart of the derivation of the finite element method. It is important to show that individual element stiffness matrices can be determined, regardless of the rest of the geometry of the system. From this point, a global stiffness matrix is developed, in order to determine displacements in a larger structure.

In most cases, more information than just the displacements are required for an analysis. Elements can be derived which relate displacement functions to stress and strains within the element. This is known as a stress-displacement relationship and values for stresses and strains can be calculated at various points within a structure due to load cases. This derivation is beyond the scope of this simple introduction.

Comparison of Analytical and Numerical Results

To validate the numerical solution, comparisons were made between values of natural frequency obtained from a closed-form solution for a cantilever beam and values obtained from a numerical analysis of the same beam. The analytical calculations and solution are summarized in Figure 3.3. Table 3.1 compares the natural frequencies obtained from the analytical and finite element solutions. The values of the natural frequencies in both the X-X and Y-Y directions compare well and provide confidence that the finite element program can be used to model more complex geometries and boundary conditions which do not have simple, closed-form solutions.

Shape: HS 3x5.7
Material: Steel
Length: 6 foot
Boundary: fixed-free
Units: in-lbs

Properties: $L := 72$ $A := 1.67$

$I_x := 2.52$ $I_y := .455$

$\rho := .000738$ $\gamma := \rho \cdot A$

$E := 29000000$

Iyy:

$$\omega_{(i)} := \frac{(\lambda L_i)^2}{L^2} \cdot \sqrt{\frac{E \cdot I_y}{\gamma}}$$

$\omega_1 = 70.169$ $\omega_2 = 439.807$ $\omega_3 = 1231.456$ $\omega_4 = 2413.162$ $\omega_5 = 3989.131$

$$\omega_i := \frac{\omega_i}{2 \cdot \pi} \text{ Hz}$$

$\omega_1 = 11.168$ $\omega_2 = 69.997$ $\omega_3 = 195.992$ $\omega_4 = 384.067$ $\omega_5 = 634.89$

Ixx:

$$\omega_{(i)} := \frac{(\lambda L_i)^2}{L^2} \cdot \sqrt{\frac{E \cdot I_x}{\gamma}}$$

$\omega_1 = 165.136$ $\omega_2 = 1035.038$ $\omega_3 = 2898.1$ $\omega_4 = 5679.12$ $\omega_5 = 9387.995$

$$\omega_i := \frac{\omega_i}{2 \cdot \pi} \text{ Hz}$$

$\omega_1 = 26.282$ $\omega_2 = 164.731$ $\omega_3 = 461.247$ $\omega_4 = 903.86$ $\omega_5 = 1494.146$

Figure 3.3 Summary of Closed-Form Calculations

Table 3.1 Comparison of Analytical and Numerical Solutions

	Natural Frequency (Hz)	
Mode of Vibration	Analytical	Numerical
Y-Y Direction		
1	11.2	11.2
2	70.0	70.1
3	196.0	196.4
4	384.1	384.9
5	634.9	636.2
X-X Direction		
1	26.3	26.3
2	164.7	165.1
3	461.3	462.2
4	903.9	905.7
5	1494.2	1497.2

4 Tests on Small-Scale Piles

Tests on small-scale piles were performed to obtain experimental pile response data under controlled laboratory conditions for a variety of pile lengths and configurations. The following sections describe the experimental facility, the configuration of the piles, and the results of tests on the small-scale piles with both free and embedded end conditions.

Small-Scale Pile Facility

Flexural wave testing on the small-scale piles was performed in the Civil Engineering Laboratories Building on the Georgia Institute of Technology campus. A photograph of the test facility is shown in Figure 4.1. The experimental pile facility contained a 12 ft long by 9 ft wide by 5 ft deep concrete pit. The pit extended 4.5 ft below the floor surface with a 6 in. rim extending up around the pit. Figure 4.2 and Figure 4.3 show two vertical channel sections (C9 x 13.4) bolted to the rim of the pit on each side of the 9 ft width. A horizontal W10 x 45 steel section, with a plate welded to each end, was connected to a channel section on each end of the pit and ran parallel to the 12 ft length of the pit. The vertical channel sections and the end plates on the horizontal members had pre-bored holes. These pre-bored holes were used to connect the vertical and horizontal members together. The holes also enabled the horizontal sections to be

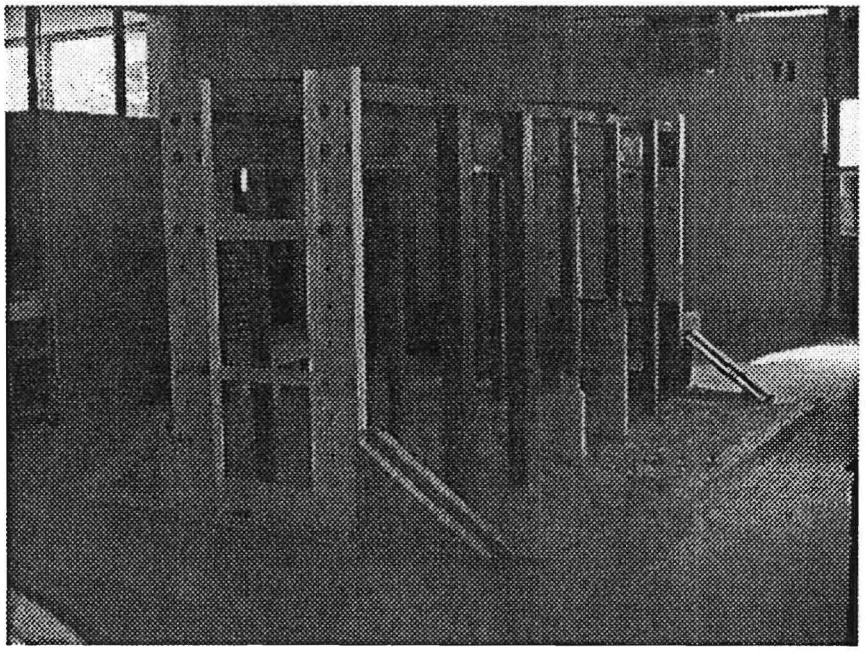

Figure 4.1 Experimental Facility for Testing Small-Scale Piles

placed at different heights if necessary. The horizontal sections were placed at 5 ft above the pit rim for all of the lab tests. The figures also show that the horizontal W10 x 45 members were connected to each other by two 3 ft x 2 ft x 1 inch thick plates that were bolted to the bottom flange of the section. Four S3 x 5.7 sections were welded at angles to the top flange of the horizontal members to help stiffen the system. Once the frame was completely assembled, five vertical model pile sections (labeled A-E and F-J) were welded to the flange edges of each of the W10 x 45 horizontal members.

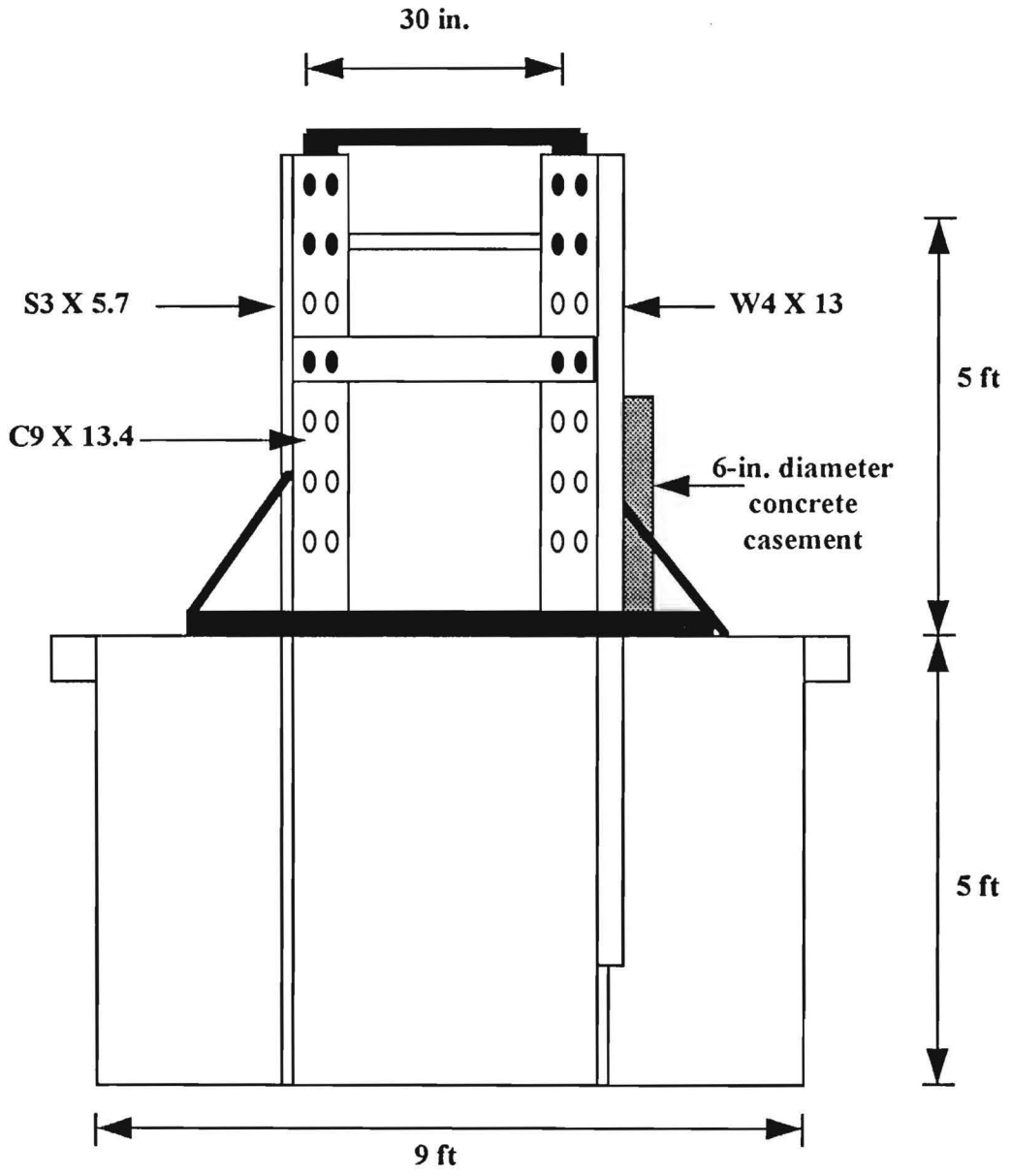

Figure 4.2 End View of Experimental Facility for Testing Small-Scale Piles

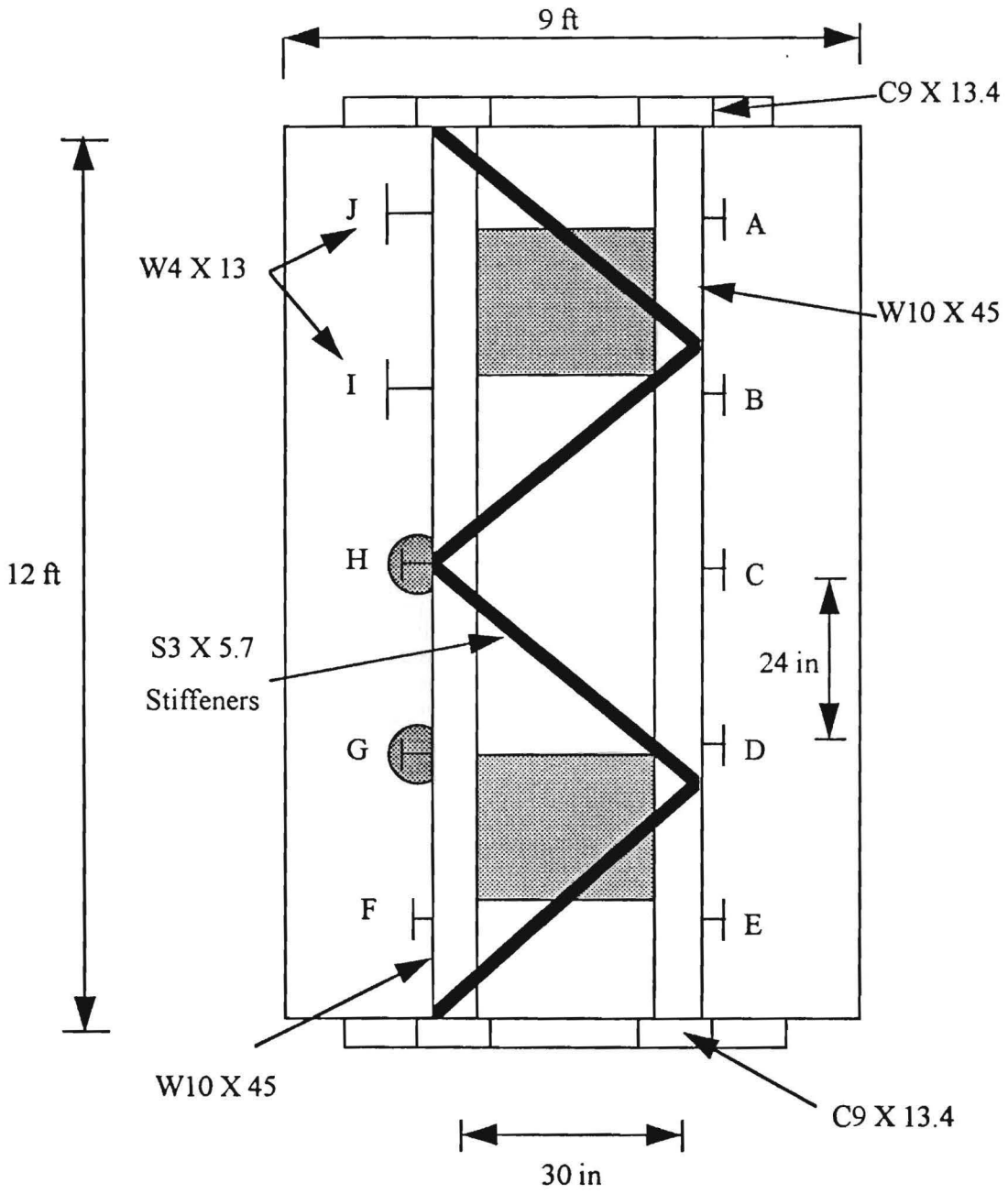

Figure 4.3 Plan View of Experimental Facility for Testing Small-Scale Piles

Test Pile Sections

The pile sections that were used in the laboratory testing were chosen based on bridge design information given by the Georgia Department of Transportation (Gratton, personal communication). The Georgia DOT indicated that a typical steel H pile section is an HP 12 x 53 that is 15 to 60 feet in length with a concrete casement from the ground line to 2 feet above the waterline. These dimensions yield an average ratio of length to section depth (L/D) of 37.5. The test pile sections have an average length of 8 feet since the lengths ranged from a minimum of 6 feet and maximum of 10 feet. This 8-foot average length was then divided by the L/D ratio of 37.5 to yield a test pile section depth of 2.6 inches. Therefore, an S3 x 5.7 was chosen to be the primary representative pile section. Two W4 x 13.0 sections were also used to change the section dimensions for some the tests. As shown in Figure 4.3, each pile was designated with an alphabetic label.

Figure 4.4 shows the right elevation of the test pit. On the right horizontal section five S3 X 5.7 sections, Piles A through E, were welded to the flanges of the horizontal member on 24-in. centers with lengths varying from 6 to 10 feet. This test setup corresponded to a pile embedment depth of 1 foot for Pile A to 5 feet for Pile E. In this basic pile setup the primary variable that was changed was the pile length. This setup would enable tests to be conducted to assess the effects of pile length on the natural frequency and mode shapes of the piles.

Figure 4.5 shows the left elevation of the test pit. The left horizontal member also had 5 test sections, Piles F through J, welded to it. These piles were setup to test the influence of other parameters in addition to the length. The following piles were welded to the left horizontal member:

- Pile F, an S3 x 5.7 section that rests on the concrete pit bottom to simulate an end bearing pile. This pile was intended to examine the influence on pile response of a fixed response to end condition as opposed to the floating end conditions of piles A through E.

- Pile G, an S3 x 5.7 section 9-ft long with concrete casement extending 2.5 feet above the top of the soil, and Pile H, an S3 x 5.7 section 7-ft long with concrete casement extending 1.25 feet above the top of the soil. These piles were used to investigate the effects of a concrete casement on flexural waves. The concrete casement is used on bridges to help protect the steel sections from corrosion. The casements were constructed by splitting a 6-in. diameter PVC pipe length-wise to make a form. The forms were taped together around the test piles and filled with Sak-Crete.

- Pile I, a 7-ft long W4 x 13 section, and Pile J, a 9-ft long W4 x 13 section. These W4 x 13 sections were intended to investigate a change in section to compare with Piles B and D which are S3 x 5.7 sections.

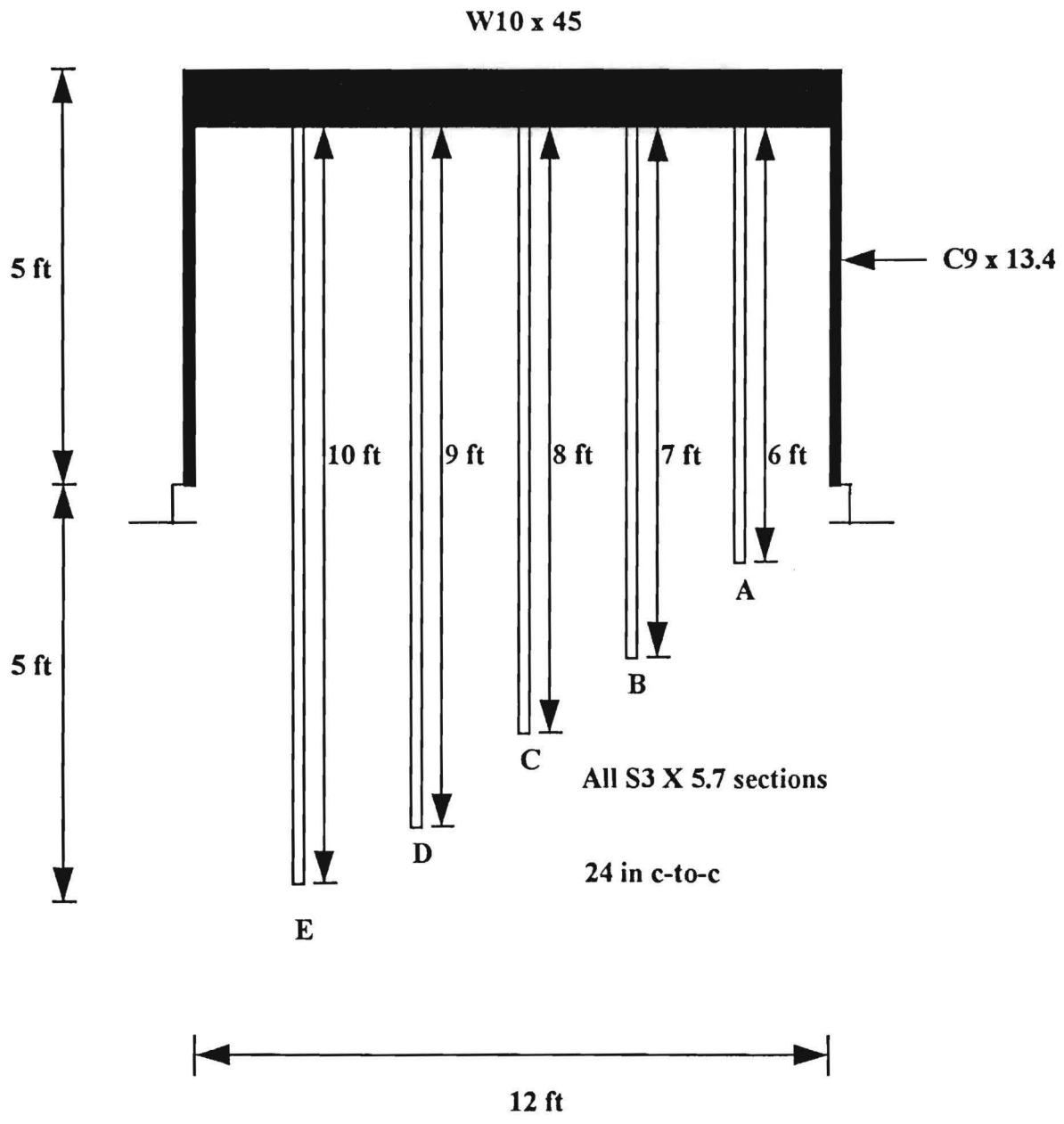

Figure 4.4 Right Elevation View of Small-Scale Pile Test Facility

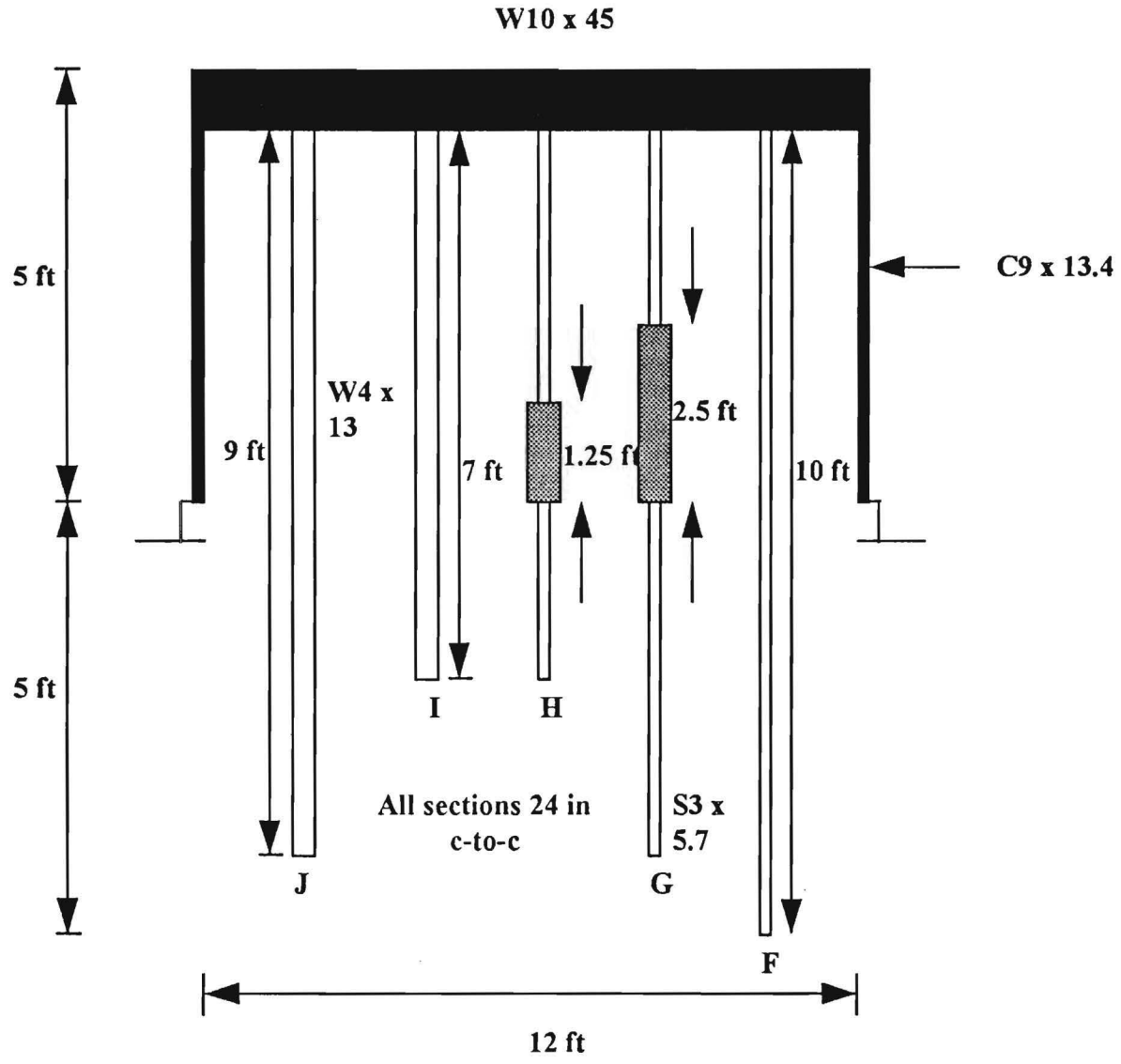

Figure 4.5 Left Elevation View of Small-Scale Pile Test Facility

Tests on Fixed-Free Piles

The first phase of the flexural wave testing was begun prior to the sand placement but after the piles had been welded to the frame. The first tests were performed at this time to test the pile in a fixed-free condition The main objective of this first phase of testing was to provide simple boundary conditions which could be modeled easily in the finite element analysis described in Chapter 3. The response of a beam with fixed-free

boundary conditions also has a closed-form solution which can be compared to the experimental and finite element solutions.

Test Equipment and Configuration

The testing configuration for the fixed-free pile testing is presented in Figure 4.6. The hammer (source) used to induce the flexural waves was a PCB Piezotronics, Inc. Model 086C50 modally tuned hammer with a built-in force transducer. The hammer is 8 in. long with a head diameter of 0.6 in. and a tip diameter of 0.25 in. It has a force range of 0 to 5000 lb. This hammer has a calibrated sensitivity of 0.98 mV/lb. The hammer has 3 tips that can be attached to the built-in force transducer. Each tip varies in hardness. Two of the tips are made of plastic and the third is made of metal. Harder tips induce higher-frequency waves into the pile. The metal tip was used for the fixed-free pile testing since higher frequencies were desired. The pile response was measured by a Wilcoxon Research Model 732A piezoelectric accelerometer (receiver). This accelerometer has a traceable frequency response range of 10 Hz to 10 kHz. The calibration voltage sensitivity for this particular accelerometer is 10.2 mV/g. The accelerometer was attached to the pile with a magnet. The magnet is 0.75 in. in diameter and 0.5 in. thick with a bolt protruding from one circular side and a magnetized disk on the other. The accelerometer was threaded onto the bolt and mounted horizontally on the pile with the magnet. The hammer and the accelerometer response measurements were recorded by a Hewlett-Packard Model 3562A Dynamic Signal Analyzer. This analyzer has the ability to process the pile response in the time and frequency domains. The data is processed from the time to the frequency domain by the use of a Fast Fourier Transform. The signal analyzer has two external 3.25 in. floppy disk drives which enables the user to save the pile response measurements on disk for later manipulation.

Test Method

Pile A was the chosen for testing with a free end condition. The locations of the hammer and accelerometer were varied along the length of the pile at positions designated 1 through 9 as shown in Figure 4.6. The ninth position was not placed at the top of the pile since there would be almost no pile response there due to the fixed end condition at the top of the pile. A typical test measurement consisted of placing the accelerometer at a designated position (1 through 9) along the pile and inducing flexural waves at another designated position (1 through 9) with the hammer. The fixed-free pile tests were designated by the letter R with the hammer position and accelerometer positions being designated in that order by a numeral. For example, test R_{23} indicates a fixed-free pile test with the hammer located at position 2 and the accelerometer located at position 3. For each impact of the hammer, the FFT analyzer calculated and displayed the inertance frequency response function (FRF) between the hammer (input) and accelerometer (output):

$$\text{Inertance} = \frac{\ddot{U}(f)}{P(f)} \tag{4.1}$$

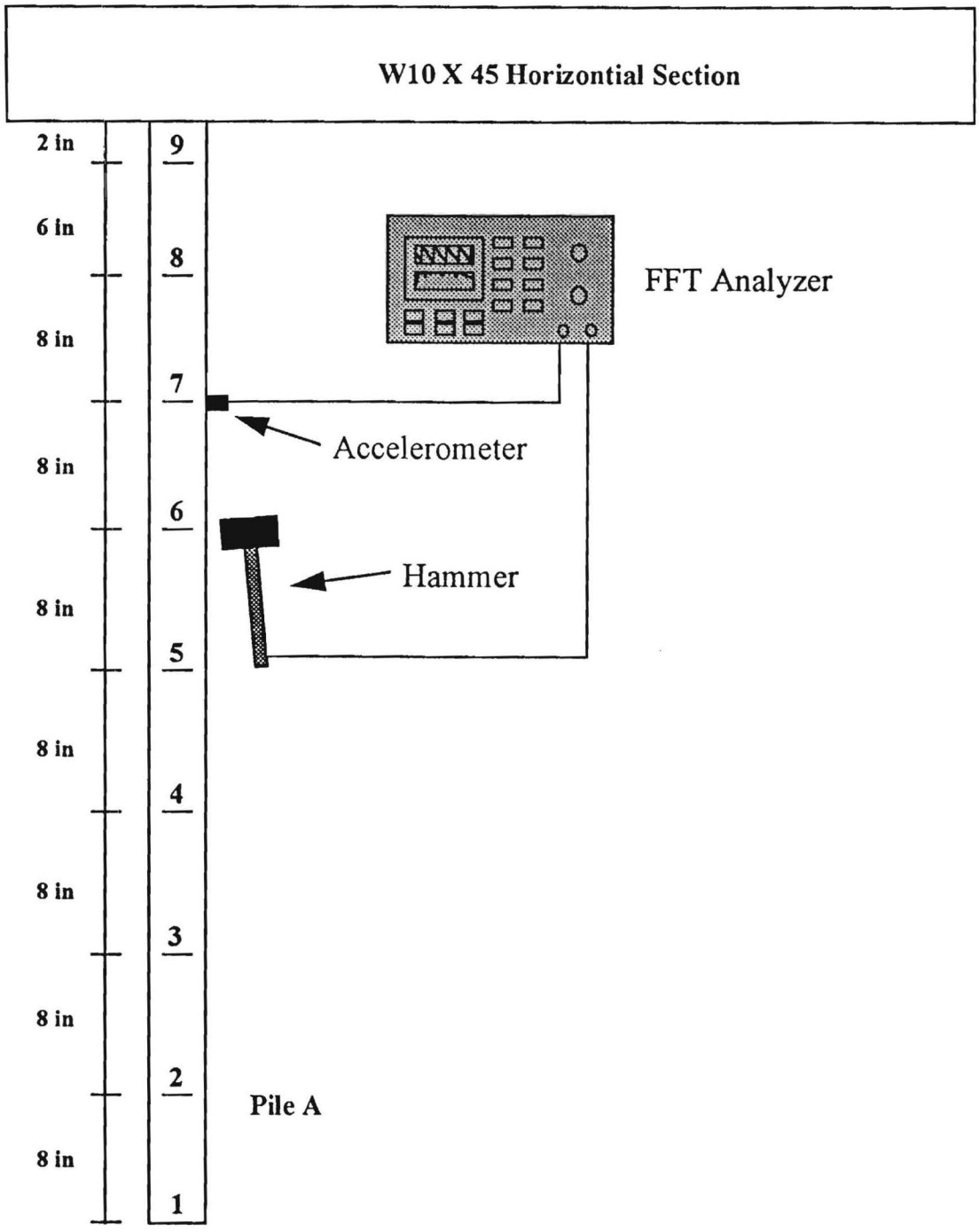

Figure 4.6 Test Configuration Used for Testing Pile A with Free End Condition

Five individual frequency response functions were averaged in the frequency domain to reduce the influence of random noise on the final measurement. Since the pile section (S3 x 5.7) is not symmetric, tests were performed in the direction of both the X-X axis and Y-Y axis. Figure 4.7 shows the orientation of the X-X and Y-Y axes with respect to the cross-section of the S3 x 5.7 pile.

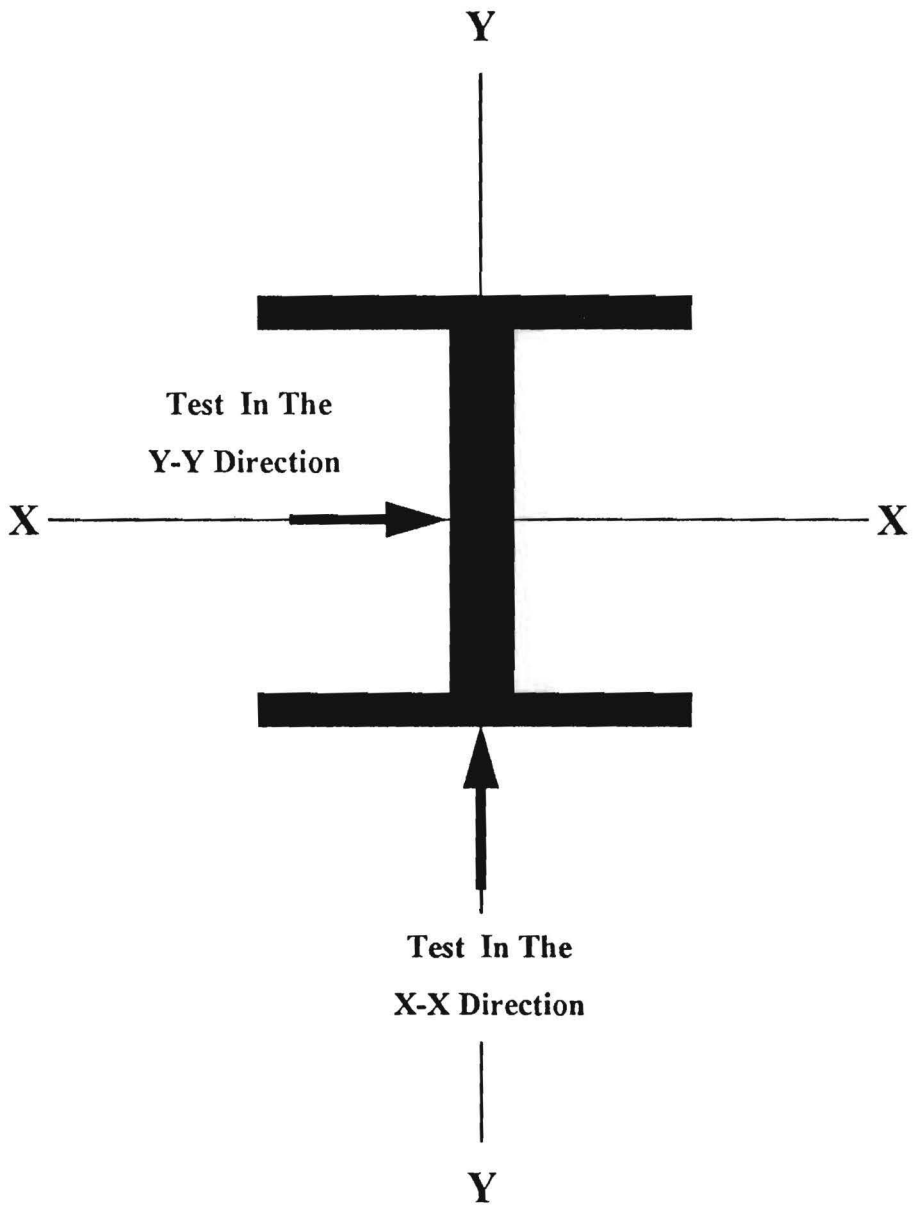

Figure 4.7 Definition of X-X and Y-Y Directions

Test Results

Figure 4.8 shows a typical frequency response function of Pile A with a free end condition. The source and receiver were both placed at Position 1 (R_{11}) and the pile was tested in the Y-Y direction. The magnitude plot is characterized by numerous sharp peaks corresponding to the natural frequencies of different modes of vibration of the pile. The first five flexural modes are labeled with numerals indicating the mode number. Three additional modes labeled as "Coupled" are spurious modes involving torsional and longitudinal motion. These modes arise because it is nearly impossible to strike the pile in such a way as to excite pure flexural modes.

Additional tests were performed with the source and receiver placed at different positions on the pile as described above. Figure 4.9 shows the frequency response function measured with the source at Position 2 and the receiver at Position 3 (R_{23}). Note that the amplitude of Modes 2 and 3 is greatly diminished in comparison with R_{11}. Modes 1, 4, and 5 as well as the coupled modes remain approximately the same as R_{11}. This difference is attributed to the mode shapes associated with each natural frequency. Figure 4.10 illustrates the mode shapes of the first five modes of vibration of a pile fixed at the upper end and free at the bottom. Note that Modes 2 and 3 have nodal points (points with zero deflection) at approximately the same positions as the source and receiver (63 in. and 54 in. from the top of the pile, respectively). Thus, Mode 2 is not strongly excited by the source placed at Position 2 (63 in. from the top of the pile). Similarly, the receiver at Position 3 (54 in. from the top of the pile) is not well placed to measure the response of the pile associated with Mode 3.

To provide the best opportunity for all of the modes to be excited and measured, measurements were performed at 45 different combinations of source and receiver positions along the length of the pile. A "matrix of frequency response measurements" was used to organize the test program. Each row of the matrix corresponds to a single source position and each column corresponds to one receiver position. Maxwell's reciprocal theorem states that 'the displacement at point i due to a unit load at another point j is equal to the displacement at point j due to unit load at point i, provided that the displacements and forces 'correspond,' i.e., that they are measured in the same direction at each point" (Fung, 1964). Thus, the frequency response function R_{23} should be the same as R_{32} and, in general, the matrix of frequency response functions will be symmetric. Figure 4.11 shows the comparison of R_{23} and R_{32}. The two frequency response functions are approximately equal. Comparisons for other source and receiver positions yielded similar agreement. As a result, only the lower diagonal of the matrix of frequency response functions was measured to minimize testing time.

Figure 4.12 shows all 45 frequency response measurements for Pile A. Each "waterfall" plot in Figure 4.12 contains the frequency response functions measured at the 9 different receiver locations for a common source position. Plotting several frequency response functions in this way allows trends in natural frequencies, etc. to be more easily observed.

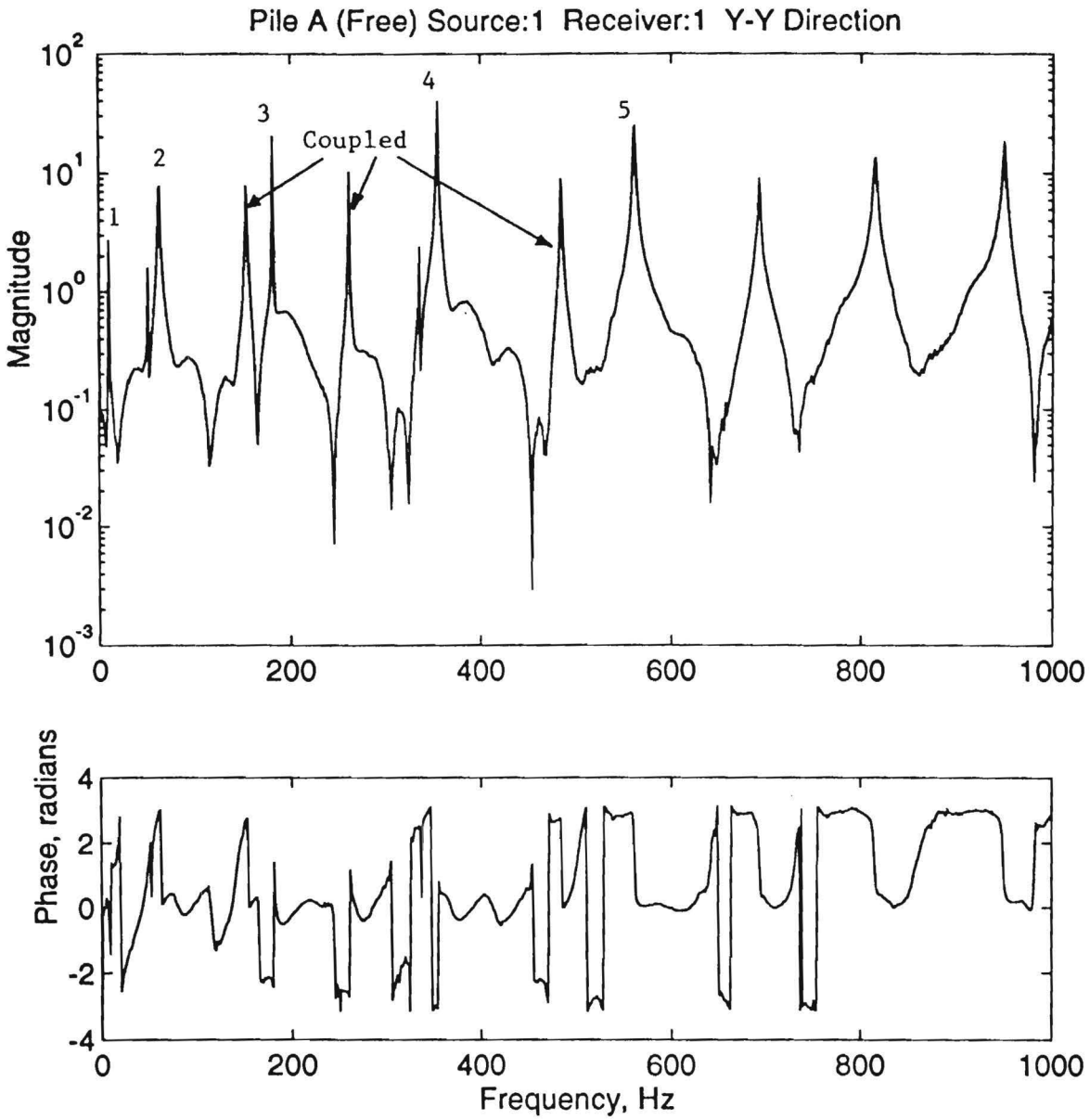

Figure 4.8 Frequency Response Function (R_{11}) for Pile A with Free End Condition

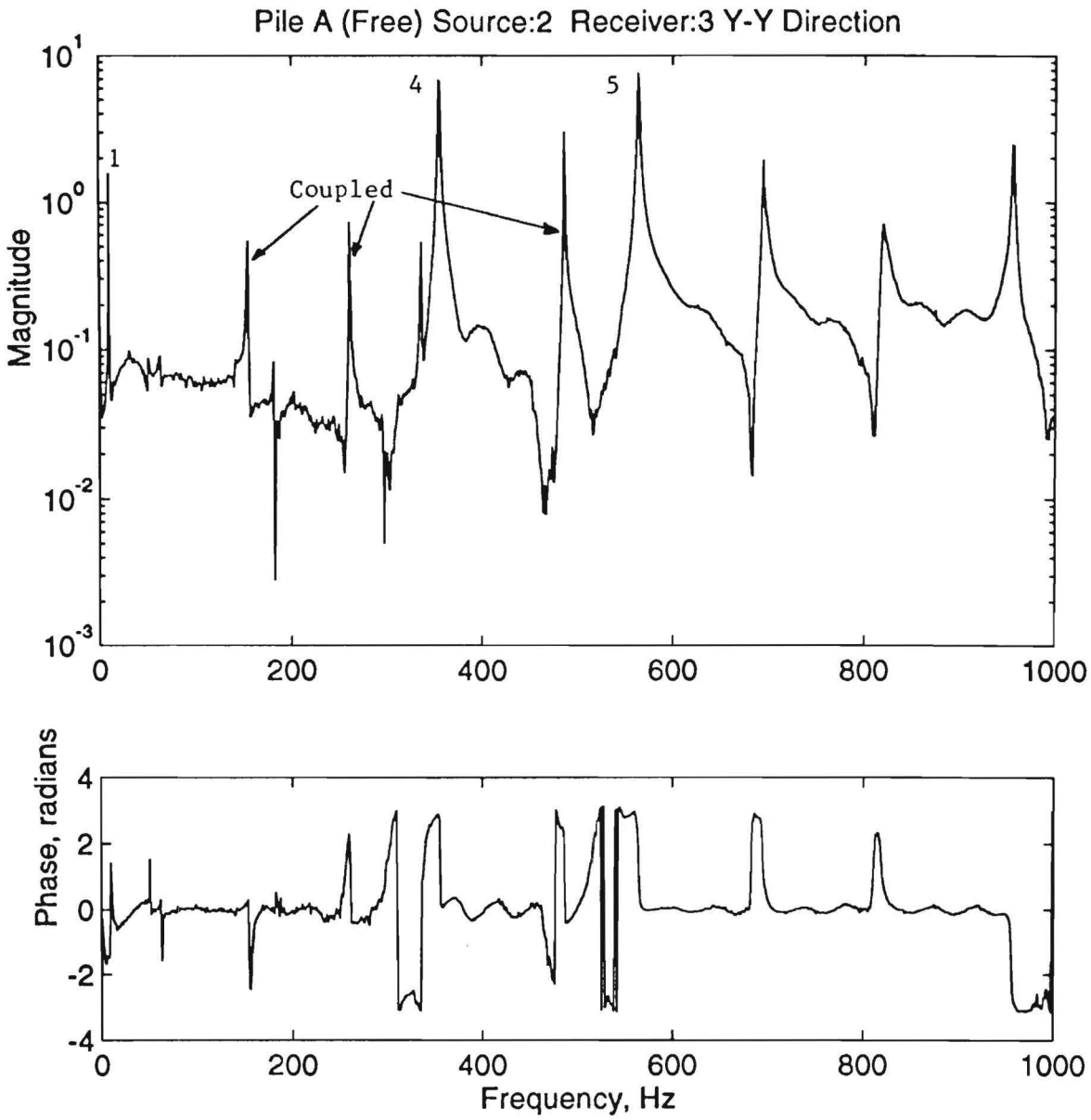

Figure 4.9 Frequency Response Function (R_{23}) for Pile A with Free End Condition

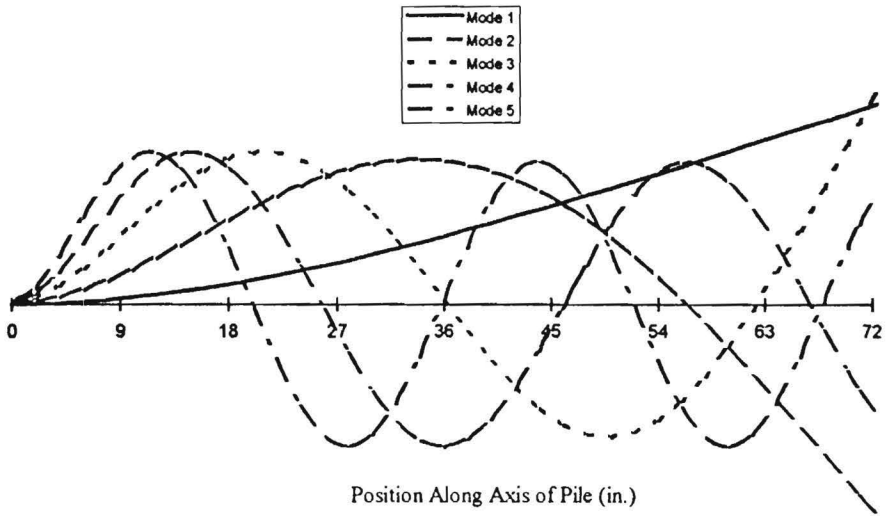

Figure 4.10 Mode Shapes of a Fixed-Free Pile

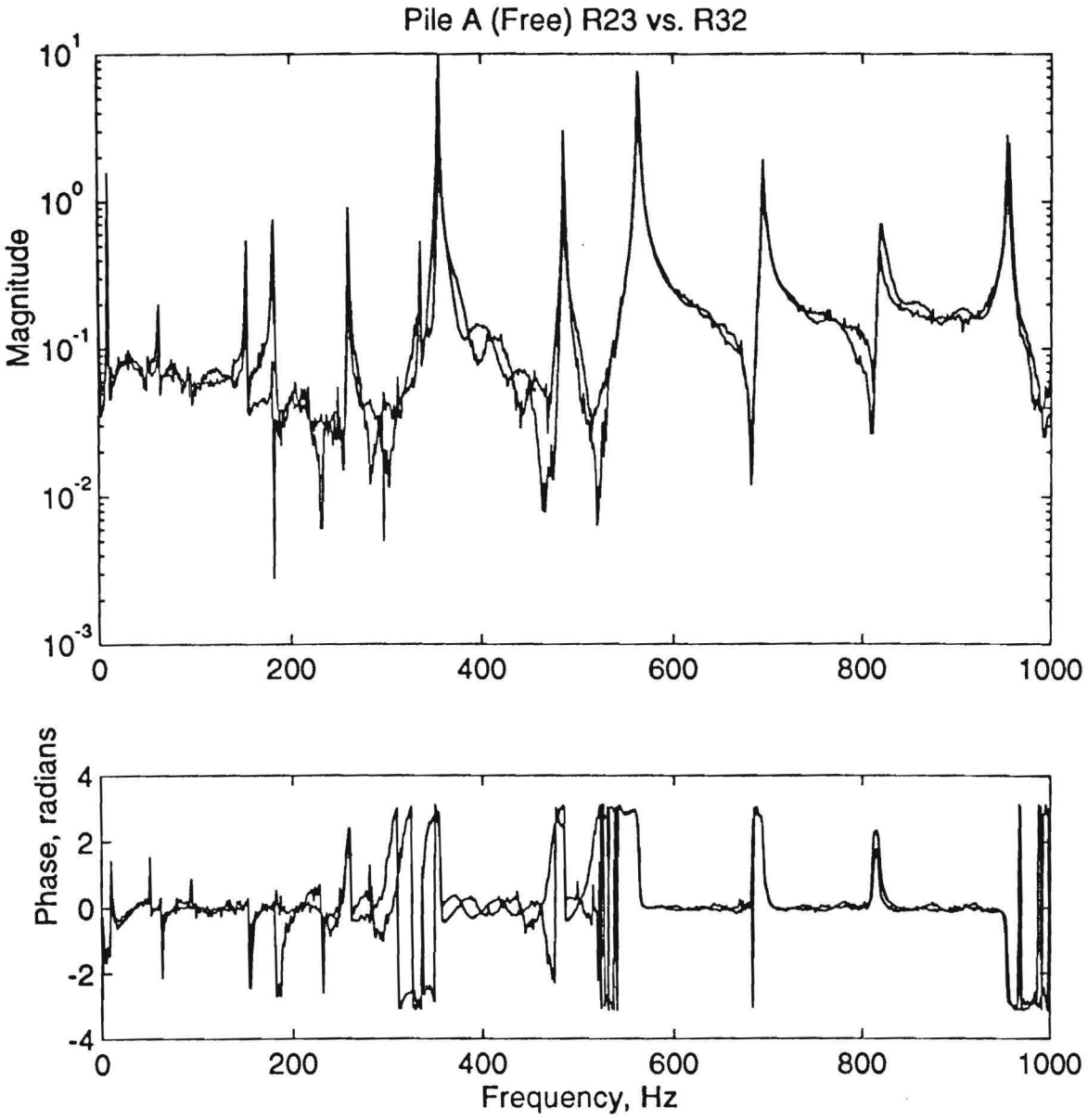

Figure 4.11 Comparison of Frequency Response Functions for Pile A with Free End Condition

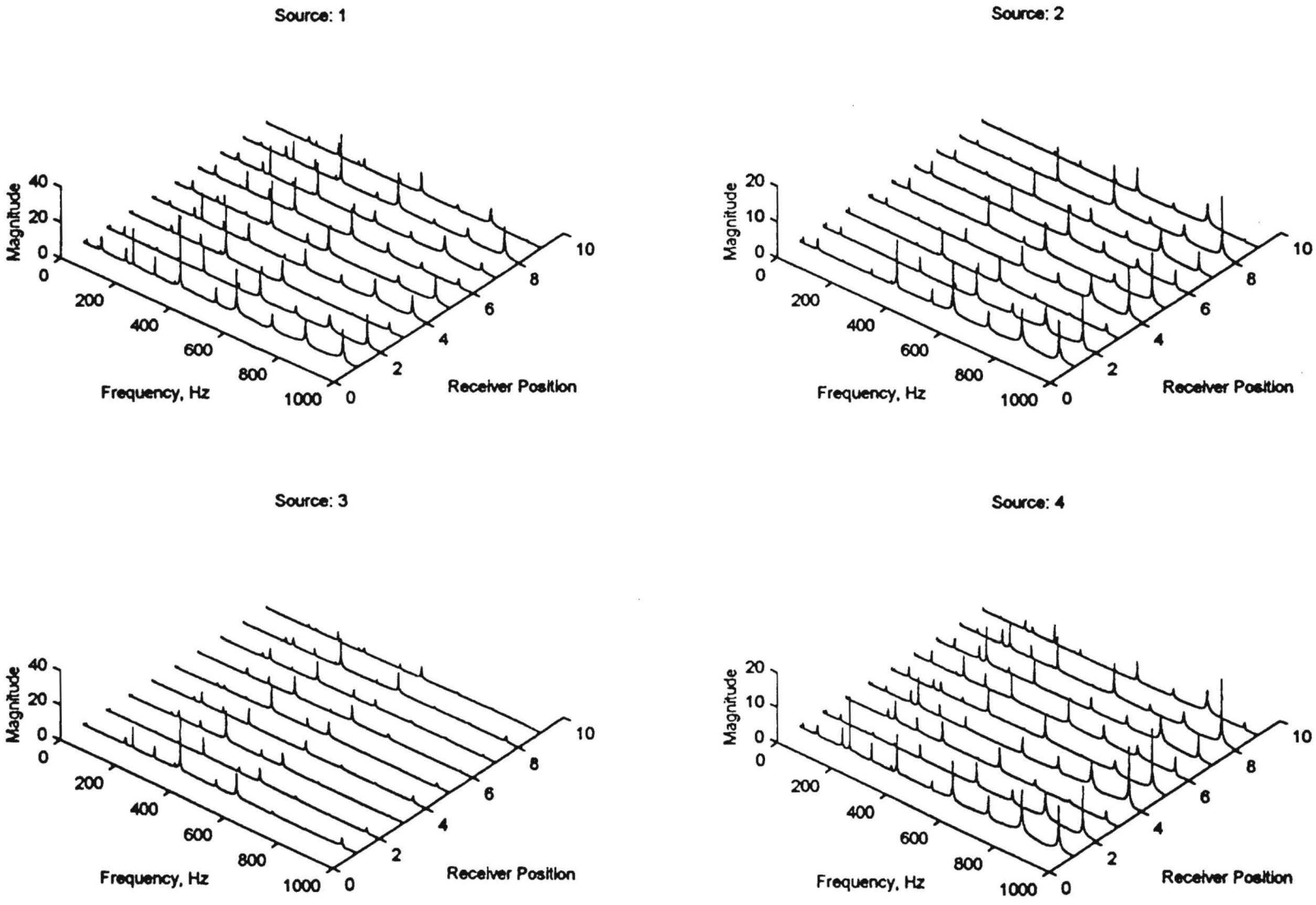

Figure 4.12 Waterfall Plots for Pile A with Free End Condition

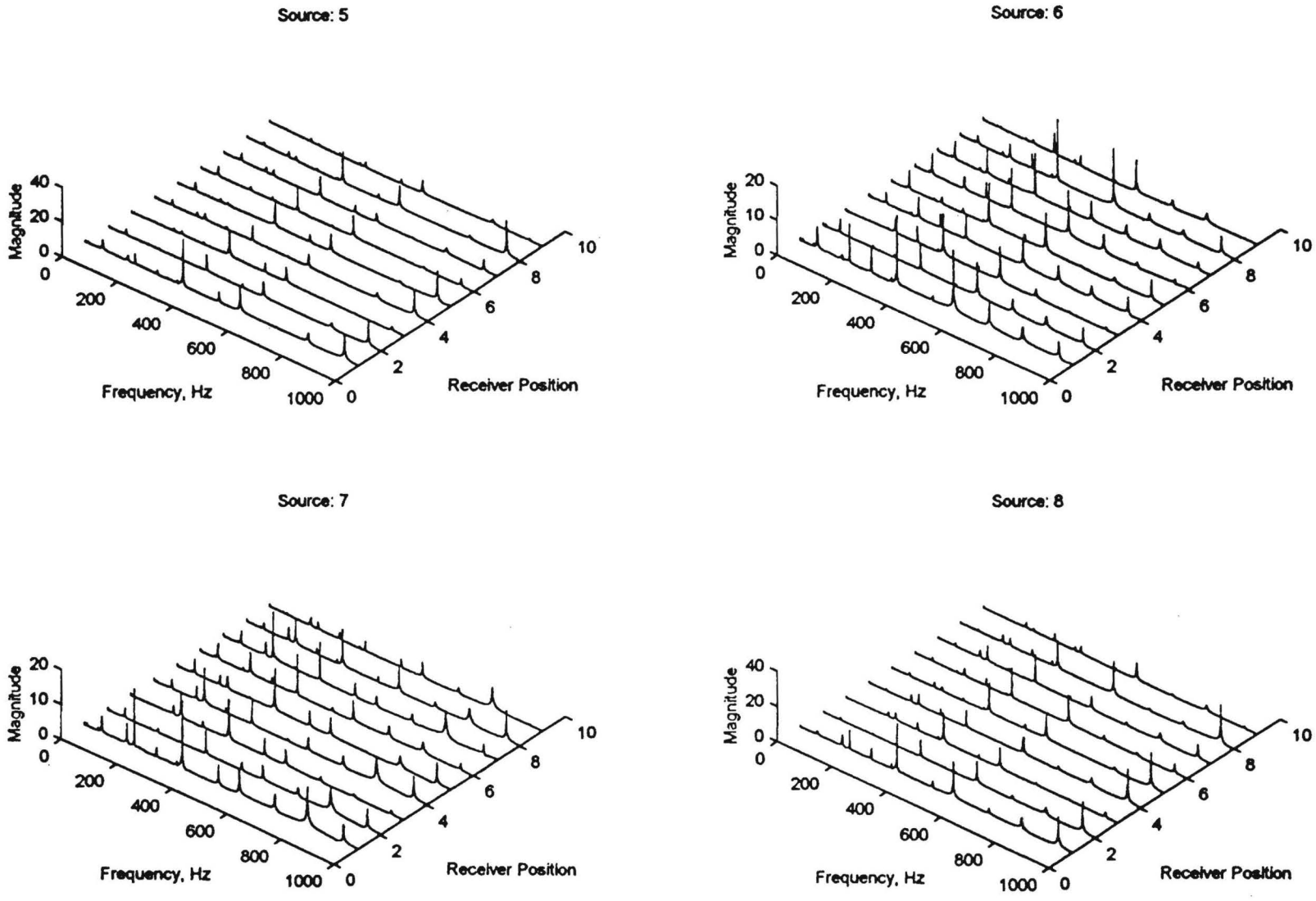

Figure 4.12 Waterfall Plots for Pile A with Free End Condition (continued)

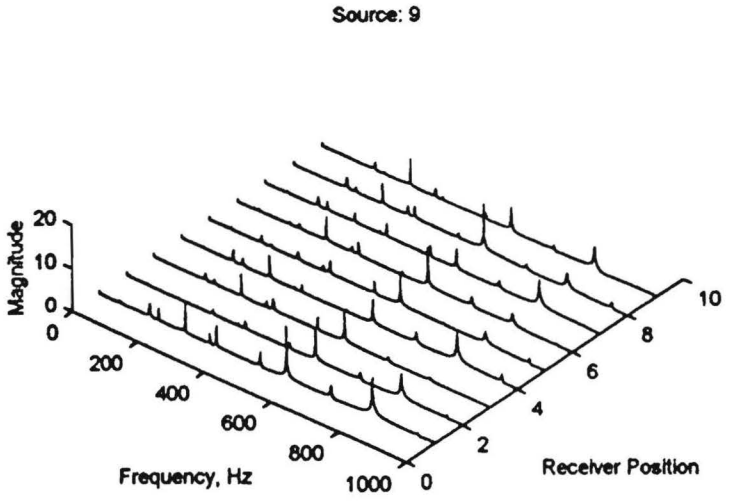

Figure 4.12 Waterfall Plots for Pile A with Free End Condition (continued)

Comparison of Experimental, Analytical, and Numerical Results on Fixed-Free Piles

Table 4.1 shows a comparison between the natural frequencies in both the X-X and Y-Y directions for the experimental, analytical, and numerical results. The analytical and numerical values were obtained using a fixed boundary condition at the upper end of the pile.

Table 4.1 Comparison of Experimental, Analytical, and Numerical Results on Fixed-Free Piles with Fixed End Condition

	Natural Frequency (Hz)		
Mode of Vibration	Experimental	Analytical	Numerical
Y-Y Direction			
1	10.0	11.2	11.2
2	63.3	70.0	70.1
3	181.3	196.0	196.4
4	356.0	384.1	384.9
5	564.0	634.9	636.2
X-X Direction			
1	22.5	26.3	26.34
2	155.7	165.1	165.1
3	390.0	461.2	462.2
4	760.0	903.9	905.7
5	1150.0	1494.2	1497.2

Both the analytical and numerical analyses yield natural frequencies that are larger than those observed experimentally. The difference becomes larger at higher frequencies (higher modes). The finite element model used must be refined somewhat to more closely approximate the natural frequencies of the experimental system. The fixed boundary condition at the top of the beam in the finite element model results in the system more stiff than its experimental counterpart. The finite element boundary condition was changed to two "pinned" connections in the locations of the welds. As a result, the rotational stiffness is a function of the elements themselves, rather than infinite as for the fixed connection. Translational

stiffness will remain infinite. Table 4.2 shows the comparison of the experimental and numerical solutions with the pinned end condition. (Note that the analytical solution could not be calculated for this more complex boundary condition.) The match between experimental and numerical values is improved, suggesting that the pinned connections model the actual end conditions more accurately. As such, pinned connections are used in all subsequent modeling of embedded piles.

Table 4.2 Comparison of Experimental, Analytical, and Numerical Results on Fixed-Free Piles with Pinned End Condition

	Natural Frequency (Hz)		
Mode of Vibration	Experimental	Numerical	Error
Y-Y Direction			
1	10.0	10.4	4%
2	63.3	66.1	4%
3	181.3	187.5	3%
4	356.0	363.9	2%
5	564.0	599.3	6%
X-X Direction			
1	22.5	23.8	5%
2	155.7	148.0	-5%
3	390.0	401.9	3%
4	760.0	750.6	-1%
5	1150.0	1168.7	2%

Tests on Embedded Piles

Following the tests performed on Pile A with a free end condition, the test facility was backfilled with sand to simulate embedded piles. The following sections describe the properties of the sand and the methods used to compact the soil around the piles. Note that for these tests "perfect insertion" was used (i.e., the sand was compacted around the pre-placed piles) rather than driving the piles as is usually the case.

Sand Fill

The sand that was used for fill in this testing is a Chattahoochee River sand. The sand was visually classified as a white-tan, medium to fine, poorly graded, micaceous sand (SP). The grain size distribution for the sand is presented in Figure 4.13. The maximum dry density of the sand was determined by ASTM D 4253-93. The average dry density of the six tests was 98.6 pcf. The minimum density of the sand was determined using ASTM D 4254 - 91. Three tests were performed using Methods A and B of this standard. The average minimum density from the six tests was 80.8 pcf.

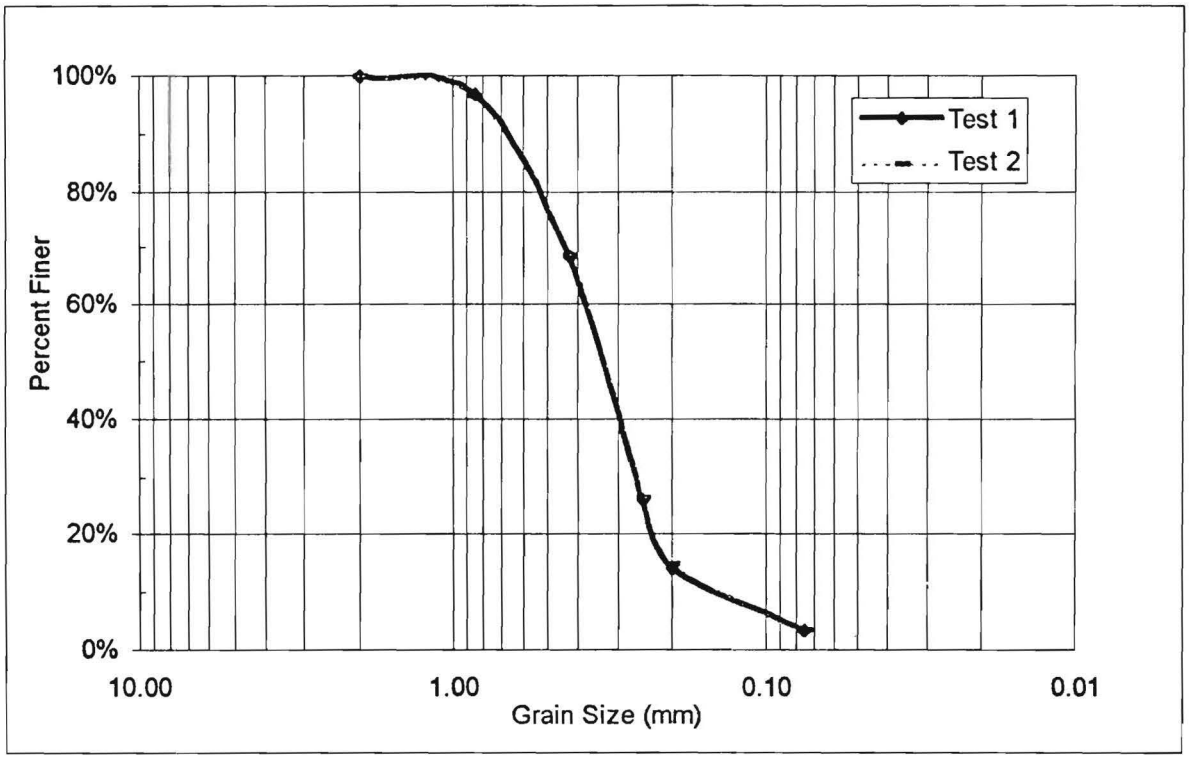

Figure 4.13 Grain Size Distribution for Chattahoochee River Sand

Sand Placement

The sand was placed in 6-in. thick lifts. The lifts were compacted with a Wacker Corporation vibratory plate compactor with a plate size of approximately 18-in. square. This size compactor enabled the operator to carefully maneuver it around each of the test pile sections so that the sand could be more uniformly compacted. This was especially important since the nature of the pile-sand interface influences the attenuation of the flexural waves. The lifts were compacted to greater than 95 percent of the maximum dry density of the sand. Density control tests were performed with a nuclear moisture-density gauge.

Test Configuration and Equipment

The test configuration and equipment were similar to those used for testing the fixed-free pile. Figure 4.14 shows the numbering scheme used to perform frequency response measurements. The source and receiver were placed at one of nine positions along the length of the pile. Tests were performed in both the X-X and Y-Y directions. As in the case of the fixed-free piles, a matrix of frequency response measurements was developed to organize the measurements.

Test Results

Figure 4.15 shows a typical frequency response measurement for an embedded pile. The measurement was performed in the Y-Y direction on Pile A with both the source and receiver at position 1. Like tests performed on the fixed-free piles, the frequency response is characterized by several peaks corresponding to different modes of vibration of the pile. At higher frequencies, the peaks are more rounded as a result of higher damping attributed to the surrounding soil. To excite and measure as many modes as possible, the frequency response measurements were repeated at 45 different combinations of source and receiver positions. Figure 4.16 shows the results of these measurements using the waterfall format introduced previously.

Similar sets of measurements were obtained on the other 9 small-scale piles. An example of the difference in frequency response measurements from the 10 small-scale piles is shown in Fig. 4.17. The figure contains the frequency response measurement in the Y-Y direction with the source and receiver at position 1 for all 10 piles. Qualitatively, the response of Piles A through F appears similar. The primary difference between these piles is the embedded length. Pile A has the least embedment (1 ft) and Piles E and F have the largest embedment (5 ft). Pile F also simulates an "end bearing" pile whereas Pile E is "floating." The frequencies at which the peak responses occur are similar (but not identical). Another difference is in the width of the peaks; the peaks appear to broaden as pile embedment increases. This is expected since greater embedment will result in additional damping of each mode of vibration. Piles G and H are encased. The casing clearly influences the frequency response. It is not known why the response of Pile H differs substantially from that of Pile G. Pile I and J differ in cross section (W4 x 13) compared to the other 8 piles (S3 x 5.7). Pile I is embedded 2 ft and Pile J is embedded 4 ft. Both frequency responses are qualitatively similar. It is important to note that comparisons involving other source and receiver locations or the X-X direction may yield different information than that drawn from Figure 4.17.

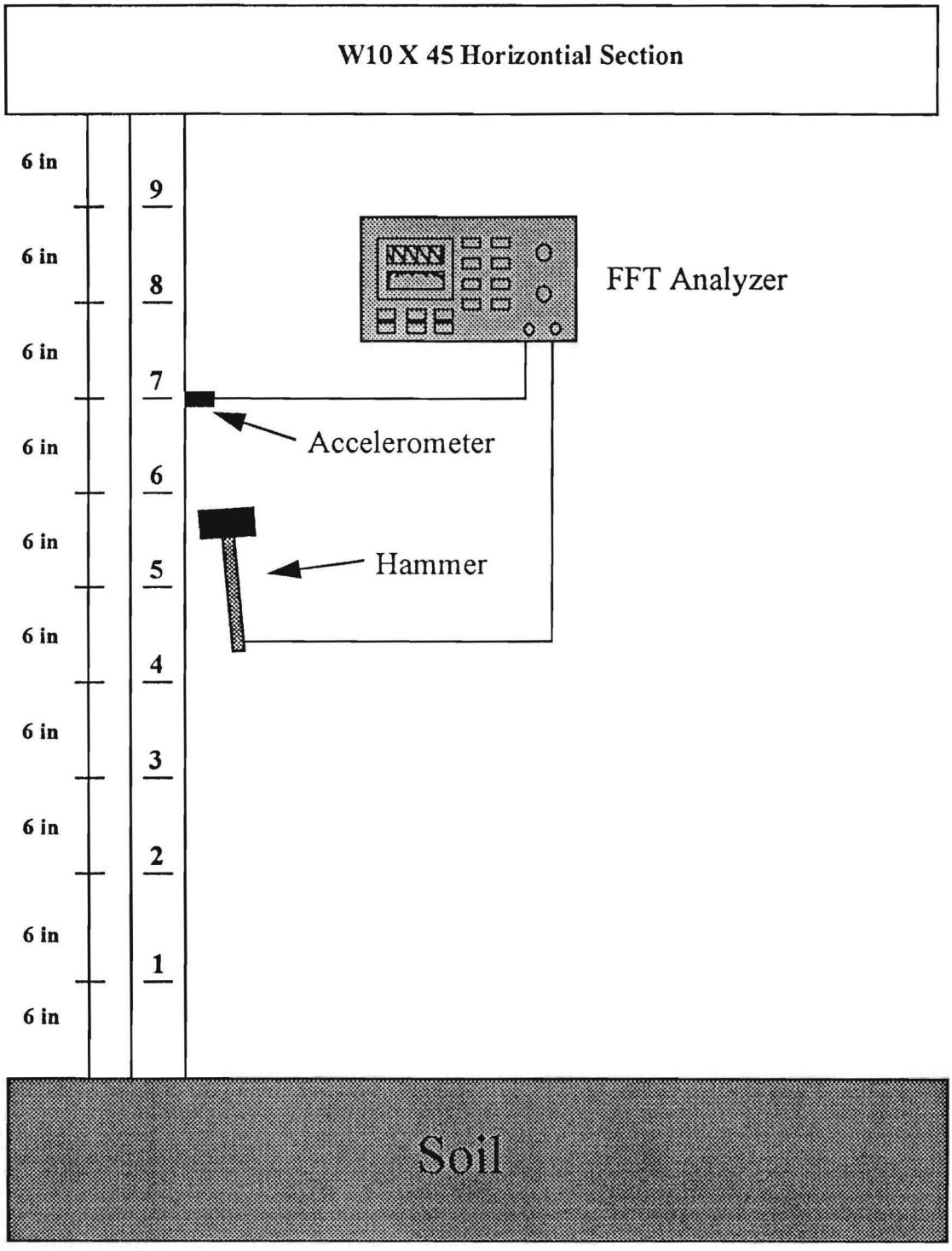

Figure 4.14 Test Configuration Used for Embedded Piles

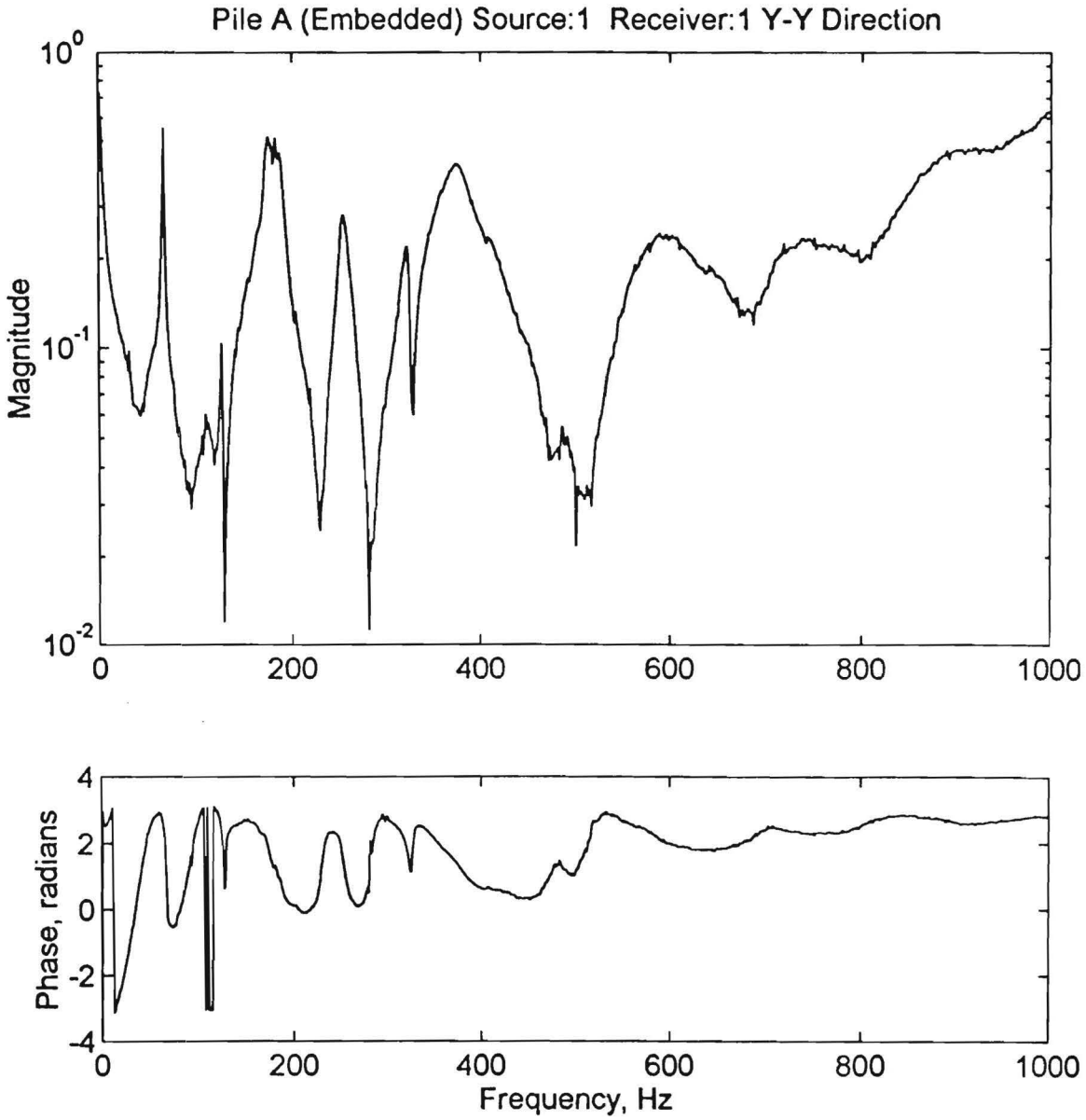

Figure 4.15 Frequency Response Function (R_{11}) for Pile A with Embedded End Condition

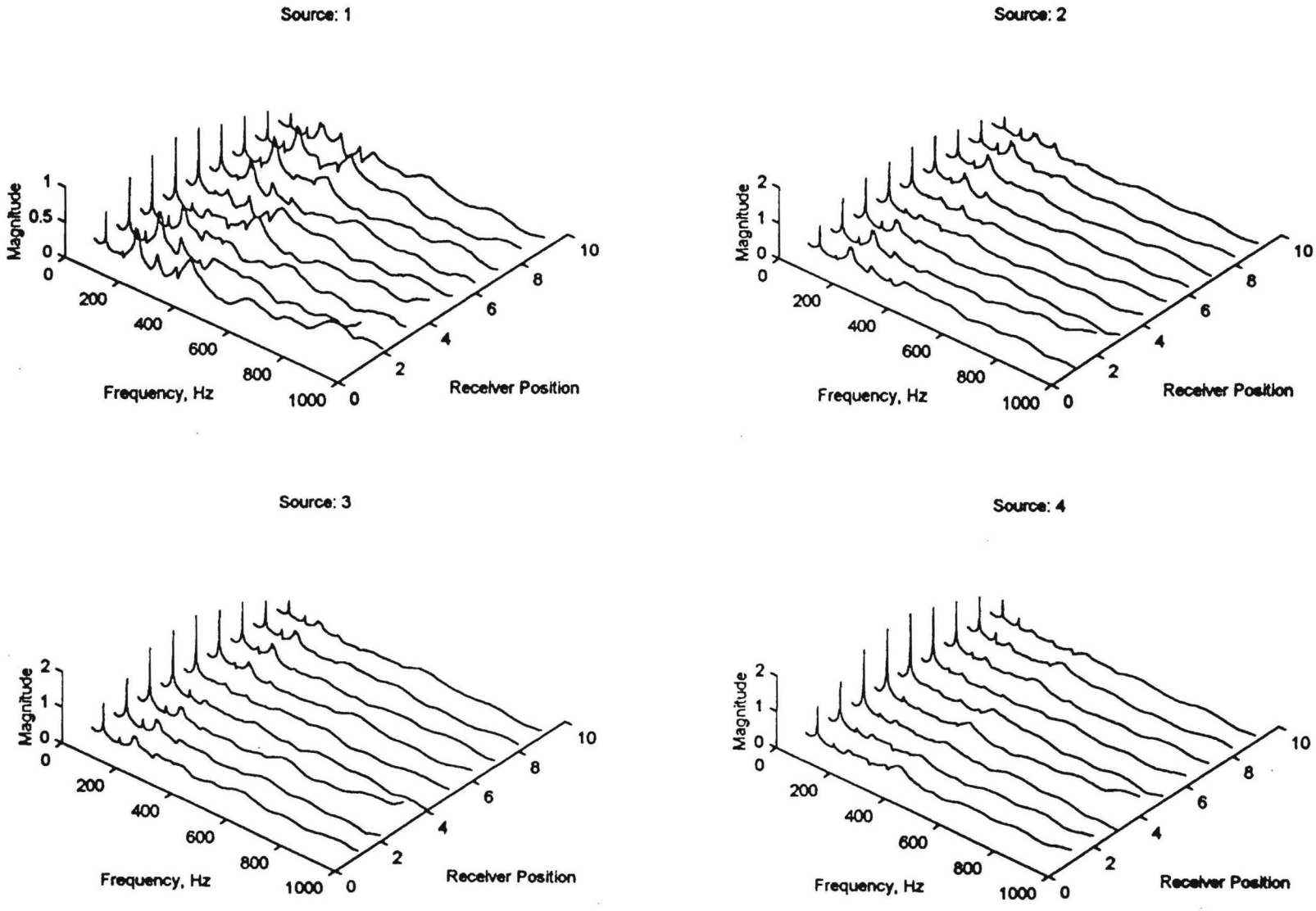

Figure 4.16 Waterfall Plots for Pile A with Embedded End Condition

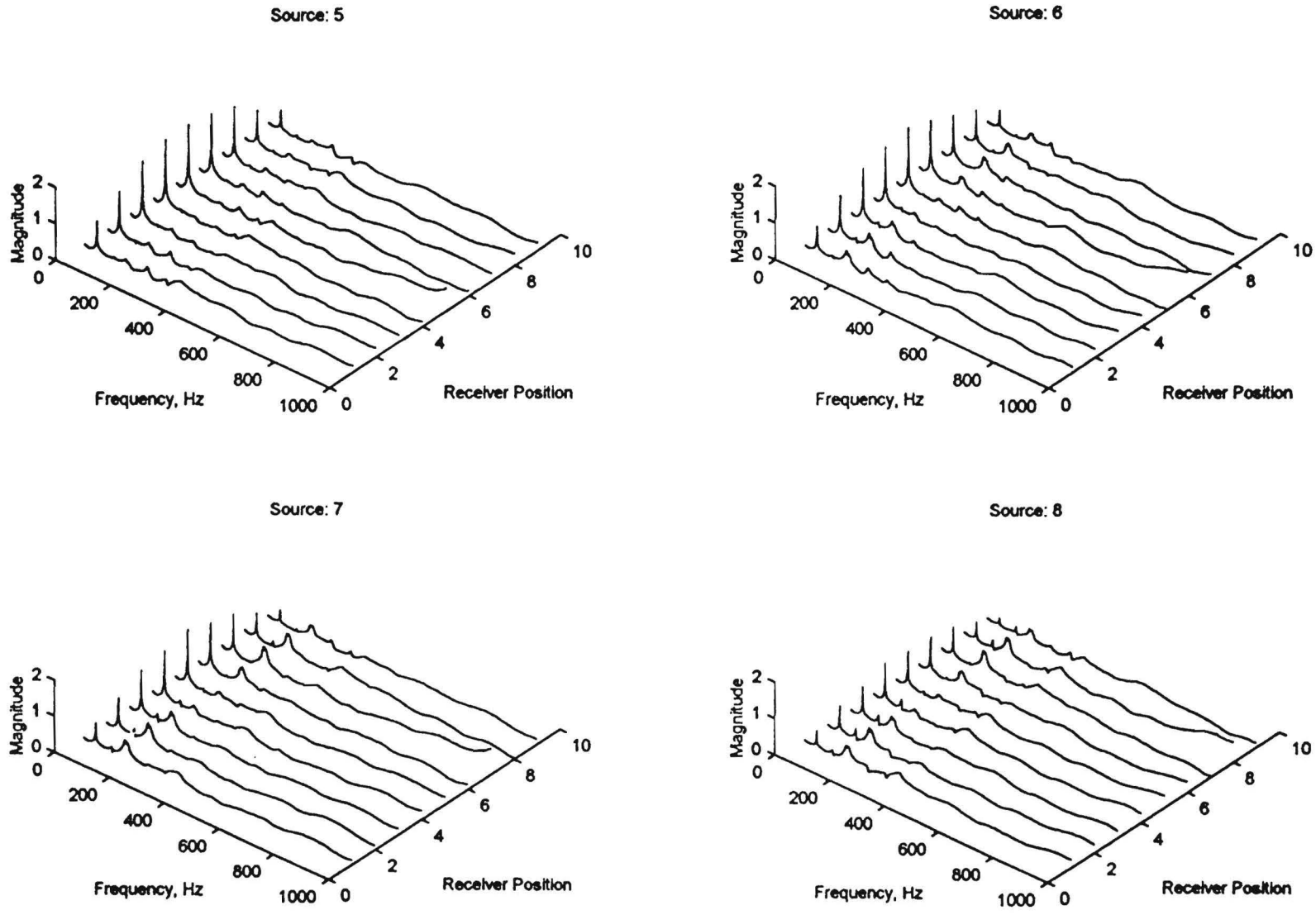

Figure 4.16 Waterfall Plots for Pile A with Embedded End Condition (continued)

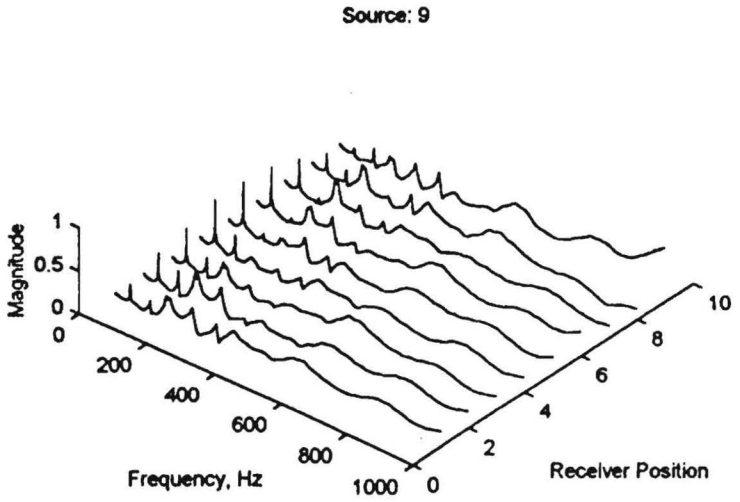

Figure 4.16 Waterfall Plots for Pile A with Embedded End Condition (continued)

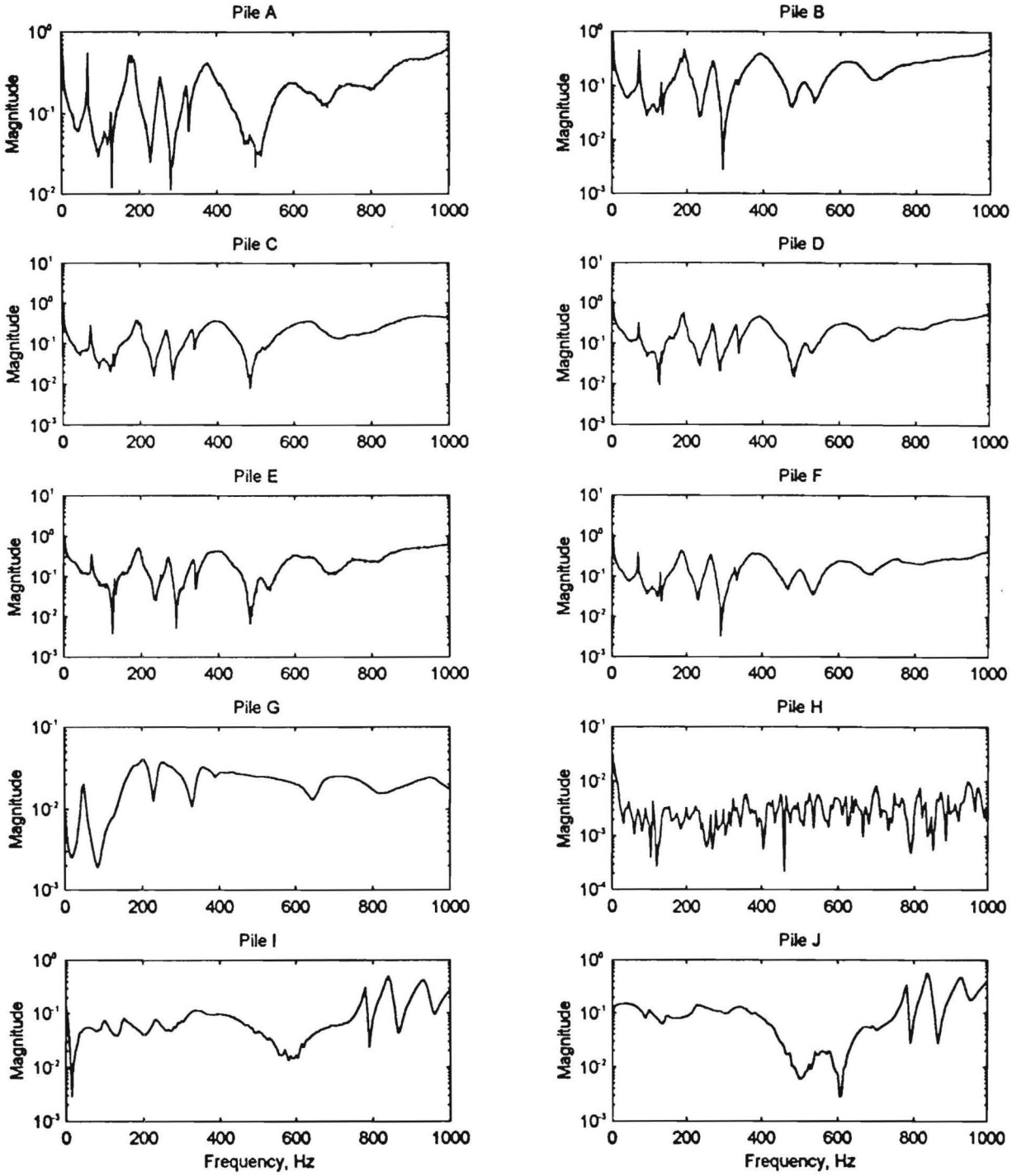

Figure 4.17 Comparison of Frequency Response Functions for Embedded Piles

Comparison of Experimental and Numerical Results on Embedded Piles

Finite element analyses were performed to model the response of embedded piles. The soil reactions in the finite element model are modeled through the use of Winkler springs (Novak et al., 1978). Figures 4.18 and 4.19 show several examples of the comparison between experimental and numerical frequency response functions. Three arbitrarily selected source-receiver combinations are presented for Pile A (Figure 4.18) and Pile E (Figure 4.19). Both figures are for measurements in the Y-Y direction. To facilitate comparison between the experimental and numerical data, the magnitude of each frequency response function was normalized to a maximum value of one. This normalization is necessary because of the different units used for the experimental (volts/volt) and numerical (in^2/sec/lb.) frequency response functions.

At frequencies less than approximately 300 to 400 Hz, the numerical frequency response functions match the predominant peaks in the experimental frequency response functions reasonably well. Many of the peaks which are present in the experimental data but not in the numerical data can be attributed to spurious modes of vibration resulting from longitudinal and torsional motion as discussed previously. In the finite element analyses, the piles were modeled as prismatic members with the same area moments of inertia as the corresponding S or W section. Thus, the finite element analyses are not able to model these other modes of vibration that occur in the actual pile. At frequencies greater than 300 to 400 Hz, the experimental frequency response functions yield larger magnitudes than the numerical frequency response functions.

Sensitivity Study

To aid in understanding limitations in using pile frequency response functions as the basis for assessing pile embedment, a numerical sensitivity study was performed. The study examined the influence of embedment on the first three natural frequencies corresponding to flexural vibrations in the Y-Y direction. A prismatic pile with properties equivalent to the S3 x 5.7 piles was used in the finite element analyses. The results are shown in Figure 4.20. The results indicate that the frequencies of vibration are sensitive to the embedment depth for embedments less than approximately 30 in. For the S3 x 5.7 section, this depth is approximately 10 times the section depth (3.0 in.). These results provide an indication of the maximum embedment depth that can be detected using a frequency response function approach. For an HP12 x 53 pile which is commonly found on full-scale bridges, this limitation implies that the maximum depth of embedment that is able to be resolved is approximately 10 ft. Yu and Roesset (1995) found that the maximum observable embedment depth for concrete piles was approximately 15 ft using a similar frequency domain analysis. The limitation is likely more severe for steel H sections because of the greater attenuation of energy resulting from the larger surface area of an H section.

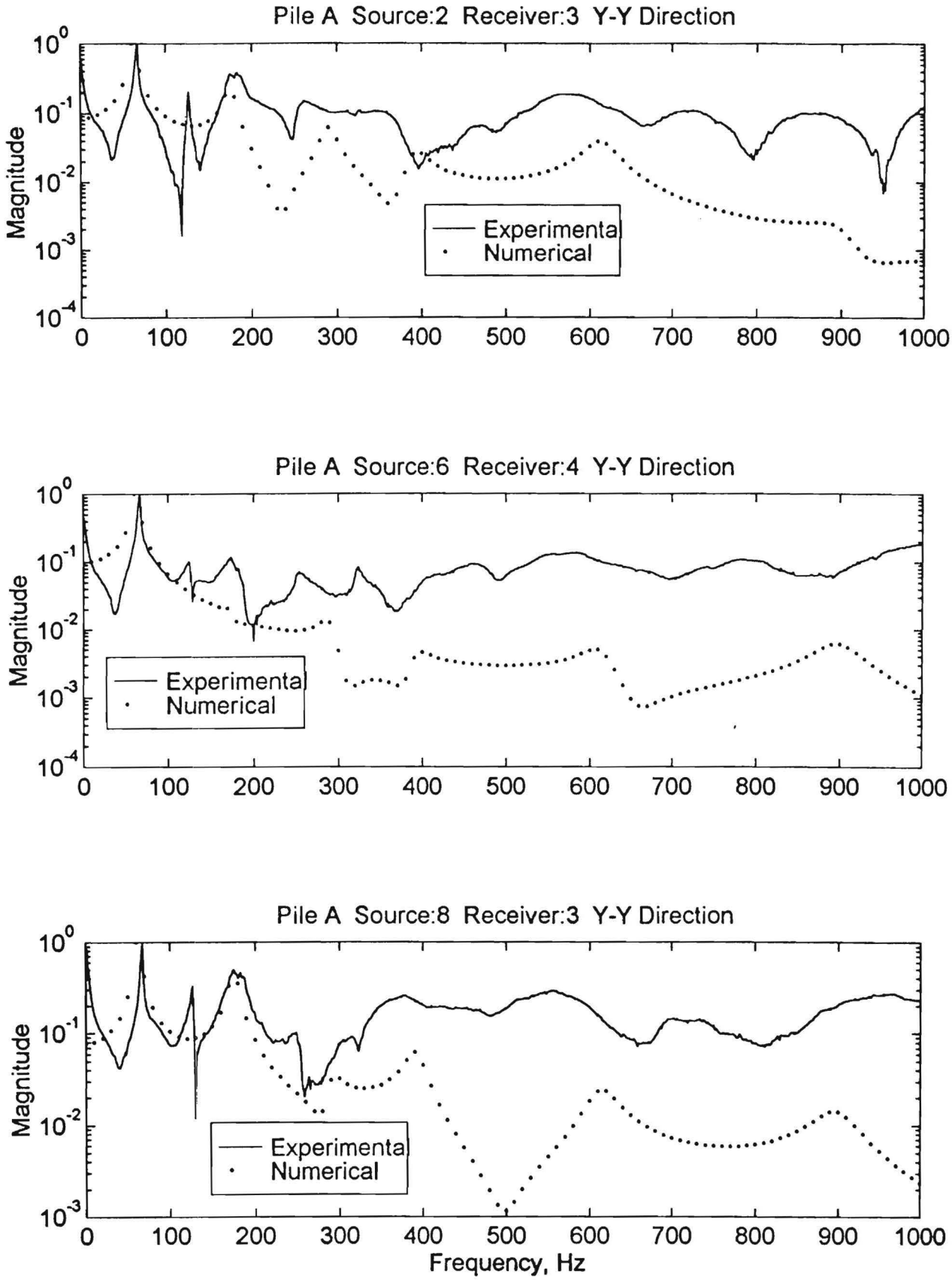

Figure 4.18 Comparison of Experimental and Numerical Frequency Response Functions for Pile A

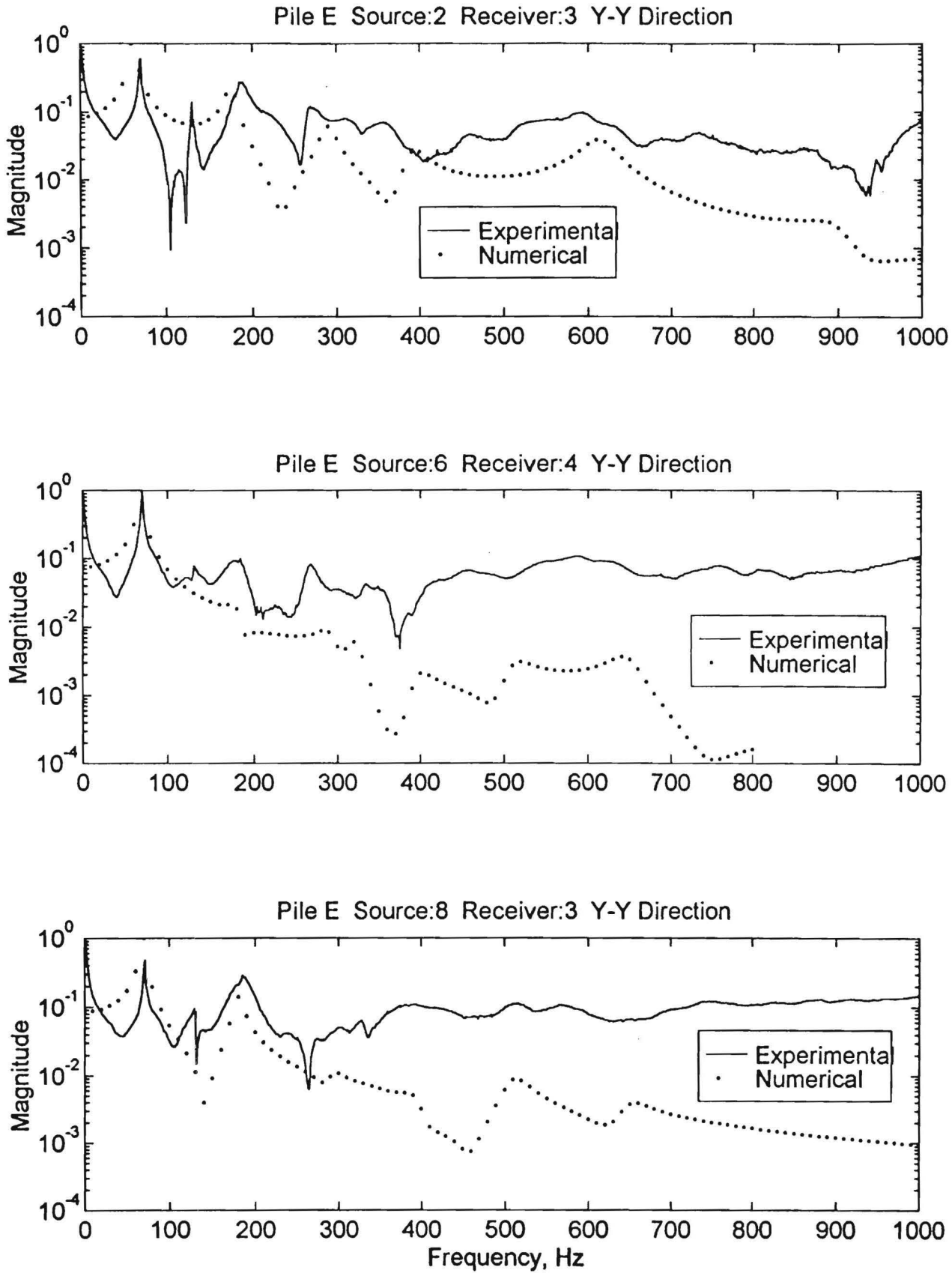

Figure 4.19 Comparison of Experimental and Numerical Frequency Response Functions for Pile E

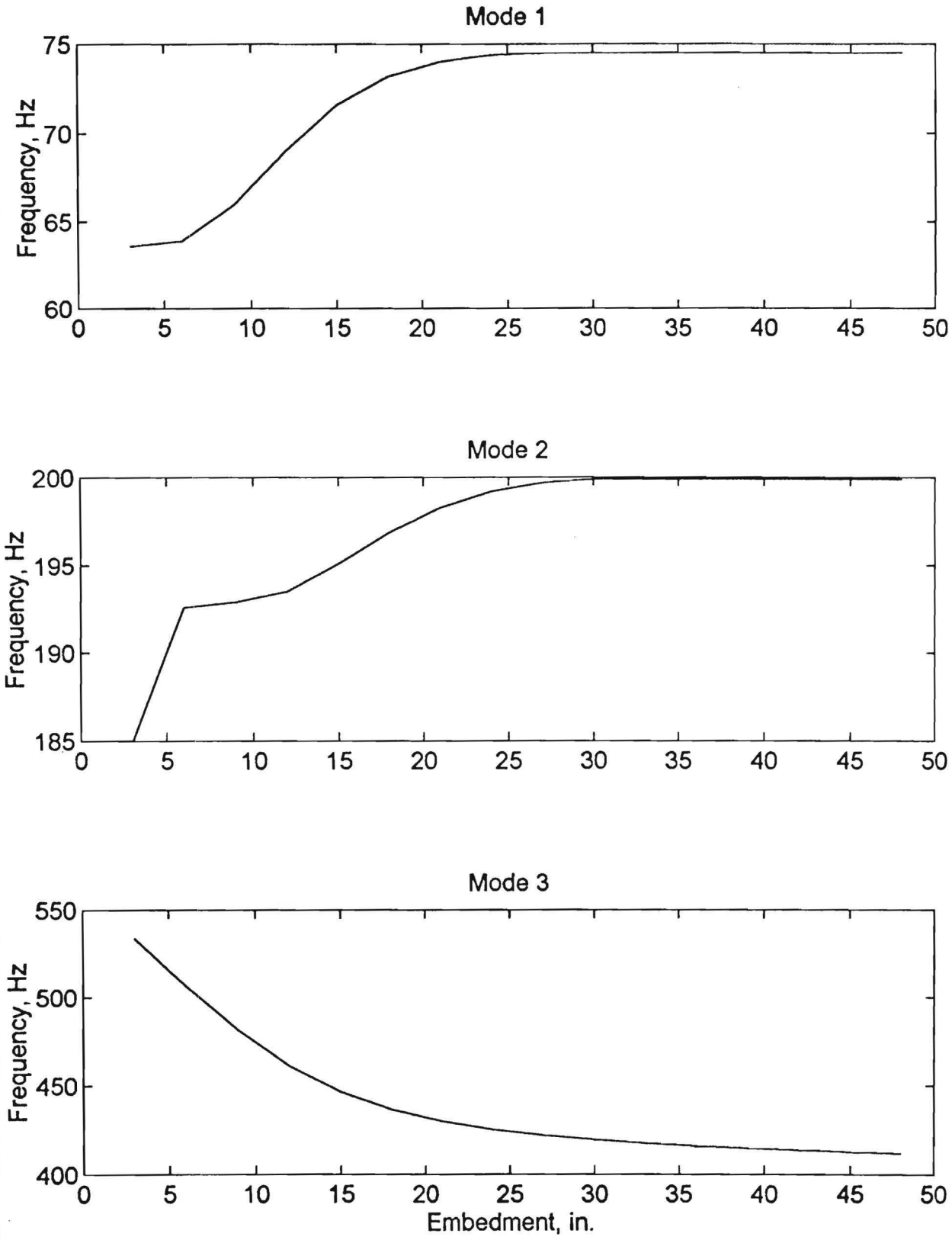

Figure 4.20 Influence of Embedment Depth on Natural Frequencies of Vibration

5 Tests on Full-Scale Piles

Following the tests on the small-scale piles, a full-scale bridge was selected to perform additional nondestructive flexural wave tests. The purpose of the full-scale test was to evaluate the test method under more realistic field conditions.

Bridge Site

The bridge site is located on Merck Road over Camp Creek in southwest Fulton County, Georgia. As-built plans and pile tip elevations of the bridge were provided by the Georgia Department of Transportation. A photograph of the bridge is shown in Figure 5.1.

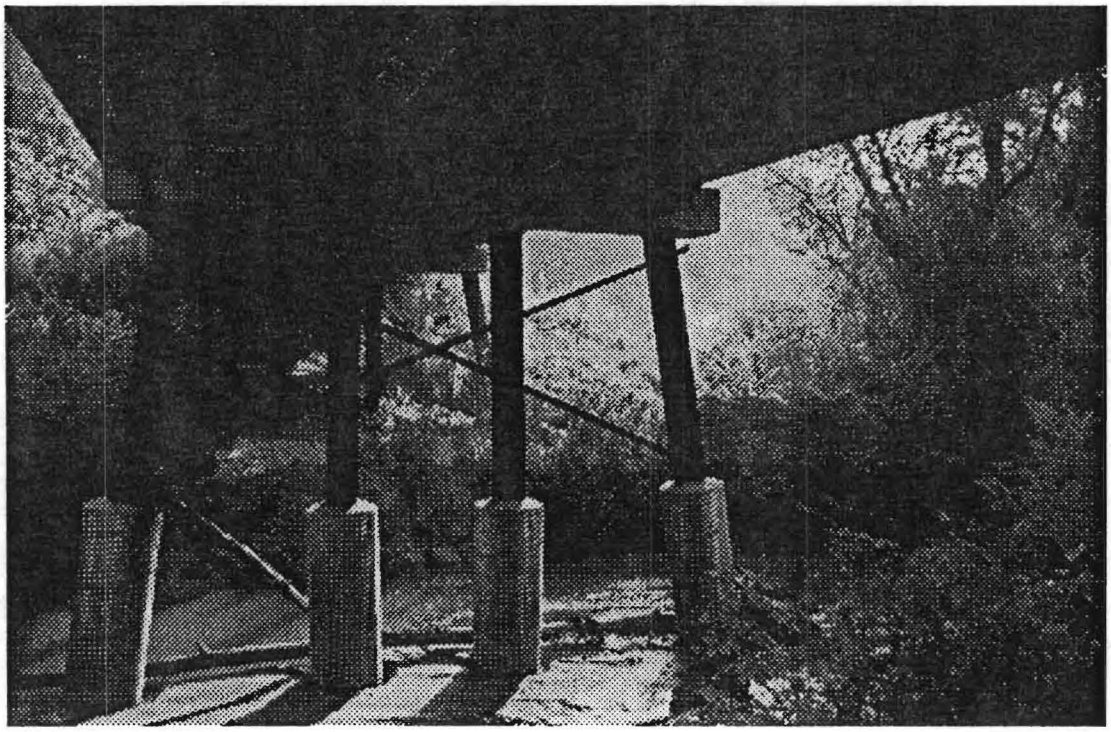

Figure 5.1 Bridge at Merck Road over Camp Creek

The bridge runs in a north-south direction and is supported by 6 bents with 4 piles per bent. The abutment bent piles are HP 10 x 57 sections and the intermediate bent piles are HP 14 x 73 sections. The bents are designated by numbers form 1 to 6 with Bent 1 starting numerically at the south abutment to Bent

6 at the north abutment. The bent piles are numbered from 1 to 4 from left to right as viewed by an observer facing north. Bent 4 is located in the channel of Camp Creek and the piles are encased in concrete (Bent 4 is shown in Figure 5.1). The concrete casements are made of 3-ft diameter corrugated steel pipe placed around the pile and filled with concrete. Bent 4 also had cross or sway bracing that connects the four piles to each other.

Test Setup

Field tests were performed on Pile 2 of both Bents 3 and 4. Bent 3 is on the bank of Camp Creek, and thus was not surrounded by water. Although Bent 4 was in the stream channel, there was such low flow on the day that testing was performed that the water level did not interfere with the tests.

The test configurations for the pile are shown in Figures 5.2 and 5.3. A photograph of the test equipment is shown in Figure 5.4. The pile response was measured with a Wilcoxon Research Model 728T piezoelectric accelerometer. The Model 728T is more sensitive than the Model 732A used in the scale model testing, and thus was able to record the smaller amplitude vibrations more reliably. This accelerometer has a traceable frequency response range of 1 Hz to 12 kHz. The calibration voltage sensitivity for this accelerometer is 517 mV/g. The accelerometer was attached to the pile using the same magnetic mounting base as described in Chapter 4. The hammer (source) used for the field testing was a PCB Piezotronics, Inc. Model GK291B50 modally tuned hammer with a built-in force transducer. The hammer is approximately the size of a large sledge hammer and weighs 12 lb. It has a force range of 0 to 5000 lb. This hammer has a calibrated sensitivity of 1 mV/lbf. The larger hammer also has 3 tips that can be attached to the built-in force transducer. The hard tip (#084A33) was used for all of the field measurements to excite higher natural frequencies. The field measurements were recorded by a Hewlett Packard Model 3560A Dynamic Signal Analyzer. The HP Model 3560A was used, instead of the HP Model 3562A, since it is battery operated and is much more portable than the HP Model 3562A. The HP 3560A was set up exactly as the HP 3562A was for the scale model testing as described in Chapter 4. The HP 3560A has built-in storage to which the measurements could be saved and transferred later to a personal computer.

Test Method

The test method used for the field testing was similar to that of the scale model tests. The positions of the source and receiver were varied on each pile depending on the length of exposed pile. Figure 5.2 shows that Pile 2 on Bent 3 had 10 ft of exposed pile length between the pile cap and the ground line. The source and receiver locations were placed at 1 ft increments and were labeled from 1 at the top to 10 near the ground line. Figure 5.3 shows the measurement locations for Pile 2 on Bent 4. The test measurements were performed up to 6 ft above the pile casement. The test were performed by standing on the pile casement and inducing the flexural waves into the steel pile. The tests were performed only up to 6 ft since accessibility was limited without a longer ladder or a truck with boom attachment.

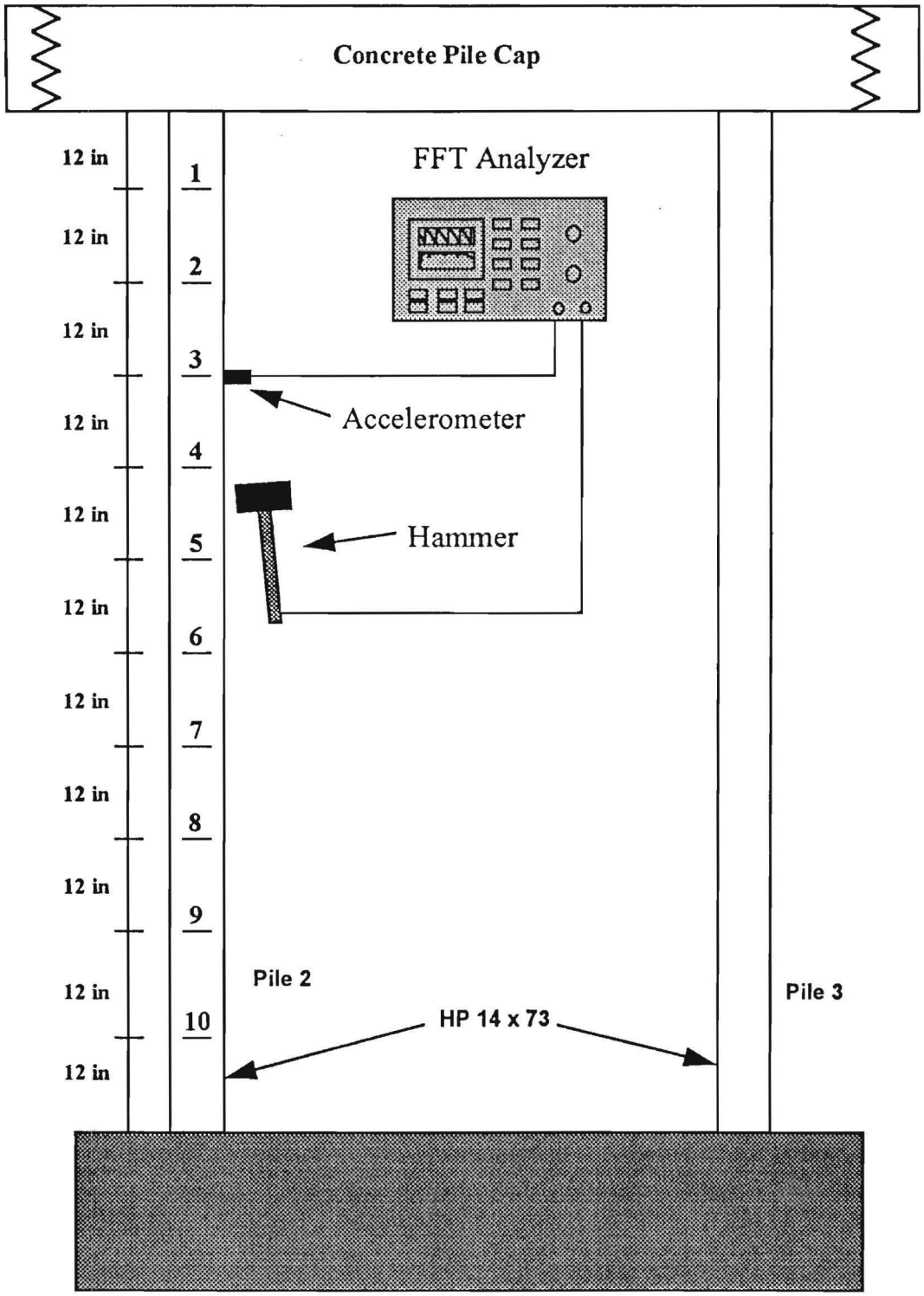

Figure 5.2 Field Test Configuration for Bent 3 - Pile 2

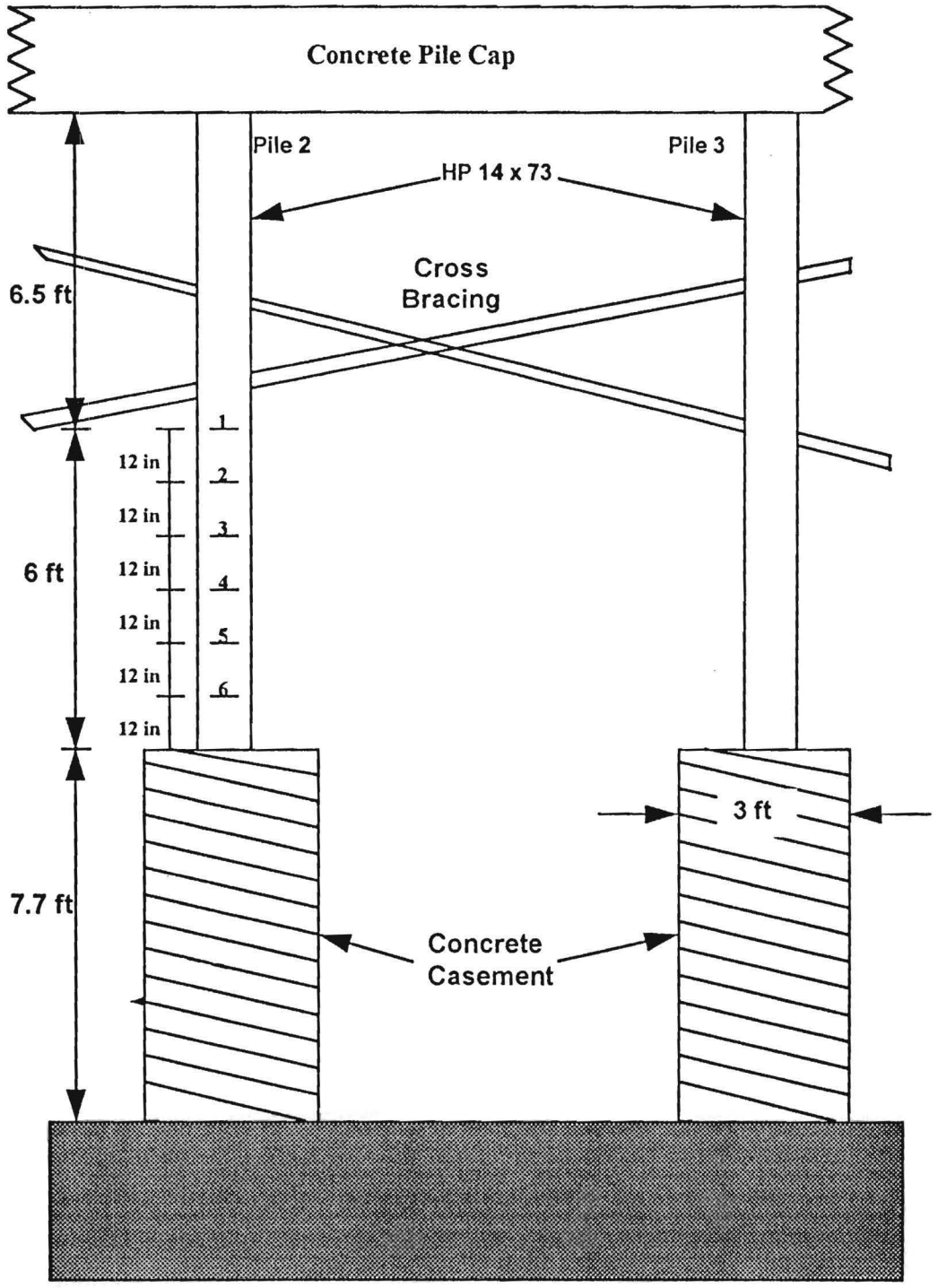

Figure 5.3 Field Test Configuration for Bent 4 - Pile 2

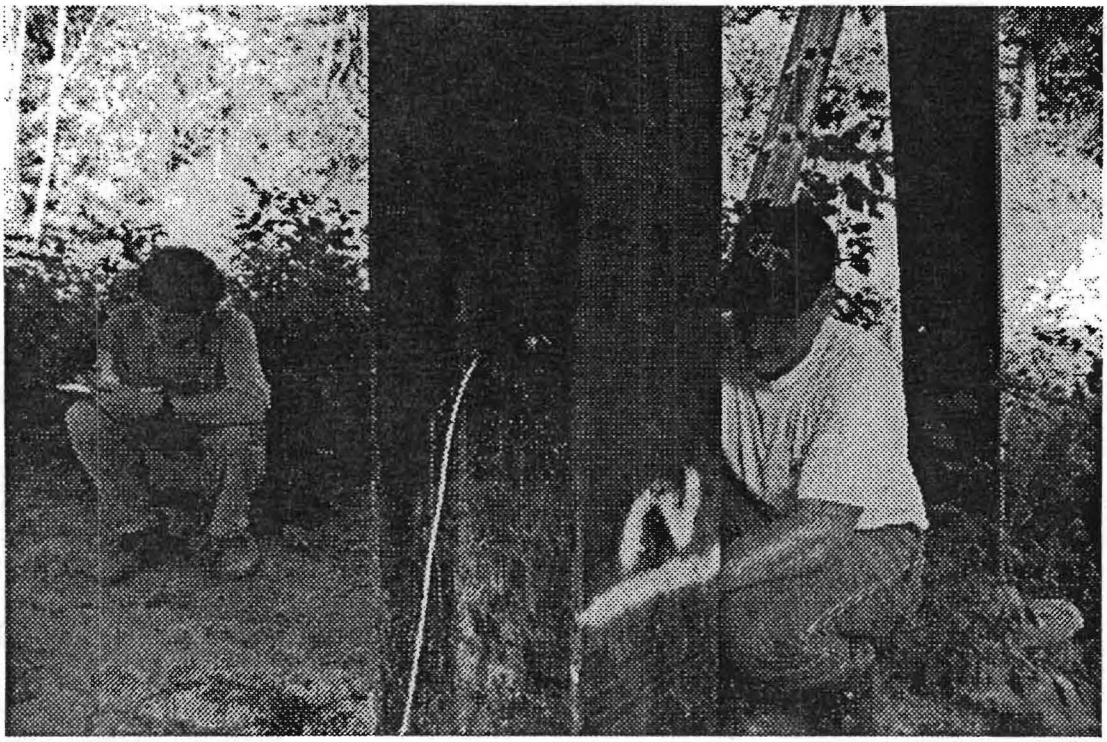

Figure 5.4 Photograph of Field Test

Pile 2 on Bent 3 was tested in both the X-X and the Y-Y directions . A limited number of source-receiver combinations were tested in each direction. In the Y-Y direction, the source and receiver were varied at the even number positions. In the X-X direction, the source was placed at the even positions and the receiver was placed at positions 8, 5 and 3. Pile 2 on Bent 4 was tested only in the Y-Y direction with the source placed at the 6 locations shown in Figure 5.3 The response of the pile was measured only at the even numbered positions. For each source-receiver combination, the frequency response function was measured using five averages.

Test Results

Figure 5.5 shows the frequency response function measured with the source at position 6 and the receiver at position 10 in the Y-Y direction on Pile 2 on Bent 3. This frequency response function is typical of those measured in the Y-Y direction on the non-cased bridge piles. The response is similar to the frequency response function measured on the non-cased small-scale pile in the laboratory; the plot is characterized by several broad peaks that reflect the high attenuation resulting from the soil surrounding the pile. Figure 5.6 shows a waterfall plot of the frequency response functions measured on Bent 3 - Pile 2. Figure 5.7 shows a typical frequency response function measured on the encased pile (Bent 4 - Pile 2).

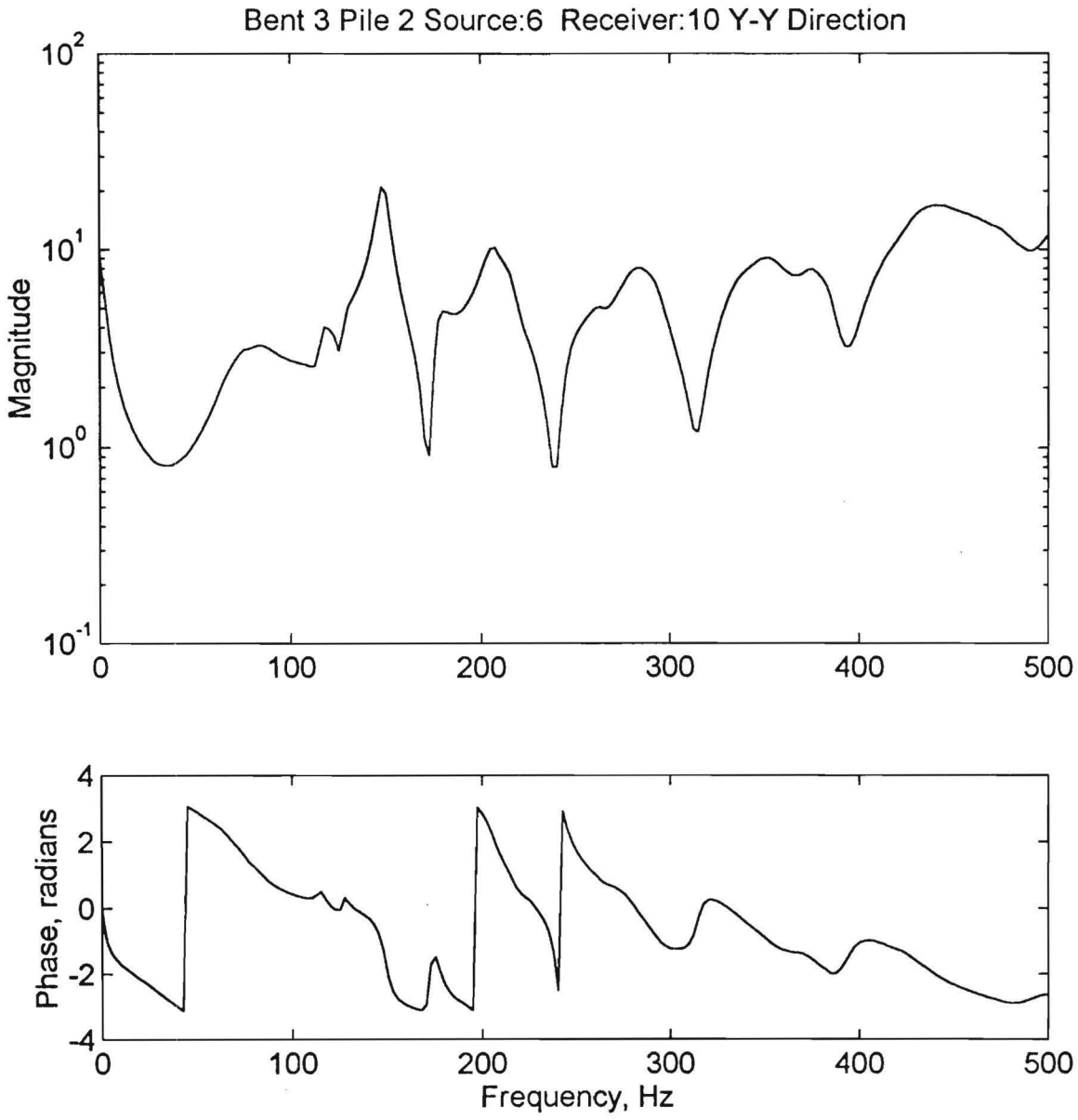

Figure 5.5 Typical Frequency Response Function for Bent 3 - Pile 2

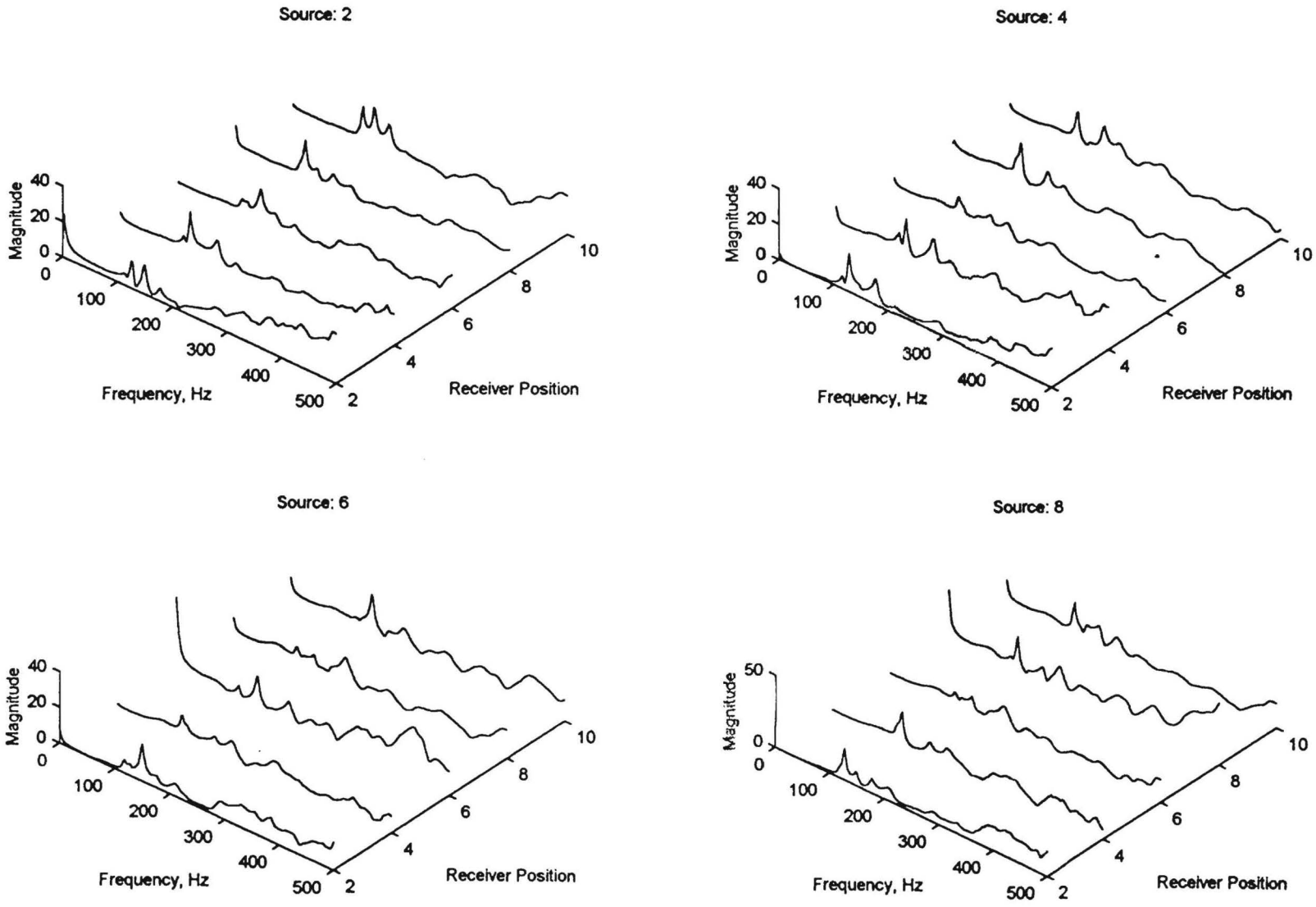

Figure 5.6 Waterfall Plots for Bent 3 - Pile 2

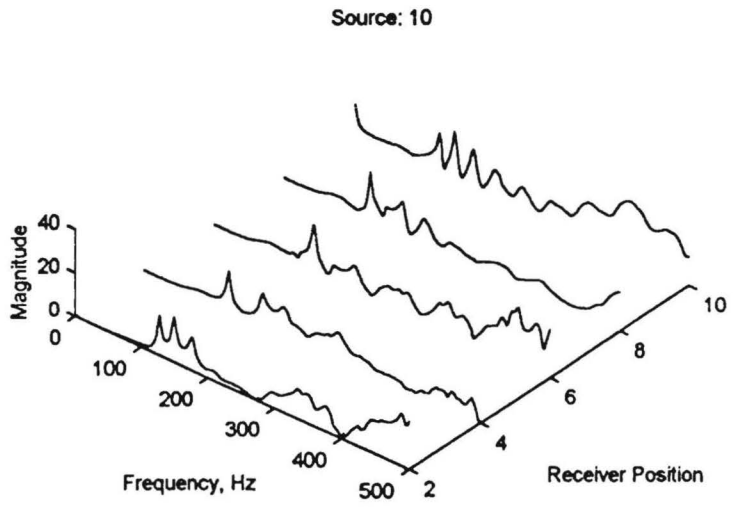

Figure 5.6 Waterfall Plots for Bent 3 - Pile 2 (continued)

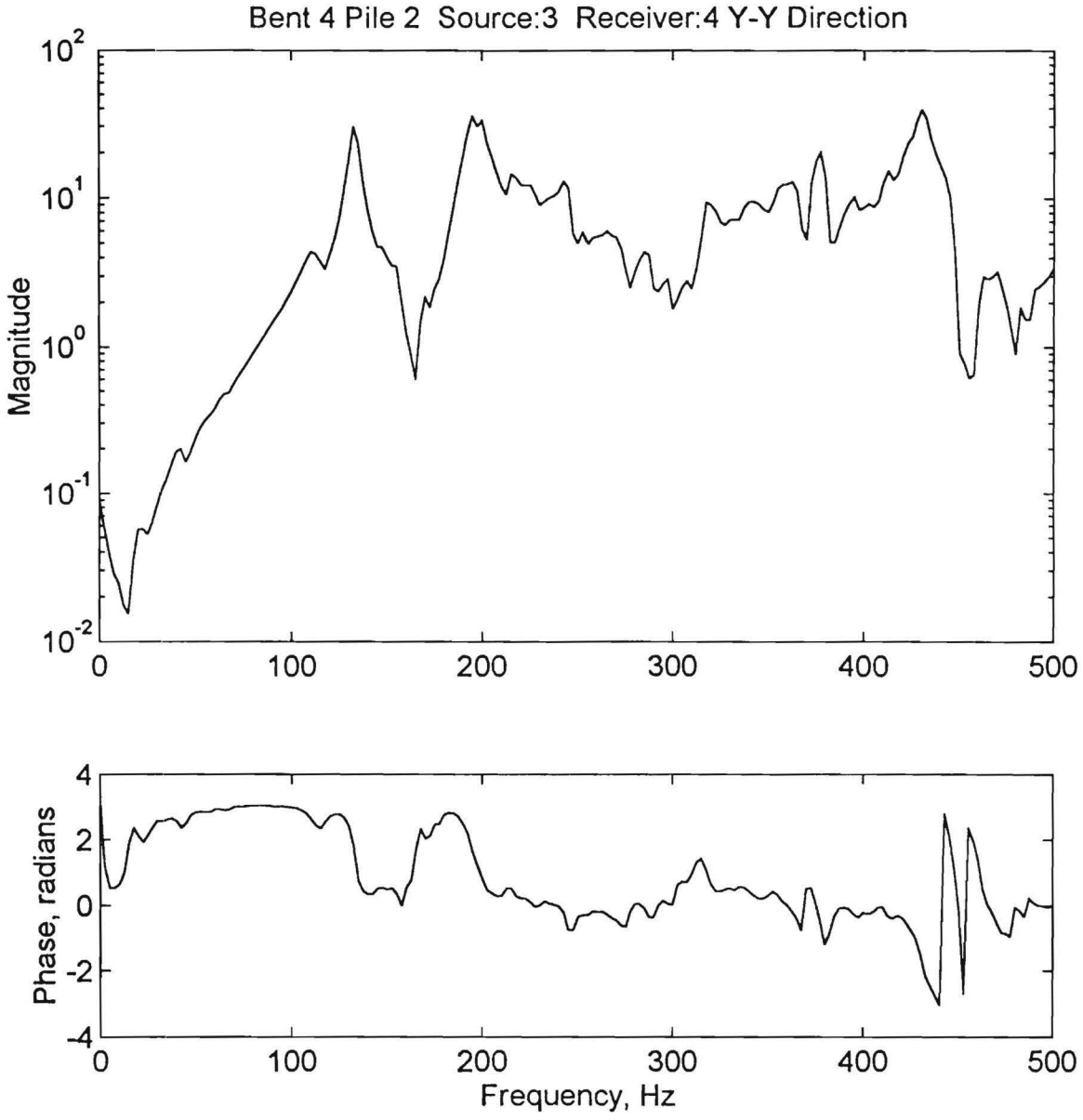

Figure 5.7 Typical Frequency Response Function for Bent 4 - Pile 2

6 Summary

Nondestructive tests on foundations were initially developed to provide a quality control test for cast-in-place deep foundations. In recent years, these nondestructive tests have been adapted to address the "unknown foundation" problem. Many of these tests rely on longitudinal waves that are difficult to generate if the bridge superstructure interferes with access to the top of the pile. The purpose of this study was to evaluate the use of flexural waves to determine pile tip elevations of unknown foundations. The basis of the approach taken in this study is the measurement of a large number of frequency response functions at various source and receiver positions along the exposed length of the pile. The natural frequencies and mode shapes obtained from the frequency response functions are functions of the embedded length of the pile. As such, the natural frequencies and mode shapes can be used to backcalculate the embedded length.

This study consisted of an experimental study on 10 small-scale piles, numerical calculations of pile response using the finite element method, and a trial test on a full-scale bridge. The 10 small-scale piles were selected so as to study the influence of embedment depth, tip condition (i.e., floating vs. end bearing), presence of concrete casing, and section geometry on the frequency response of the pile. Initially, tests on the small-scale piles were performed without any soil embedment. The purpose of these tests was to obtain experimental data which could be used to "calibrate" the finite element model of the pile. By adjusting the boundary condition at the upper end of the pile from a fixed boundary to one with two pinned connections, the experimental and numerical natural frequencies were made to match. These tests provided confidence in the ability to model the piles numerically.

Following this initial series of tests, the piles were embedded by placing and compacting sand around the piles. Nine different source and receiver positions were chosen on each of the 10 small-scale piles. Frequency response measurements were made using 45 different combinations of source and receiver positions to excite and record as many modes of propagation as possible within the pile. These measurements provide a comprehensive set of experimental frequency response data from which to develop an interpretive procedure to determine pile embedment depth.

The embedded piles were also modeled numerically using the finite element program I-DEAS. Comparisons between the experimental and numerical frequency response functions yielded satisfactory matches at frequencies less than approximately 300 to 400 Hz. The experimental data contained additional natural frequencies corresponding to spurious modes of vibration involving longitudinal and torsional motion. These modes were not contained in the numerical analyses because the pile was modeled numerically as a prismatic member (i.e. the actual S or W section shape was not modeled). The satisfactory match between experimental and numerical frequency response functions at lower frequencies provides a basis for iteratively matching experimental and numerical frequency response functions to determine the embedment depth.

Finite element analyses were also used in a parametric study of embedment depth. It was determined that the natural frequencies of the first three modes of vibration are sensitive to the embedment depth for embedment depths less than approximately 10 times the section depth. Similar results have been found in other studies (Yu and Roesset, 1995). The reason for this limitation is the attenuation of energy by the surrounding soil. For steel H sections, the limitation is more severe because of the large surface area available to dissipate energy.

A trial test was conducted on full-scale piles to evaluate the practical application of the approach. Two concerns that arose from the full-scale test are problems related to access to portions of the pile well above the ground line and short exposed lengths limiting the number of source and receiver positions that are available for use in making frequency response measurements.

7 References

Davis, A.G. and Dunn, C.S. (1974). "From Theory to Field Experience with the Nondestructive Vibration Testing of Piles." *Proceedings*, Institution of Civil Engineers, Part 2, 57, 571-593.

Douglas, R.A., and Holt, J.D. (1993). "Determining Length of Install Timber Pilings by Dispersive Wave Propagation Methods." Center for Transportation Engineering Studies, North Carolina State University, June.

Fung, Y.C. (1964). *Foundations of Solid Mechanics*. Prentice-Hall, Englewood Cliffs, New Jersey, 525 pp.

Holt, J.D., and Douglas, R.A. (1994). "A Field Test Procedure for Finding the Overall Lengths of Installed Timber Piles by Dispersive Wave Propagation Methods." Technical Report No. NC/R&D/94-001, ITRE, North Carolina State University, March.

Malhotra, V.M., (1976), "Testing Hardened Concrete: Non-Destructive Methods," American Concrete Institute, Detroit, Michigan, Iowa State University Press, Ames, 87 pp.

Novak, M., Nogami, T., and Aboul-Ella, F. (1978). "Dynamic Soil Reactions for Plane Strain Case." *Journal of the Engineering Mechanics Division*, ASCE, Vol. 104, No. EM4, August, pp. 953-959.

O'Neill, M. W., (1992), "Construction Practices and Defects in Drilled Shafts," *Integrity Testing of Foundations 1991*, Transportation Research Record 1331, Transportation Research Board, Washington, DC, pp. 6-14.

Olson, L.D. and Wright, C.C. (1989). "Nondestructive Testing of Deep Foundations with Sonic Methods." *Foundation Engineering: Current Principles and Practices*. ASCE, Vol. 2, pp. 1173-1183.

Olson, L.D., Jalinoos, F., and Aouad, M.F. (1995). "Determination of Unknown Subsurface Bridge Foundations." Draft Final Report, NCHRP Project E 21-5, National Cooperative Highway Research Program, Transportation Research Board, National Research Council, Washington, D.C., April, 264 pp.

Paquet, J. (1968). "Étude Vibratoire Des Pieux En Béton Résponse Harmonique Et Impulsionelle: Application Au Controle (in French). *Annalles de l'Institut Technique du Batiment et des Travaux Publics*, No. 245, May, pp. 788-803.

Rix, G.J., Jacobs, L.J., and Reichert, C.D. (1993). "Evaluation of Nondestructive Test Methods for Length, Diameter, and Stiffness Measurements on Drilled Shafts." *Field Performance of Structures and Nondestructive Evaluation of Subsurface Infrastructure*. Transportation Research Record No. 1415, Transportation Research Board, pp. 69-77.

Stain, R.T. (1982). "Integrity Testing." *Civil Engineering*. April, 54-59.

School of Civil and Environmental Engineering

Nondestructive Assessment of Pile Tip Elevations Using Flexural Waves

Glenn J. Rix, Ph.D.

Laurence J. Jacobs, Ph.D.

Patrick B. Rhodes

Raymond Q. Raparelli

Georgia Department of Transportation Project No. 9406

December 1995

Report No. GIT-CEE/GEO-95-5

Georgia Institute of Technology
Georgia Institute of Technology
Georgia Institute of Technology
Georgia Institute of Technology
Georgia Institute of Technology
Georgia Institute of Technology
Georgia Institute of Technology
Georgia Institute of Technology
Georgia Institute of Technology
Georgia Institute of Technology
Georgia Institute of Technology
Georgia Institute of Technology
Georgia Institute of Technology
Georgia Institute of Technology
Georgia Institute of Technology
Georgia Institute of Technology
Georgia Institute of Technology
Georgia Institute of Technology
Georgia Institute of Technology
Georgia Institute of Technology
Georgia Institute of Technology
Georgia Institute of Technology
Georgia Institute of Technology
Georgia Institute of Technology
Georgia Institute of Technology
Georgia Institute of Technology
Georgia Institute of Technology
Georgia Institute of Technology
Georgia Institute of Technology
Georgia Institute of Technology
Georgia Institute of Technology
Georgia Institute of Technology
Georgia Institute of Technology
Georgia Institute of Technology
Georgia Institute of Technology
Georgia Institute of Technology
Georgia Institute of Technology
Georgia Institute of Technology
Georgia Institute of Technology
Georgia Institute of Technology
Georgia Institute of Technology
Georgia Institute of Technology
Georgia Institute of Technology
Georgia Institute of Technology

Table of Contents

TABLE OF CONTENTS i

LIST OF TABLES iii

LIST OF FIGURES iv

1 INTRODUCTION 1

PURPOSE 1
METHOD 1
REPORT ORGANIZATION 2

2 REVIEW OF EXISTING NONDESTRUCTIVE TEST METHODS 3

NDT OVERVIEW 3
SONIC ECHO 3
IMPULSE RESPONSE 4
APPLICATION OF NDT METHODS TO UNKNOWN FOUNDATIONS 6
Flexural Wave Tests 6

3 NUMERICAL MODELING 12

FINITE ELEMENT ANALYSIS 12
ANALYTICAL DERIVATION 14
COMPARISON OF ANALYTICAL AND NUMERICAL RESULTS 17
INFLUENCE OF SOIL EMBEDMENT 20

4 TESTS ON SMALL-SCALE PILES 24

SMALL-SCALE PILE FACILITY 24
Test Pile Sections 27
TESTS ON FIXED-FREE PILES 29
Test Equipment and Configuration 30
Test Method 30
Test Results 33
Comparison of Experimental, Analytical, and Numerical Results on Fixed-Free Piles 41
TESTS ON EMBEDDED PILES 42
Sand Fill 43
Sand Placement 43
Test Configuration and Equipment 44
Test Results 44
Comparison of Experimental and Numerical Results on Embedded Piles 51

5 TESTS ON FULL-SCALE PILES **54**

BRIDGE SITE 54
TEST SETUP 55
TEST METHOD 55
TEST RESULTS 58

6 MODAL ANALYSIS **63**

GRAPHICAL TOOLS 63
DERIVATION OF MATHEMATICAL MODEL 66

7 SUMMARY **67**

8 REFERENCES **69**

List of Tables

TABLE 3.1 COMPARISON OF ANALYTICAL AND NUMERICAL RESULTS 20

TABLE 4.1 COMPARISON OF EXPERIMENTAL, ANALYTICAL, AND NUMERICAL RESULTS ON FIXED-FREE PILES WITH FIXED END CONDITION 41

TABLE 4.2 COMPARISON OF EXPERIMENTAL, ANALYTICAL, AND NUMERICAL RESULTS ON FIXED-FREE PILES WITH PINNED END CONDITION 42

List of Figures

FIGURE 2.1 TEST CONFIGURATION USED FOR NONDESTRUCTIVE TESTS 4

FIGURE 2.2 ACCELERATION TIME HISTORY OBSERVED AT THE TOP OF DRILLED SHAFT 5

FIGURE 2.3 MOBILITY FREQUENCY RESPONSE FUNCTION 5

FIGURE 2.4 PARALLEL SEISMIC METHOD 7

FIGURE 2.5 TEST CONFIGURATION FOR FLEXURAL WAVE TEST DEVELOPED BY DOUGLAS AND HOLT (1993) 8

FIGURE 2.6 DETERMINATION OF BENDING WAVE VELOCITY USING SHORT KERNEL METHOD 9

FIGURE 2.7 DETERMINATION OF PILE LENGTH USING SHORT KERNEL METHOD 10

FIGURE 3.1 ELASTIC SPRING 12

FIGURE 3.2 BEAM ELEMENT 15

FIGURE 3.3 SOLVING FOR ROOTS OF THE CHARACTERISTIC EQUATION 17

FIGURE 3.4 ANALYTICAL SOLUTION FOR NATURAL FREQUENCIES OF CANTILEVR S3 X 5.7 18

FIGURE 3.5 FINITE ELEMENT MODEL OF CANTILEVERED BEAM 19

FIGURE 3.6 MATHCAD SOLUTION - VARIABLE BEAM LENGTH ON ELASTIC FOUNDATION 21

FIGURE 3.7 USE OF SPRINGS TO MODEL SOIL RESISTANCE 22

FIGURE 3.8 INFLUENCE OF EMBEDMENT DEPTH ON NATURAL FREQUENCIES OF VIBRATION 23

FIGURE 4.1 EXPERIMENTAL FACILITY FOR TESTING SMALL-SCALE PILES 24

FIGURE 4.2 END VIEW OF EXPERIMENTAL FACILITY FOR TESTING SMALL-SCALE PILES 25

FIGURE 4.3 PLAN VIEW OF EXPERIMENTAL FACILITY FOR TESTING SMALL-SCALE PILES 26

FIGURE 4.4 RIGHT ELEVATION VIEW OF SMALL-SCALE PILE TEST FACILITY 28

FIGURE 4.5 LEFT ELEVATION VIEW OF SMALL-SCALE PILE TEST FACILITY 29

FIGURE 4.6 TEST CONFIGURATION USED FOR TESTING PILE A WITH FREE END CONDITION 31

FIGURE 4.7 DEFINITION OF X-X AND Y-Y DIRECTIONS 32

FIGURE 4.8 FREQUENCY RESPONSE FUNCTION (R_{11}) FOR PILE A WITH FREE END CONDITION 34

FIGURE 4.9 FREQUENCY RESPONSE FUNCTION (R_{23}) FOR PILE A WITH FREE END CONDITION 35

FIGURE 4.10 MODE SHAPES OF A FIXED-FREE PILE 36

FIGURE 4.11 COMPARISON OF FREQUENCY RESPONSE FUNCTIONS FOR PILE A WITH FREE END CONDITION 37

FIGURE 4.12 WATERFALL PLOTS FOR PILE A WITH FREE END CONDITION 38

FIGURE 4.13 GRAIN SIZE DISTRIBUTION FOR CHATTAHOOCHEE RIVER SAND 43

FIGURE 4.14 TEST CONFIGURATION USED FOR EMBEDDED PILES 45

FIGURE 4.15 FREQUENCY RESPONSE FUNCTION (R_{11}) FOR PILE A WITH EMBEDDED END CONDITION 46

FIGURE 4.16 WATERFALL PLOTS FOR PILE A WITH EMBEDDED END CONDITION 47

FIGURE 4.17 COMPARISON OF FREQUENCY RESPONSE FUNCTIONS FOR EMBEDDED PILES 50

FIGURE 4.18 COMPARISON OF EXPERIMENTAL AND NUMERICAL FREQUENCY RESPONSE FUNCTIONS FOR PILE A 52

FIGURE 4.19 COMPARISON OF EXPERIMENTAL AND NUMERICAL FREQUENCY RESPONSE FUNCTIONS FOR PILE E 53

FIGURE 5.1 BRIDGE AT MERCK ROAD OVER CAMP CREEK 54

FIGURE 5.2 FIELD TEST CONFIGURATION FOR BENT 3 - PILE 2 56

FIGURE 5.3 FIELD TEST CONFIGURATION FOR BENT 4 - PILE 2 57

FIGURE 5.4 PHOTOGRAPH OF FIELD TEST 58

FIGURE 5.5 TYPICAL FREQUENCY RESPONSE FUNCTION FOR BENT 3 - PILE 2 59

FIGURE 5.6 WATERFALL PLOTS FOR BENT 3 - PILE 2 60

FIGURE 5.7 TYPICAL FREQUENCY RESPONSE FUNCTION FOR BENT 4 - PILE 2 62

FIGURE 6.1 COMPARISON OF FREQUENCY RESPONSE FUNCTIONS FOR PILE A 64

FIGURE 6.2 COMPARISON OF FREQUENCY RESPONSE FUNCTIONS FOR PILE E 64

FIGURE 6.3 FREQUENCY RESPONSE FUNCTION FOR PILE E 65

FIGURE 6.4 MODE INDICATOR FUNCTION FOR PILE E 65

1 Introduction

For approximately 6000 of Georgia's 14,500 bridges, pile tip elevations are unknown because design and construction records no longer exist (Gratton, personal communication). This lack of information is critical because it is difficult to determine the capacity of these piles - particularly in the presence of scour. The unknown bridge foundation problem is an important problem for federal and state agencies and has been the focus of several studies (Olson et al., 1995; Douglas and Holt, 1993) The unknown bridge foundation problem is one in which either the type and depth of foundation is unknown, or the type of foundation is known but the depth is unknown.

Although soil borings and other intrusive tests are capable of determining pile tip elevations, the time and cost of performing these tests on a large number of bridges is prohibitive. Nondestructive tests are an effective alternative for assessing pile tip elevations. The principle employed in these nondestructive tests is to generate stress waves by impacting the pile on an exposed surface. These stress waves then propagate downward along the pile and are reflected at the tip. The arrival of the reflected wave is monitored by sensors attached to the pile.

Purpose

This study focuses on bridges which are supported by exposed pile foundations that have unknown lengths. The purpose of this study is to evaluate the nondestructive use of flexural waves to determine the length of these bridge pile foundations. Many nondestructive test methods rely on the use of longitudinal waves excited axially down a pile. This type of testing is not feasible since the bridge superstructure prevents access to the top of a pile. Although the theory behind flexural wave testing is more complicated than that of the traditional longitudinal wave testing, flexural or bending waves can be excited laterally on the side of the pile with no physical interference from the bridge superstructure. The pile in most cases can be modeled as a long slender member since its ratio of length to section depth ratio is large. The propagation of the flexural waves within the beam is a function of its length, mass density, moment of inertia, elastic modulus and end conditions. When dealing with bridge piles the primary unknown is the embedment length since all of the other variables can be assumed or measured.

Method

This research used analytical and numerical modeling, tests on small-scale piles, and tests on full-scale bridges to initiate development of a method to determine unknown bridge pile lengths based on flexural waves. Analytical models with closed-form solutions and numerical models based on the finite element method were developed to aid in understanding the response of piles with varying geometries and boundary

conditions. Experimental frequency response measurements were performed on 10 small-scale bridge piles that were embedded in a 12 ft x 9 ft x 5 ft deep pit. Measurements were made of pile response to flexural waves induced in each pile. The measurements on small-scale piles were complemented with a test performed on a full-scale bridge selected by the Georgia Department of Transportation. The experimental data on small and full-scale piles was then compared to numerical solutions of pile response. An interpretive scheme based on modal analysis principles which permits the length of the piles to be determined from flexural wave testing was also investigated.

Report Organization

Chapter 2 reviews the development of nondestructive test methods to assess the integrity of cast-in-place foundations. Results of recent efforts to adapt these nondestructive test methods to the unknown foundation problem are also reviewed. Chapter 3 presents the theory of flexural wave propagation in long, slender members. Examples of closed-form solutions are presented for simple boundary conditions. Fundamentals of finite element numerical analyses are also presented to model more complex and realistic boundary conditions such as those of an embedded pile. Tests on the small-scale piles are presented and discussed in Chapter 4. Chapter 5 presents test data measured on a full-scale bridge in southeast Atlanta. In Chapter 6, the potential uses of modal analysis techniques to interpret pile response data are explored. A summary of the research study is presented in Chapter 7.

2 Review of Existing Nondestructive Test Methods

NDT Overview

Nondestructive tests (NDT) of piles were first developed as a technique to determine the integrity of cast-in-place pile foundations (Paquet, 1968; Davis and Dunn, 1974). These tests are frequently used to check for defects arising from drilling, casing, slurry, or concreting problems (O'Neill 1992) that could adversely affect the performance of the foundation. Most existing noninvasive NDT technologies used for integrity testing are based on the theory of one-dimensional wave propagation in a long slender member. In this context a pile is considered to be a long slender member. Access to the top of the pile is required for many of these integrity testing procedures. Typically the top of the pile is struck with an impact force and the pile response to this impact is also measured at the top of the pile. The length of the pile or the depth to any defect is a function of the amount of time it takes a longitudinal wave (or bar wave), induced by the impact force, to propagate down and back up the pile. In addition to identifying reflections from voids, the longitudinal wave velocity can be used to assess concrete quality (Malhotra, 1976).

Two commonly used noninvasive testing techniques are the Sonic Echo and the Impulse Response methods. Both methods share the same basic equipment configuration and test procedure in the field. This configuration is shown in Fig. 2.1. A transient force is applied to the top of the shaft by an instrumented 12 lb. sledge hammer. The force applied to the shaft is measured by a dynamic force transducer in the face of the hammer. The response of the pile to the impact is measured by a piezoelectric accelerometer attached to the shaft with mounting wax. Both force and acceleration are recorded by a Fast Fourier Transform (FFT) analyzer capable of processing data in either the time or frequency domain. The two methods differ in the way that the force and acceleration time histories are processed. The following sections summarize the methods of interpretation and present typical results for each test method.

Sonic Echo

Conceptually, the sonic echo method is the simplest of the two methods. The end of the shaft and any defects that exist along its length cause reflections of the seismic waves as they propagate downward through the shaft. By observing the time required for these reflections to return to the top of the shaft, the depth to the reflector can be determined:

$$z = \frac{v_c \bullet \Delta t}{2} \tag{2.1}$$

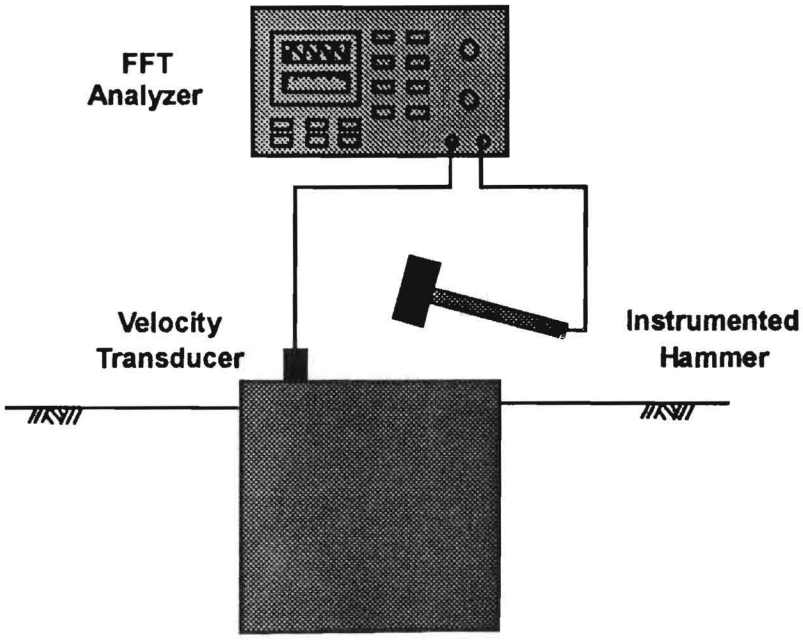

Figure 2.1 Test Configuration Used for Nondestructive Tests

where z is the depth to a reflector (a defect or the bottom of the shaft), v_c is the compression wave velocity in concrete, and Δt is the travel time of the reflected wave. Since Δt is a two-way travel time, the numerator in Eq. 2.1 must be divided by two. Davis and Dunn (1974), Stain (1982), and Olson and Wright (1989) give complete descriptions of the method.

A typical plot showing the transient impact and the pile response is shown in Figure 2.2. The time between wave arrivals is determined from the time history response of the pile measured by the accelerometer. There is a clearly identified reflection that occurs 9.47 msec after the initial impact. The compression wave velocity of the concrete measured on 6-in. by 12-in. test cylinders was equal to 3700 12,130 ft/sec. Using the observed travel time and compression wave velocity, the depth to the reflector is calculated to be 57.4 ft. The depth agrees well with the design length of 55.5 ft.

Impulse Response

An alternative to identifying reflections in the time domain is to process the data in the frequency domain. The response of the pile in the frequency domain is possible since the signal analyzer has the ability to perform a Fast Fourier Transform (FFT) on the data from the time domain. In the frequency domain a transfer function is used to describe the foundation system under consideration. A transfer functions is defined as the output of the system under consideration divided (normalized) by the input to the system. The mobility is a frequency response transfer function and is defined as:

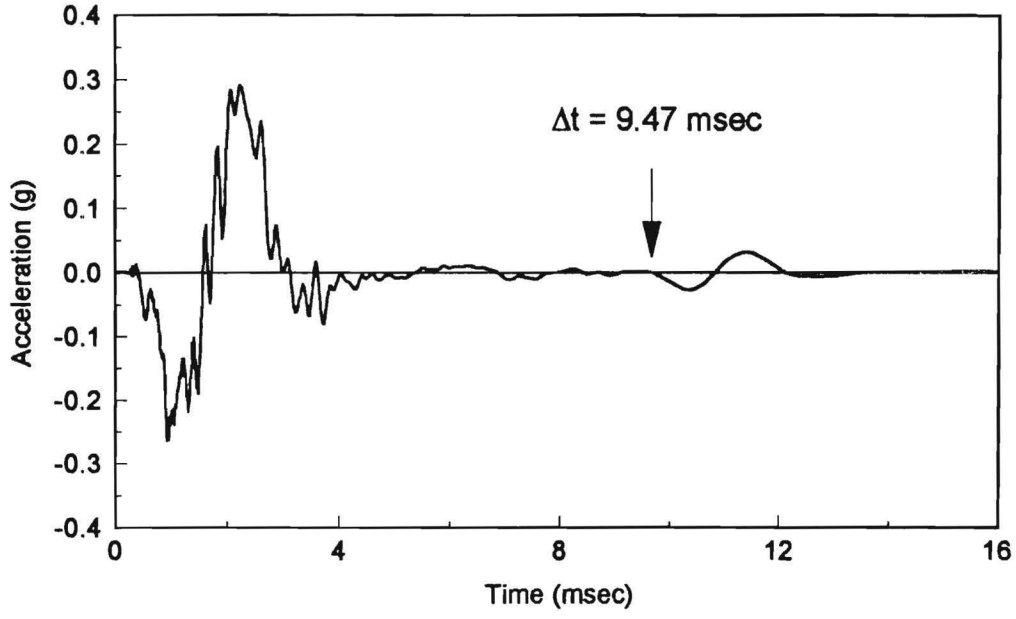

Figure 2.2 Acceleration Time History Observed At The Top Of Drilled Shaft

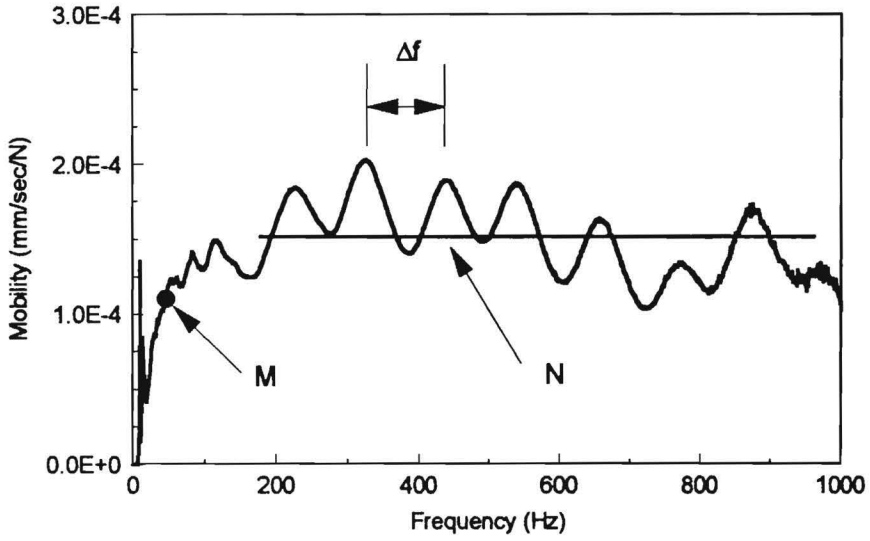

Figure 2.3 Mobility Frequency Response Function

$$\text{Mobility} = \frac{\dot{U}(f)}{P(f)} \tag{2.2}$$

where $\dot{U}$ is the particle velocity spectrum and P is the force spectrum. The particle velocity spectrum is obtained by integrating the particle acceleration spectrum The mobility is a complex-valued quantity, but typically only the magnitude is plotted. A typical plot showing the pile response in terms of the mobility is shown in Figure 2.3.

In the frequency domain the length of the pile or depth to any defects is calculated by the equation:

$$L = \frac{V_C}{2\Delta f} \tag{2.3}$$

where Δf is the change in frequencies between the adjacent peaks on the mobility vs. frequency plot. One of the advantages of this approach is that it is sometimes easier to identify peaks on the mobility vs. frequency plot than to identify reflections in the time domain. Using the value of Δf in Figure 2.3 and a V_c of 12,130 ft/sec, which was measured on concrete test cylinders, the length of the pile in the example is 56.4 ft according to Equation 2.3. The calculated length agrees well with the actual length of 55.5 ft.

Application of NDT Methods to Unknown Foundations

In recent years NDT techniques have been applied to help address the unknown bridge foundation problem. Olson et al (1995) presented a comprehensive review of all NDT techniques used to determine the depth of unknown foundations. They determined that one of the most reliable techniques is an invasive technique known as the parallel seismic method. The test configuration for the parallel seismic method is presented in Figure 2.4. In the parallel seismic method a receiver is placed in a cased, water filled borehole, drilled adjacent to the pile. The arrival of the wave is recorded by the receiver at different depths in the borehole. The length of the pile is determined from a plot of travel time vs. borehole receiver depth. The main disadvantage is that this test requires a borehole.

Flexural Wave Tests

Douglas and Holt (1993) and Holt and Douglas (1994) have developed a method to determine the length of piles using flexural waves. An illustration of the test configuration is shown in Figure 2.5. The pile is struck laterally to induce flexural waves propagating up and down within the pile. The propagation of these flexural waves is dispersive (i.e., the velocity is a function of frequency or wavelength). At low frequencies (wavelength >> pile diameter), the velocity associated with flexural waves is low. As the frequency increases, the velocity of propagation increases and approaches the Rayleigh wave velocity of the pile material.

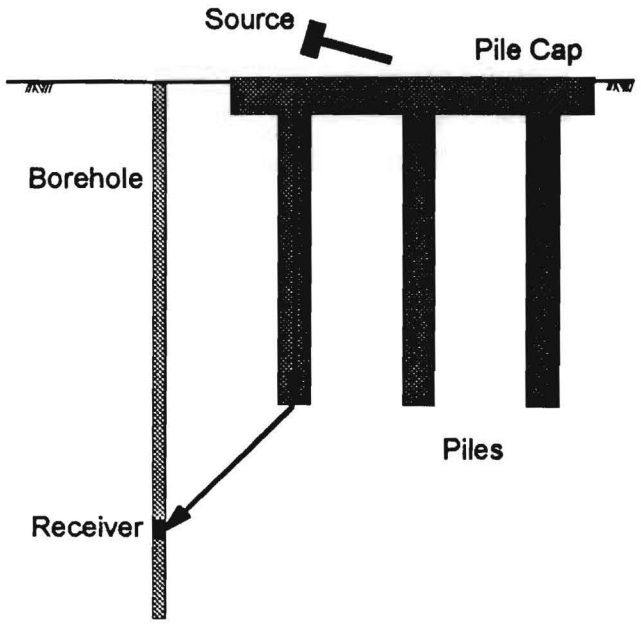

Figure 2.4 Parallel Seismic Method

The propagation of the waves in the pile is monitored by two receivers mounted horizontally on the side of the pile. Douglas and Holt (1993) used the "Short Kernel Method" (SKM) to analyze the propagation of dispersive flexural waves in timber piles. Olson et al. (1995) reviewed the short kernel method and summarized it as follows:

> "The method is similar to narrow band cross-correlation procedures between the input (the hammer blow) and the output (receiver response(s)). However, instead of measuring the hammer blow, a periodic function of 1 or more cycles is used as the 'Kernel Seed,' and a number of seeds for frequencies ranging from 500 to 4000 Hz may be cross-correlated with the receiver responses. The SKM correlation procedure amplifies bending wave energy responses with the selected seed frequency and in a way bandpass filters the response data since frequencies higher and lower than the seed frequency are filtered out. Two receivers are used in order to measure the bending wave velocity (distance divided by elapsed time between the bending wave arrival peaks) between them as determined from the peak responses in the cross-correlated data of the two receivers. The use of two receivers also allows one to determine whether the reflections of the bending wave energy are traveling back up the pile after reflection from the pile bottom, or if the bending wave energy is traveling back down the pile after reflection from the pile top or beam. This is identical to the procedures used in Sonic Echo tests when 2 receivers are used. The dispersion of the bending wave velocity is thus accounted for by calculating the bending wave velocity for each kernel seed frequency."

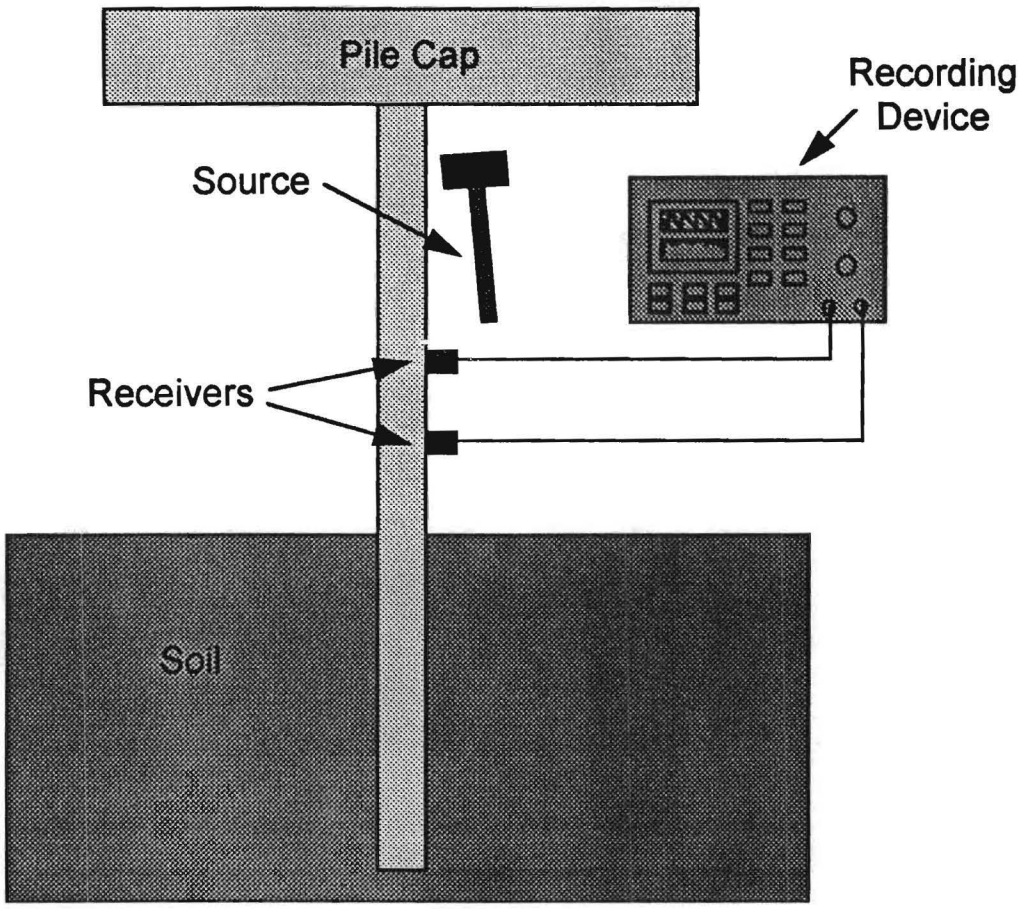

Figure 2.5 Test Configuration for Flexural Wave Test Developed by Douglas and Holt (1993)

Figures 2.6 and 2.7 illustrate the application of the Short Kernel method to a timber pile test performed by Olson et al. (1995). Figure 2.6 shows the response at each of the two accelerometers after application of the short kernel method with a kernel seed consisting of one cycle of 500 Hz. From the response, a bending wave velocity of 2480 ft/sec is calculated using the propagation delay (1.41 msec) between the two receivers. Figure 2.7 illustrates the calculation of the pile length by identifying reflected arrivals from the pile bottom. The calculated length is 27.3 ft which agrees well with the actual length of 28 ft.

Olson et al (1995) concluded that a limitation of the Short Kernel Method was that it is necessary to identify the propagation path(s) of flexural waves so as to correctly identify the propagation path of the waves reflected from the pile bottom. They concluded that identifying the correct path can be difficult for piles with several reflecting boundaries including the pile top, groundline, changes in pile geometry, etc. Olson et al. also found that using the direction of initial particle motion as an indicator to choose the correct propagation path can be misleading.

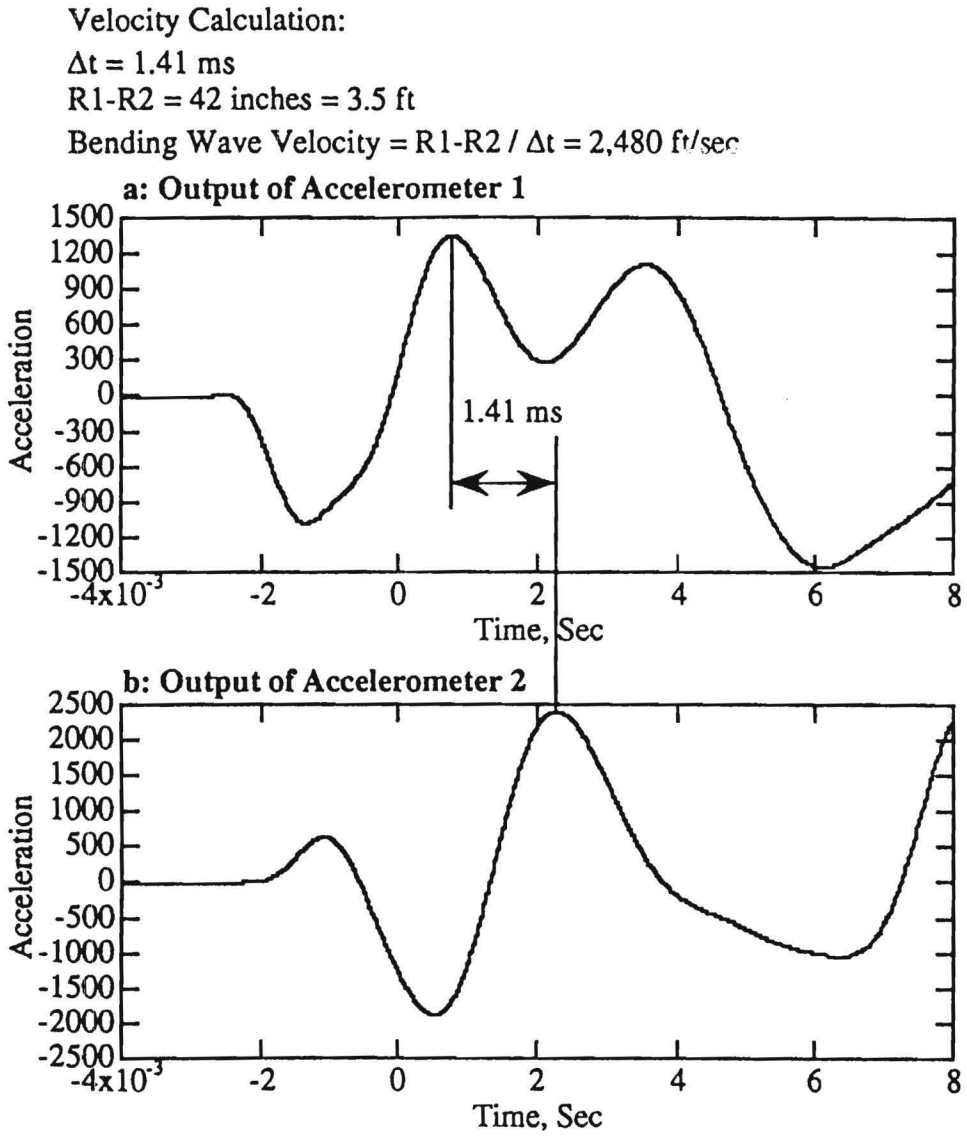

Figure 2.6 Determination of Bending Wave Velocity Using Short Kernel Method

Length Calculation:
$\Delta t = 22$ ms
$V = 2{,}480$ ft/sec
Length of Pile = $V \times \Delta t / 2 = 2{,}480 \times 22 \times 10^{-3} / 2 = 27.3$ ft

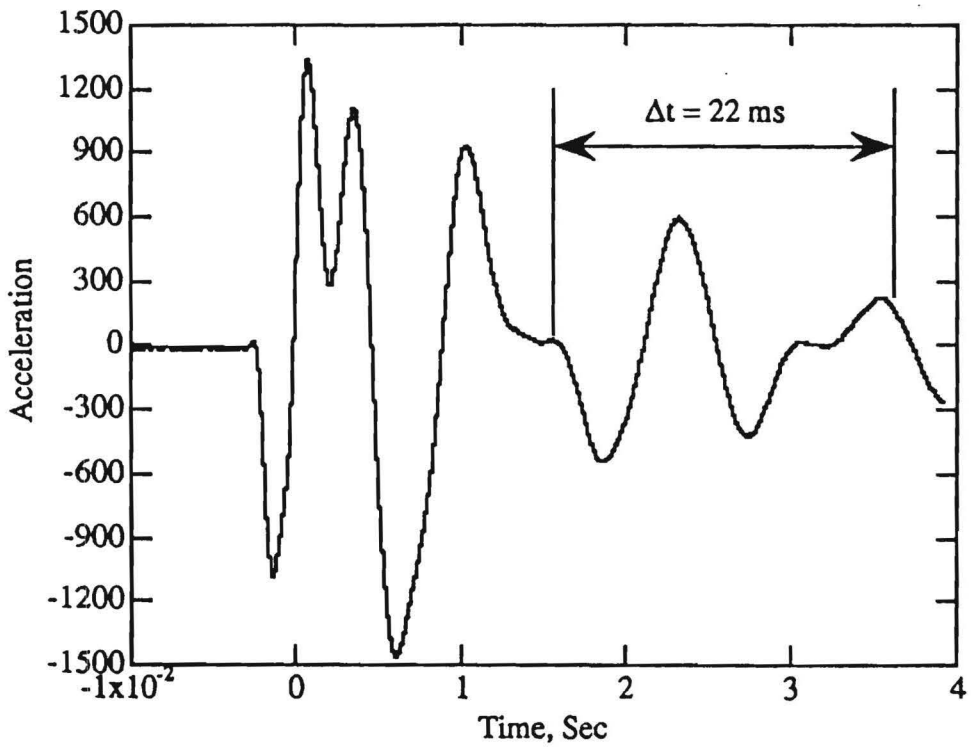

Figure 2.7 Determination of Pile Length Using Short Kernel Method

Yu and Roesset (1995) also considered frequency domain (transfer function) interpretation of bending wave test results. The interpretation is similar to the Impulse Response method described earlier which relies on longitudinal waves. The pile length is determined from the spacing between peaks, Δf, in the frequency response function between the input (hammer blow) and output (receiver response):

$$L = \frac{V_{limit}}{2\Delta f} \tag{2.4}$$

where the limiting flexural wave velocity approaches the Rayleigh wave velocity of the pile material. Since flexural waves are dispersive as described above, it is necessary to use the peaks of higher order modes (say 8th mode and higher) to determined the spacing between frequencies. For these higher modes, Δf approaches a constant value. Lower modes can be used if the appropriate value of V (accounting for dispersion) is used in Eq. 2.4.

3 Numerical Modeling

A series of analytical and numerical models were developed to study the response of long, slender members such as beams or piles to flexural waves. Closed-form solutions were developed for a cantilever beam to illustrate the basic characteristics of the response. Finite element numerical solutions using the commercially available finite element code I-DEAS by SDRC were employed to model complex pile geometry and boundary conditions such as those encountered on actual bridge foundations. The accuracy and robustness of the numerical models were validated by comparison with analytical models and the results of the experimental test program.

Finite Element Analysis

Finite element analysis is a valuable tool for structural analysis. Traditionally, engineers have analyzed a structure by first examining the behavior of individual structural elements, then combining the individual elements together such that equilibrium of forces and compatibility of displacements are satisfied. In the finite element method, a structure is idealized as a number of elements connected only at node points. Any geometry, along with any type of loading, can be modeled in this manner. Various types of elements are available for analysis. However, only bar elements are considered here.

The finite element method is based on the stiffness method:

$$\{\mathbf{F}^e\} = [\mathbf{K}^e]\{\delta^e\} \tag{3.1}$$

where $\mathbf{F}^e$ is the nodal load vector, δ^e is the nodal displacement vector and $\mathbf{K}^e$ is the element stiffness matrix.

The element stiffness matrix is developed using the number of degrees of freedom at each node of the element, and then relating the forces and displacements with unit values. A simple elastic spring illustrates this relationship. Figure 3.1 shows a spring, with F_1 and u_1 being the force and displacement at the first node, and F_2 and u_2 being the same at the second node.

Figure 3.1 Elastic Spring

The relationship between forces and displacements is:

$$\begin{Bmatrix} F_1 \\ F_2 \end{Bmatrix} = \begin{bmatrix} k_{11} & k_{12} \\ k_{21} & k_{22} \end{bmatrix} \begin{Bmatrix} u_1 \\ u_2 \end{Bmatrix} \tag{3.2}$$

The axial stiffness of the spring is known, but the individual terms in the stiffness matrix must be determined. These terms are determined by allowing each node to deform an amount u while fixing the other, and then relating the nodal forces to this deformation.

Deform node 1, node 2 fixed:

$$F_{11} = ku_1$$

$$F_{11} + F_{21} = 0$$

$$F_{21} = -ku_1$$

Deform node 2, node 1 fixed:

$$F_{22} = ku_2$$

$$F_{12} + F_{22} = 0 \tag{3.3}$$

$$F_{12} = -ku_2$$

The total forces at the nodes are:

$$F_1 = F_{11} + F_{12} \qquad F_1 = ku_1 - ku_2$$

$$F_2 = F_{21} + F_{22} \qquad F_2 = -ku_1 + ku_2 \tag{3.4}$$

This can be expressed in matrix form as follows:

$$\begin{Bmatrix} F_1 \\ F_2 \end{Bmatrix} = \begin{bmatrix} k & -k \\ -k & k \end{bmatrix} \begin{Bmatrix} u_1 \\ u_2 \end{Bmatrix} \tag{3.5}$$

giving the stiffness matrix for the single spring element:

$$\left[K^e\right] = \begin{bmatrix} k & -k \\ -k & k \end{bmatrix} \tag{3.6}$$

As can be seen in Equation 3.6, (and for all stiffness matrices), the stiffness matrix is symmetric due to the reciprocal theorem. Finite elements codes take advantage of this symmetry to reduce the amount of memory used by only storing an upper or lower triangle of the stiffness matrix. Knowing the element stiffness matrix, the deflection due to any applied load, or the loading due to any deflection consistent with the degrees of freedom of the nodes can be determined.

The procedure outlined above illustrates some of the concepts of the stiffness analysis central to the finite element method. Individual element stiffness matrices can be determined, regardless of the geometry of the system. A global stiffness matrix can be developed by combining individual element stiffness matrices to determine displacements in a larger structure.

Analytical Derivation

Simple analytical solutions for flexural beam vibrations were developed to validate the finite element models used in this study. The first step in developing an analytical model was to choose pile geometry and boundary conditions that are similar to the embedded pile, but have a closed-form analytical solution. The example used here is that of a fixed-free cantilever beam. In this context, a pile is similar to a fixed-free cantilever with the soil acting as an applied stiffness at the free end.

Euler's beam equation is one of the most fundamental ways of describing transverse beam theory. It is derived by considering an elemental length of beam, dx, and the internal shear forces and moments acting on it (Figure 3.2). This theory yields the following relationships for beams:

$$y = \text{deflection} \tag{3.7a}$$

$$\frac{\partial y}{\partial x} = \text{slope} \tag{3.7b}$$

$$EI\frac{\partial^2 y}{\partial x^2} = M\cdots(\text{moment}) \tag{3.7c}$$

$$EI\frac{\partial^3 y}{\partial x^3} = V\cdots(\text{shear}) \tag{3.7d}$$

$$EI\frac{\partial^4 y}{\partial x} = w(x)\cdots(\text{load int ensity}) \tag{3.7e}$$

Letting the mass per unit length of the beam be γ, and the acceleration of the element be $\delta^2y/\delta t^2$, Euler's beam equation is written as:

$$\frac{EI}{\gamma}\frac{\partial^4 y}{\partial x^4} + \frac{\partial^2 y}{\partial t^2} = 0 \tag{3.8}$$

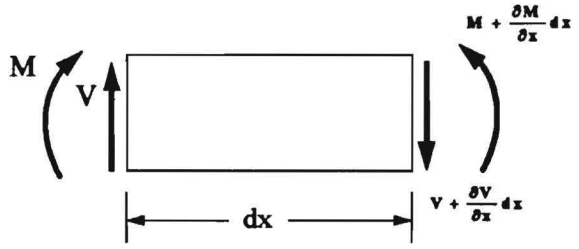

Figure 3.2 Beam Element

The general solution for the partial differential equation is:

$$y(x) = C_1 \sinh(\lambda x) + C_2 \cosh(\lambda x) + C_3 \sin(\lambda x) + C_4 \cos(\lambda x) \tag{3.9}$$

To solve for the fixed-free condition, the appropriate boundary conditions must be defined. At the end, $x = 0$, the beam is fixed such that the displacement and slope of the beam are equal to zero. At the free end, there is no moment or shear force. Therefore, the boundary conditions are as follows:

Fixed-End	Free-End
$y(0) = 0$	$\frac{\partial^2 y(L)}{\partial x^2} = 0$
$\frac{\partial y(0)}{\partial x} = 0$	$\frac{\partial^3 y(L)}{\partial x^3} = 0$

(3.10)

To evaluate the boundary conditions, the first, second, and third derivatives of Equation 3.9 are required:

$$\frac{\partial y}{\partial x} = \lambda(C_1 \cos(\lambda x) + C_2 \sinh(\lambda x) + C_3 \cos(\lambda x) - C_4 \sin(\lambda x))$$

$$\frac{\partial^2 y}{\partial x^2} = \lambda^2(C_1 \sinh(\lambda x) + C_2 \cosh(\lambda x) - C_3 \sin(\lambda x) - C_4 \cos(\lambda x)) \tag{3.11}$$

$$\frac{\partial^3 y}{\partial x^3} = \lambda^3(C_1 \cosh(\lambda x) + C_2 \sinh(\lambda x) - C_3 \cos(\lambda x) - C_4 \sin(\lambda x))$$

Substituting the appropriate values of x to lead to the following matrix formulation:

$$\begin{bmatrix} 0 & 1 & 0 & 1 \\ \lambda & 0 & \lambda & 0 \\ \lambda^2 \sinh(\lambda L) & \lambda^2 \cosh(\lambda L) & -\lambda^2 \sin(\lambda L) & -\lambda^2 \cos(\lambda L) \\ \lambda^3 \cos(\lambda L) & \lambda^3 \sinh(\lambda L) & -\lambda^3 \cos(\lambda L) & \lambda^3 \sin(\lambda L) \end{bmatrix} \begin{Bmatrix} C_1 \\ C_2 \\ C_3 \\ C_4 \end{Bmatrix} = \begin{Bmatrix} 0 \\ 0 \\ 0 \\ 0 \end{Bmatrix} \tag{3.12}$$

The determinant of this matrix must be equal to zero yielding the characteristic equation:

$$\cos(\lambda L)\cosh(\lambda L) + 1 = 0 \tag{3.13}$$

Assuming simple harmonic motion, the circular natural frequencies of the fixed-free beam are given by:

$$\omega_i = \frac{(\lambda L_i)^2}{L^2}\sqrt{\frac{EI}{\gamma}} \tag{3.14}$$

where λL_i = ith root of Equation 3.13, L is length of beam, E is Young's Modulus, I is the moment of inertia, and γ is the mass per unit length.

The roots of Equation 3.13 can be easily solved by rearranging the equation into the form:

$$\cos(\lambda L) = -\frac{1}{\cosh(\lambda L)} \tag{3.15}$$

Then the roots of Equation 3.15 can easily be found using a program such as Mathcad® by graphing each side of the equation as a separate function.

$$\begin{aligned} f_1(\lambda L) &= \cos(\lambda L) \\ f_2(\lambda L) &= \frac{-1}{\cosh(\lambda L)} \end{aligned} \tag{3.16}$$

An initial guess of the roots is made from the points of intersection of the above two equations for five natural frequencies, then the root function is used to find the exact values of λL, using the initial guess as the starting value in an iterative solver as shown in Figure 3.3.

The values calculated above can then be plugged into Equation 3.14 along with the known properties, and the natural frequencies can be obtained. This procedure can be followed for any other

boundary condition, such as pinned-pinned, fixed-fixed, etc. It is simply a matter of applying the correct boundary conditions to the solution of the beam equation.

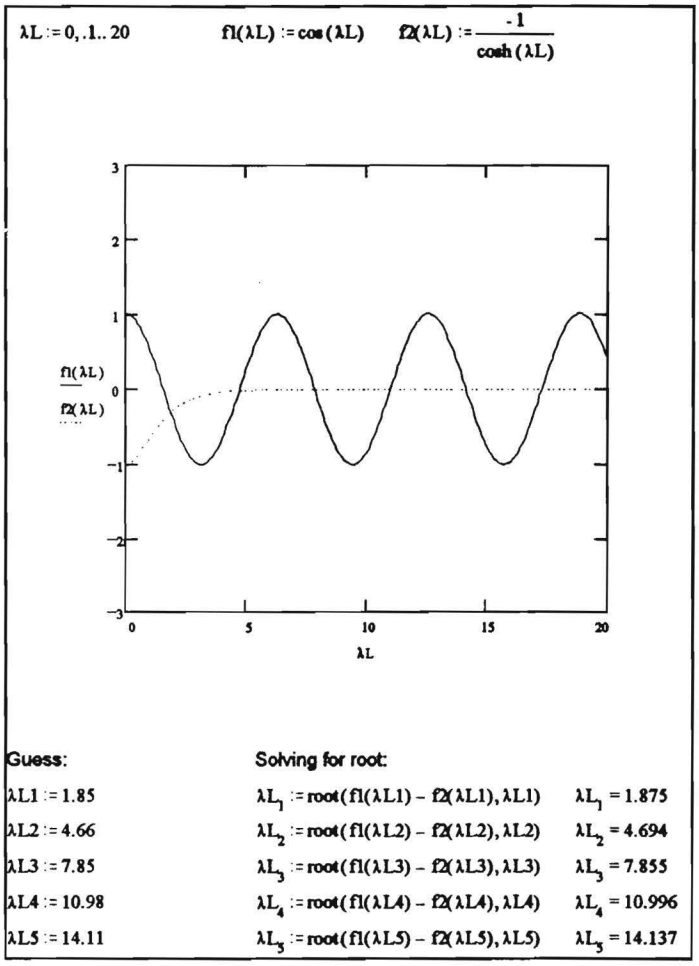

Figure 3.3 Solving for the Roots of the Characteristic Equation

Comparison of Analytical and Numerical Results

To validate the numerical solution, comparisons were made between values of natural frequency obtained from the closed-form solution for a cantilevered, 6-ft long, S3 x 5.7 steel beam and values obtained from a numerical analysis of the same beam. Calculations to obtain the first five natural frequencies of vibration are shown in Figure 3.4, using the values calculated for λL in Figure 3.3.

Shape: HS 3x5.7 Properties: $L := 72$ $A := 1.67$

Material: Steel

Length: 6 foot $I_x := 2.52$ $I_y := .455$

Boundary: fixed-free

Units: in-lbs $\rho := .000738$ $\gamma := \rho \cdot A$

$E := 29000000$

Iyy:

$$\omega_{(i)} := \frac{(\lambda L_i)^2}{L^2} \cdot \sqrt{\frac{E \cdot I_y}{\gamma}}$$

$\omega_1 = 70.169$ $\omega_2 = 439.807$ $\omega_3 = 1231.456$ $\omega_4 = 2413.162$ $\omega_5 = 3989.131$

$$\omega_i := \frac{\omega_i}{2 \cdot \pi} \text{ Hz}$$

$\omega_1 = 11.168$ $\omega_2 = 69.997$ $\omega_3 = 195.992$ $\omega_4 = 384.067$ $\omega_5 = 634.89$

Ixx:

$$\omega_{(i)} := \frac{(\lambda L_i)^2}{L^2} \cdot \sqrt{\frac{E \cdot I_x}{\gamma}}$$

$\omega_1 = 165.136$ $\omega_2 = 1035.038$ $\omega_3 = 2898.1$ $\omega_4 = 5679.12$ $\omega_5 = 9387.995$

$$\omega_i := \frac{\omega_i}{2 \cdot \pi} \text{ Hz}$$

$\omega_1 = 26.282$ $\omega_2 = 164.731$ $\omega_3 = 461.247$ $\omega_4 = 903.86$ $\omega_5 = 1494.146$

Figure 3.4 Analytical Solution for Natural Frequencies of Cantilever S3 x 5.7

The next step was to develop the corresponding numerical solution with the finite element code, I-DEAS. One-dimensional, parametric beam elements were used to model the dynamic behavior of the beam. Seventy three nodes with a 1-in. spacing were used, beginning at (0,0,0) and ending at (0,-72,0). Figure 3.5 is an illustration of the model. A fully fixed boundary condition was applied at location (0,0,0).

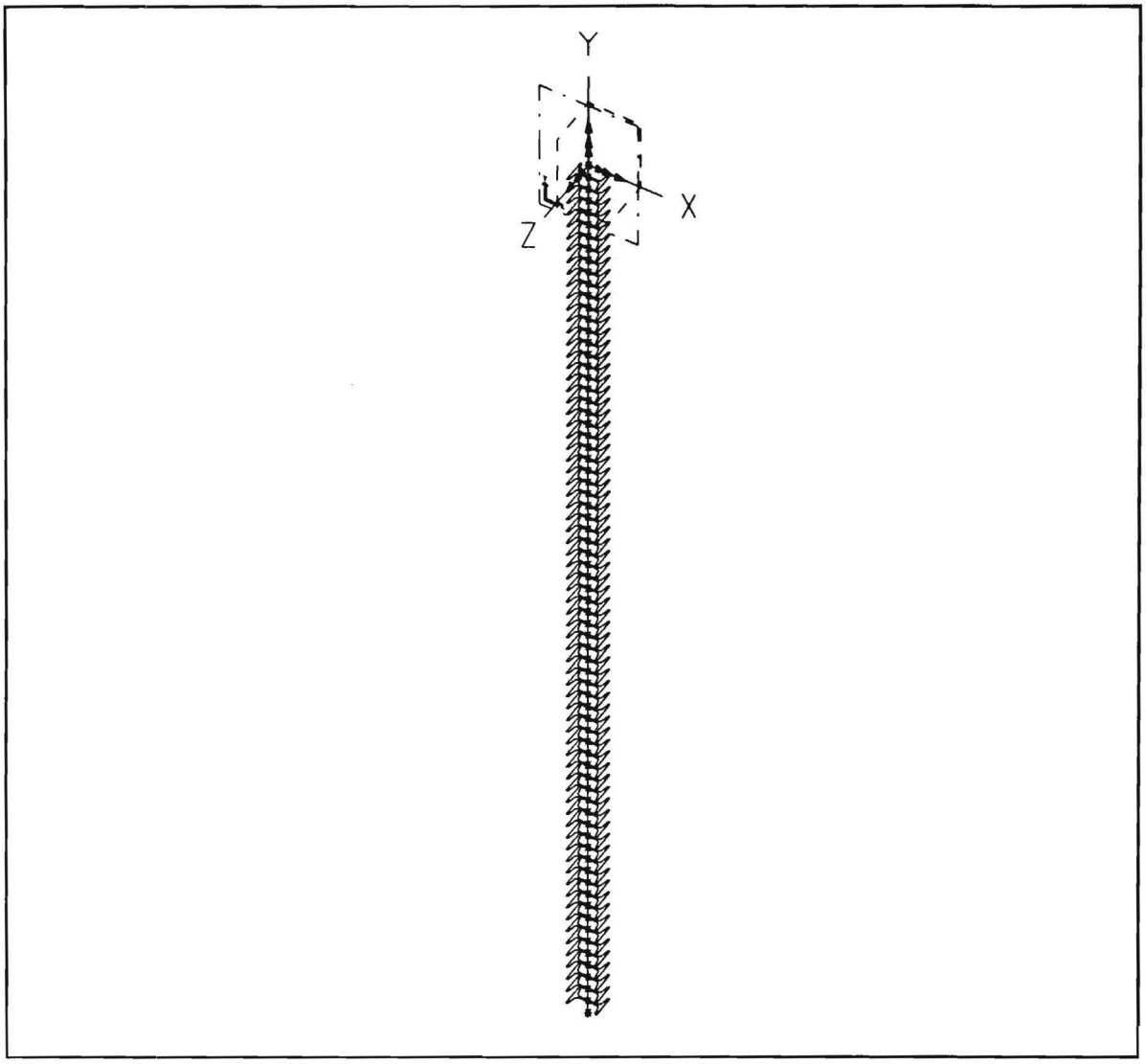

Figure 3.5 Finite Element Model of Cantilevered Beam

Table 3.1 is a summary for comparison of the analytical results obtained with Equation 3.14 and numerical results obtained from the finite element solution in I-DEAS. The values of the natural frequencies in both the X-X and Y-Y directions compare well and provide confidence that the finite element program can be used to model more complex geometries and boundary conditions which do not have closed-form analytical solutions.

Table 3.1 Comparison of Analytical and Numerical Results

	Natural Frequency (Hz)		
Mode of Vibration	Analytical	Numerical	Error
Y-Y Direction			
1	11.2	11.2	0.2%
2	70.0	70.1	0.2%
3	196.0	196.4	0.2%
4	384.1	384.9	0.2%
5	634.9	636.2	0.2%
X-X Direction			
1	26.3	26.3	0.2%
2	164.7	165.1	0.2%
3	461.3	462.2	0.2%
4	903.9	905.7	0.2%
5	1494.2	1497.2	0.2%

Influence of Soil Embedment

To aid in understanding limitations in using pile frequency response functions as the basis for assessing pile embedment, a numerical sensitivity study was performed. The limitations were first studied using a simple beam-on-elastic foundation analysis. Although the entire beam is in contact with the soil, the effect of varying the total length of the beam on the natural frequencies of vibration should yield basic trends that also apply to case where the pile is partially exposed. The total length, x, of the beam was varied from 72 to 120 in. The mass per unit length of beam is designated as γ, and the beam lays on an elastic foundation of stiffness k_0. It is assumed that the mass of the elastic foundation is negligible compared to that of the beam and that the damping is negligible as well.

The graph of the solution (Figure 3.6) shows the change in natural frequencies as a function of beam length for each of the first five natural frequencies of the beam. The variable i corresponds to the mode numbers of each natural frequency and it's associated mode shape. The mode number for the

fundamental frequency, for example, is 1. It becomes apparent that each natural frequency approaches a value of the square root of k_o/γ. Another trend apparent in this solution is that the variation in frequency is larger for higher mode numbers.

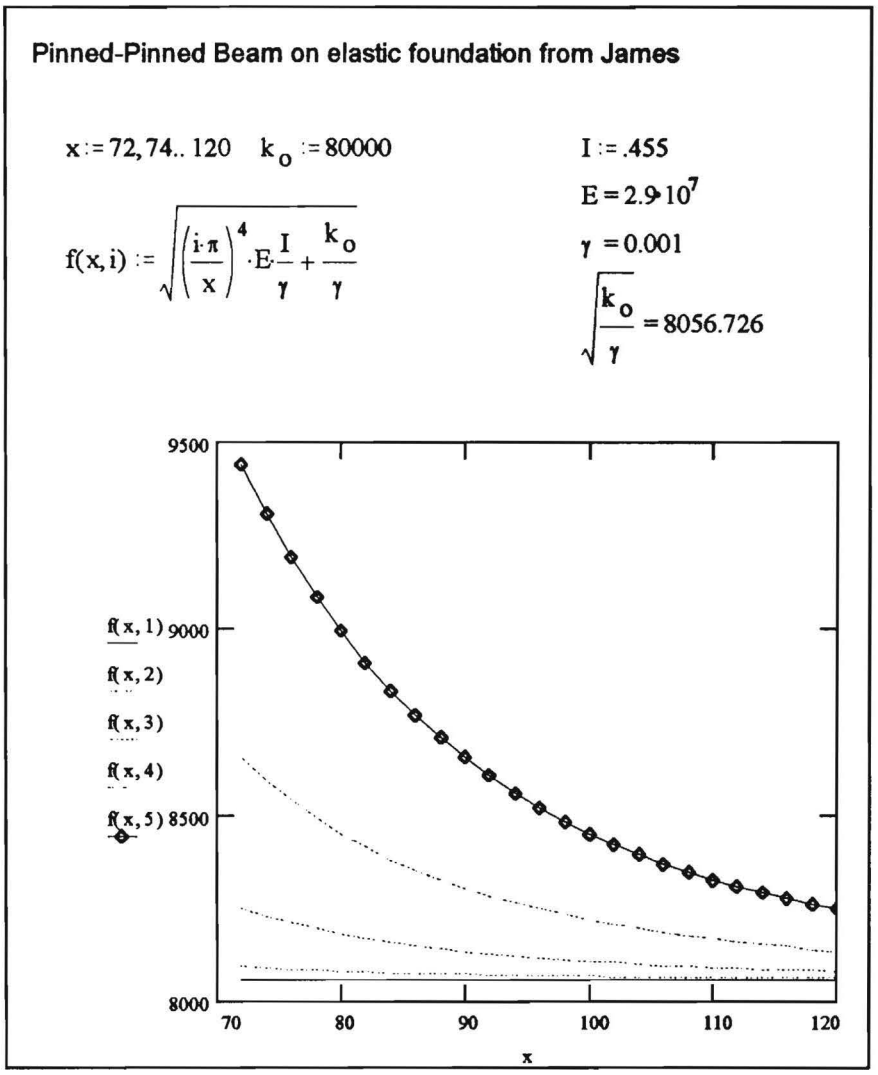

Figure 3.6 Mathcad Solution-Variable Beam length on Elastic Foundation

Finite element analyses were then used to examine the influence of embedment on the first three natural frequencies corresponding to flexural vibrations in the Y-Y direction. A pile with properties equivalent to the S3 x 5.7 piles was used in the finite element analyses. Springs were used to model the soil resistance as shown in Figure 3.7. The *exposed* length of the beams, pile properties, and the spring stiffness were kept constant. The results are shown in Figure 3.8. The results indicate that the frequencies of

vibration are sensitive to the embedment depth for embedments less than approximately 30 in. For the S3 x 5.7 section, this depth is approximately 10 times the section depth (3.0 in.).

The results of the beam-on-elastic foundation and finite element analyses provide an indication of the maximum embedment depth that can be detected using a frequency response function approach. For an HP12 x 53 pile which is commonly found on full-scale bridges, this limitation implies that the maximum depth of embedment that is able to be resolved is approximately 10 ft. Yu and Roesset (1995) found that the maximum observable embedment depth for concrete piles was approximately 15 ft using a similar frequency domain analysis. The limitation is likely more severe for steel H sections because of the greater attenuation of energy resulting from the larger surface area of an H section.

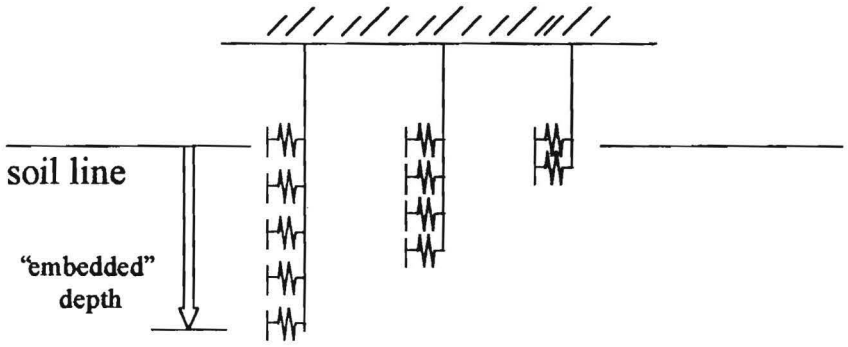

Figure 3.7 Use of Springs to Model Soil Resistance

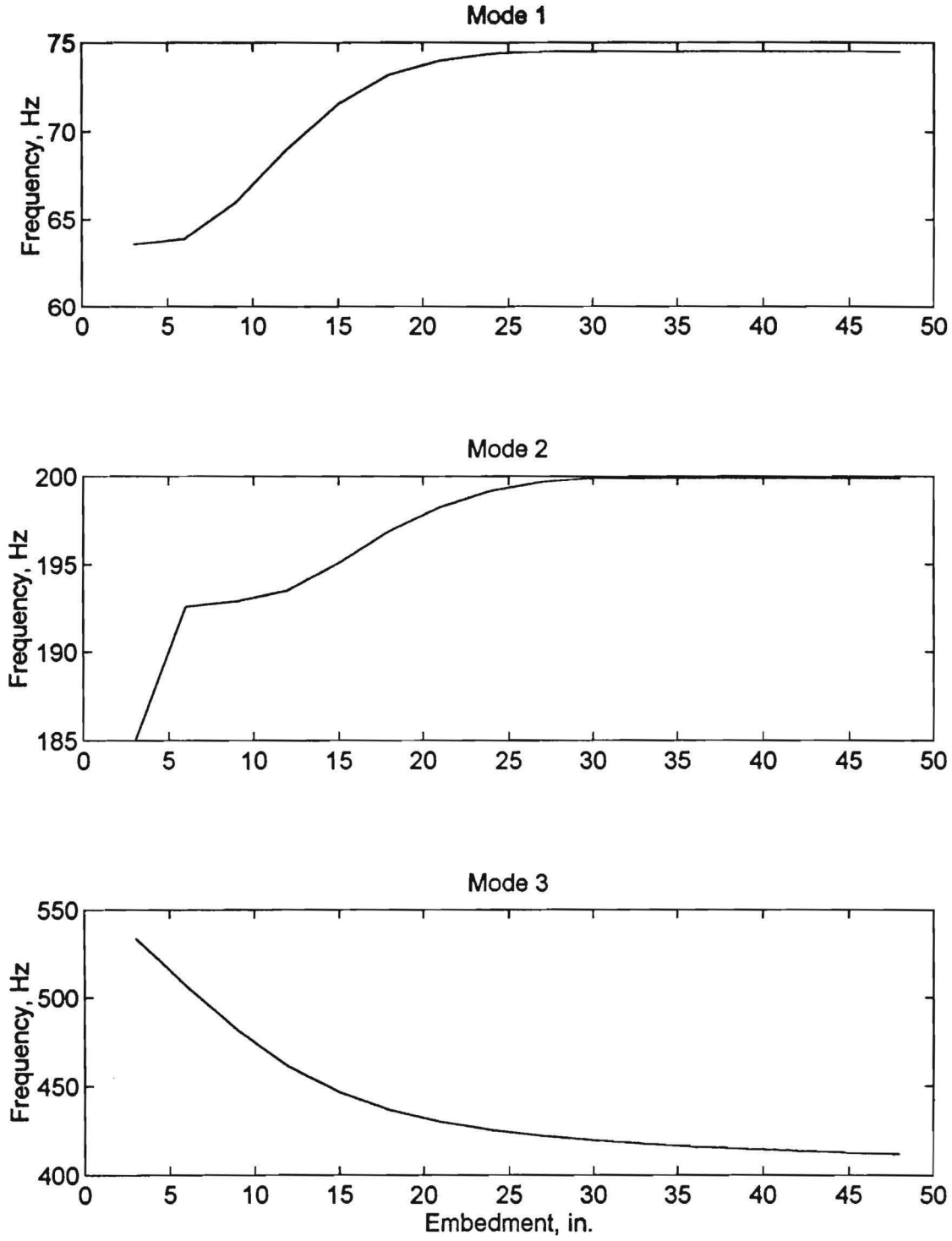

Figure 3.8 Influence of Embedment Depth on Natural Frequencies of Vibration

4 Tests on Small-Scale Piles

Tests on small-scale piles were performed to obtain experimental pile response data under controlled laboratory conditions for a variety of pile lengths and configurations. The following sections describe the experimental facility, the configuration of the piles, and the results of tests on the small-scale piles with both free and embedded end conditions.

Small-Scale Pile Facility

Flexural wave testing on the small-scale piles was performed in the Civil Engineering Laboratories Building on the Georgia Institute of Technology campus. A photograph of the test facility is shown in Figure 4.1. The experimental pile facility contained a 12 ft long by 9 ft wide by 5 ft deep concrete pit. The pit extended 4.5 ft below the floor surface with a 6 in. rim extending up around the pit. Figure 4.2 and Figure 4.3 show two vertical channel sections (C9 x 13.4) bolted to the rim of the pit on each side of the 9 ft width. A horizontal W10 x 45 steel section, with a plate welded to each end, was connected to a channel section on each end of the pit and ran parallel to the 12 ft length of the pit. The vertical channel sections and the end plates on the horizontal members had pre-bored holes. These pre-bored holes were used to connect the vertical and horizontal members together. The holes also enabled the horizontal sections to be placed at different heights if necessary. The horizontal sections were placed at 5 ft above the pit rim for all

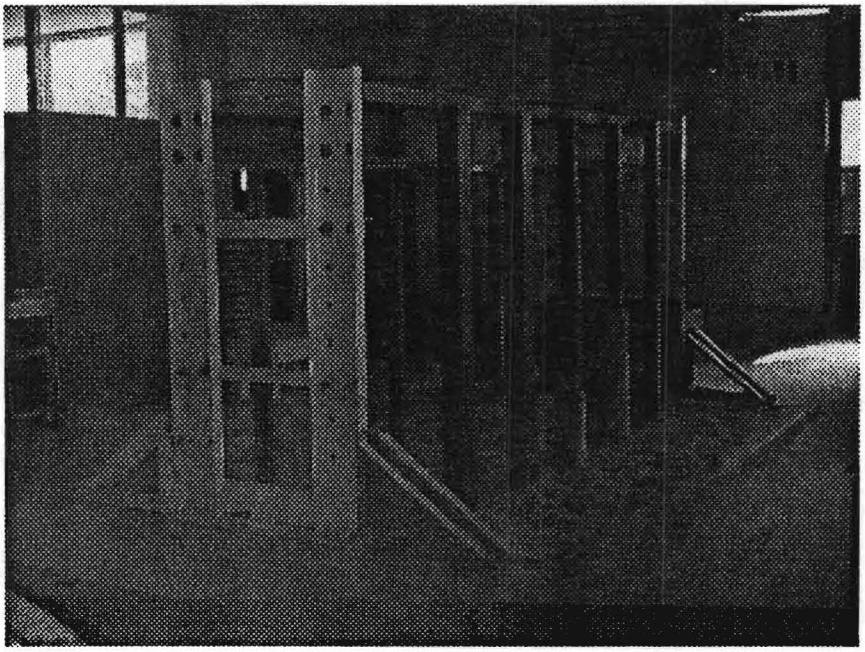

Figure 4.1 Experimental Facility for Testing Small-Scale Piles

of the lab tests. The figures also show that the horizontal W10 x 45 members were connected to each other by two 3 ft x 2 ft x 1 inch thick plates that were bolted to the bottom flange of the section. Four S3 x 5.7 sections were welded at angles to the top flange of the horizontal members to help stiffen the system. Once the frame was completely assembled, five vertical model pile sections (labeled A-E and F-J) were welded to the flange edges of each of the W10 x 45 horizontal members.

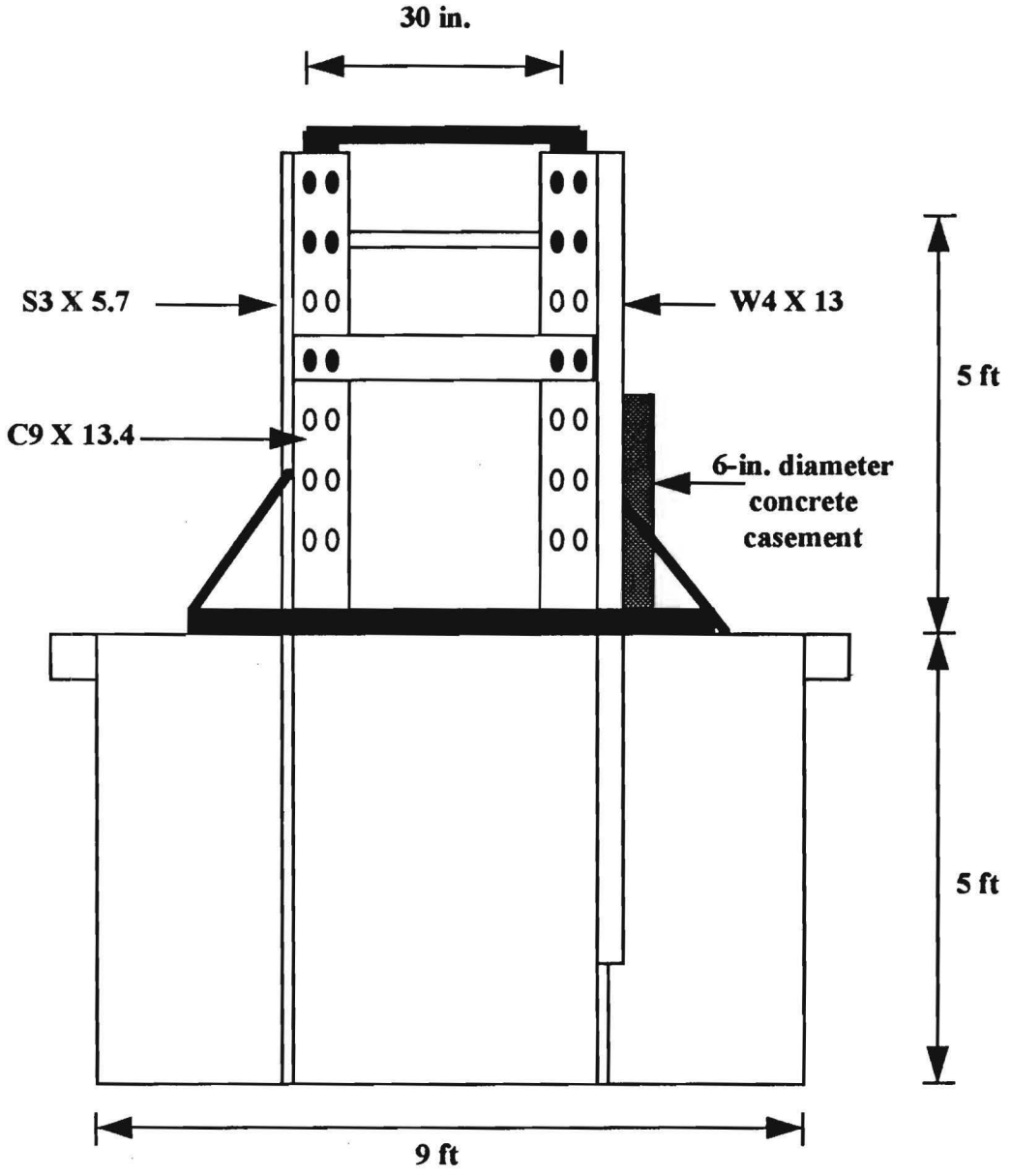

Figure 4.2 End View of Experimental Facility for Testing Small-Scale Piles

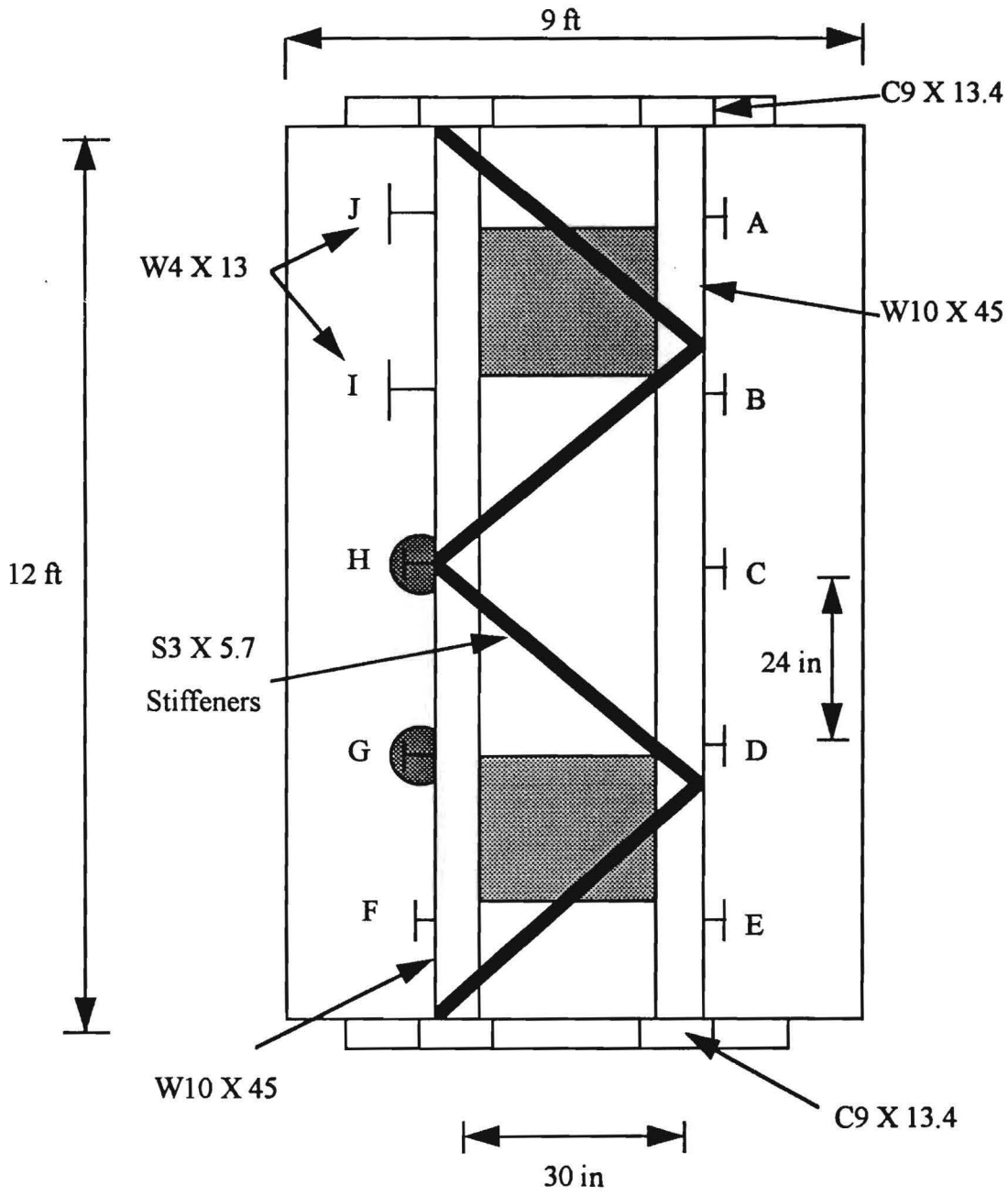

Figure 4.3 Plan View of Experimental Facility for Testing Small-Scale Piles

Test Pile Sections

The pile sections that were used in the laboratory testing were chosen based on bridge design information given by the Georgia Department of Transportation (Gratton, personal communication). The Georgia DOT indicated that a typical steel H pile section is an HP 12 x 53 that is 15 to 60 feet in length with a concrete casement from the ground line to 2 feet above the waterline. These dimensions yield an average ratio of length to section depth (L/D) of 37.5. The test pile sections have an average length of 8 feet since the lengths ranged from a minimum of 6 feet and maximum of 10 feet. This 8-foot average length was then divided by the L/D ratio of 37.5 to yield a test pile section depth of 2.6 inches. Therefore, an S3 x 5.7 was chosen to be the primary representative pile section. Two W4 x 13.0 sections were also used to change the section dimensions for some the tests. As shown in Figure 4.3, each pile was designated with an alphabetic label.

Figure 4.4 shows the right elevation of the test pit. On the right horizontal section five S3 X 5.7 sections, Piles A through E, were welded to the flanges of the horizontal member on 24-in. centers with lengths varying from 6 to 10 feet. This test setup corresponded to a pile embedment depth of 1 foot for Pile A to 5 feet for Pile E. In this basic pile setup the primary variable that was changed was the pile length. This setup would enable tests to be conducted to assess the effects of pile length on the natural frequency and mode shapes of the piles.

Figure 4.5 shows the left elevation of the test pit. The left horizontal member also had 5 test sections, Piles F through J, welded to it. These piles were setup to test the influence of other parameters in addition to the length. The following piles were welded to the left horizontal member:

- Pile F, an S3 x 5.7 section that rests on the concrete pit bottom to simulate an end bearing pile. This pile was intended to examine the influence on pile response of a fixed response to end condition as opposed to the floating end conditions of piles A through E.

- Pile G, an S3 x 5.7 section 9-ft long with concrete casement extending 2.5 feet above the top of the soil, and Pile H, an S3 x 5.7 section 7-ft long with concrete casement extending 1.25 feet above the top of the soil. These piles were used to investigate the effects of a concrete casement on flexural waves. The concrete casement is used on bridges to help protect the steel sections from corrosion. The casements were constructed by splitting a 6-in. diameter PVC pipe length-wise to make a form. The forms were taped together around the test piles and filled with Sak-Crete.

- Pile I, a 7-ft long W4 x 13 section, and Pile J, a 9-ft long W4 x 13 section. These W4 x 13 sections were intended to investigate a change in section to compare with Piles B and D which are S3 x 5.7 sections.

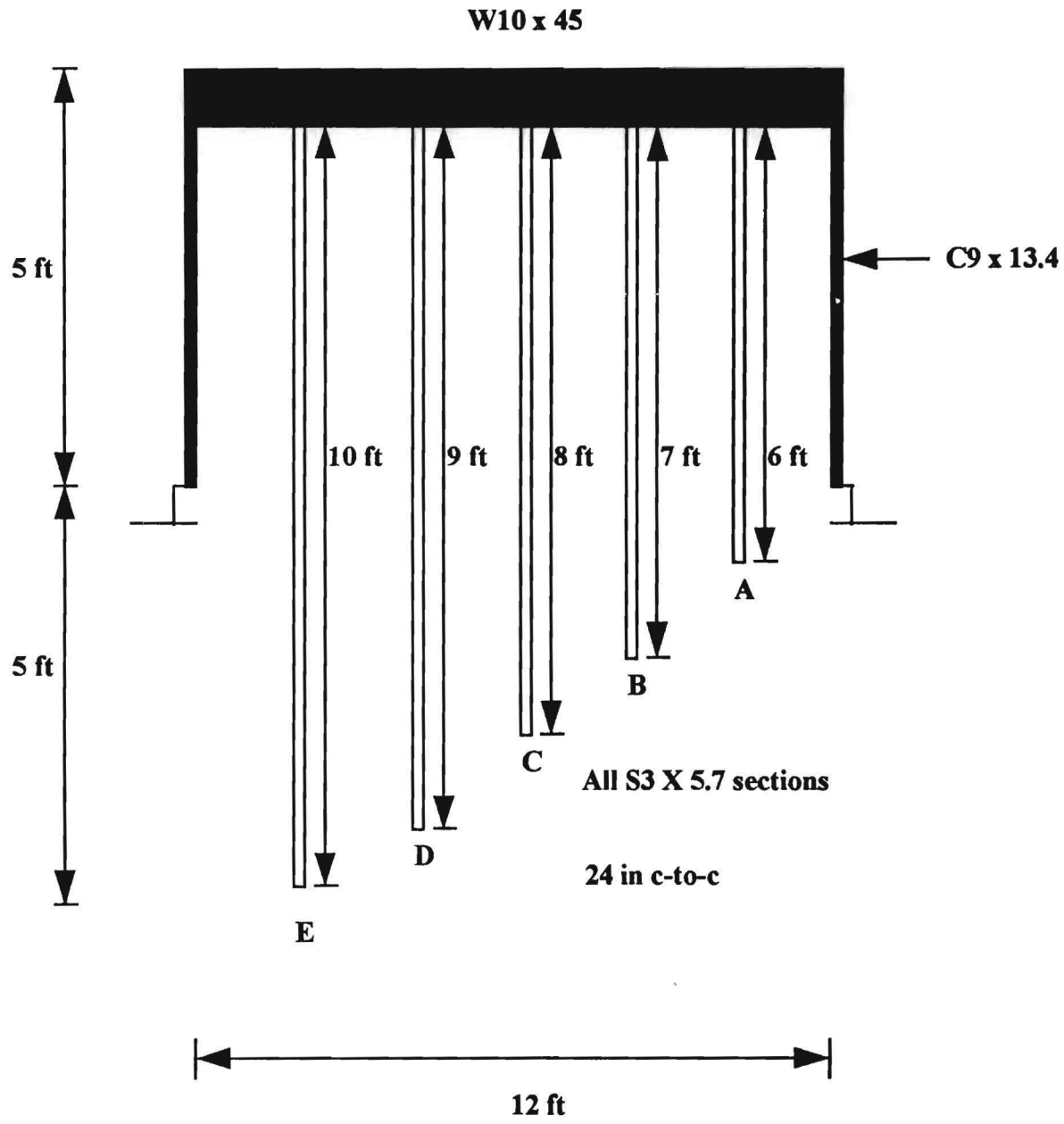

Figure 4.4 Right Elevation View of Small-Scale Pile Test Facility

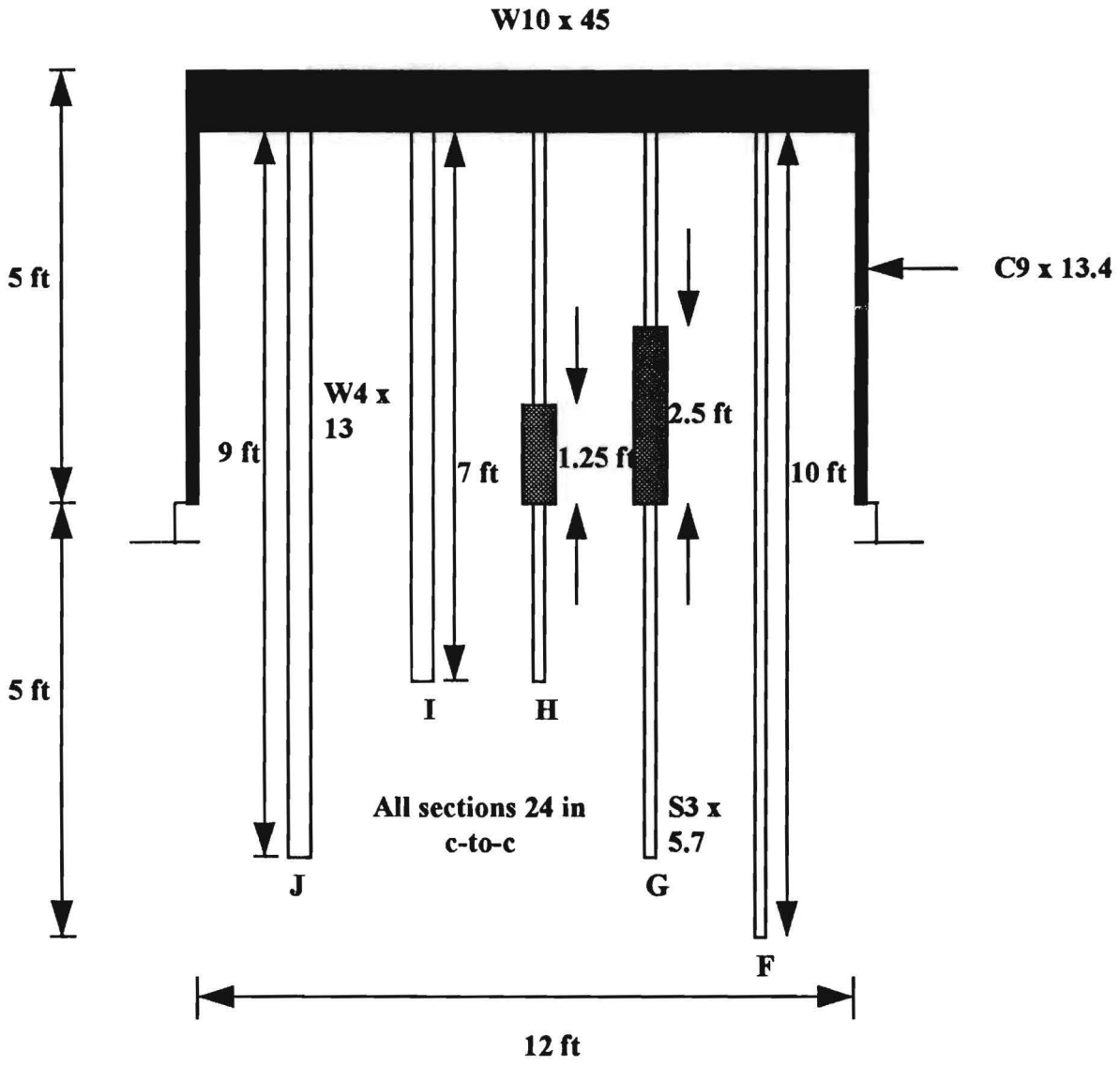

Figure 4.5 Left Elevation View of Small-Scale Pile Test Facility

Tests on Fixed-Free Piles

The first phase of the flexural wave testing was begun prior to the sand placement but after the piles had been welded to the frame. The first tests were performed at this time to test the pile in a fixed-free condition The main objective of this first phase of testing was to provide simple boundary conditions which could be modeled easily in the finite element analysis described in Chapter 3. The response of a beam with fixed-free

boundary conditions also has a closed-form solution which can be compared to the experimental and finite element solutions.

Test Equipment and Configuration

The testing configuration for the fixed-free pile testing is presented in Figure 4.6. The hammer (source) used to induce the flexural waves was a PCB Piezotronics, Inc. Model 086C50 modally tuned hammer with a built-in force transducer. The hammer is 8 in. long with a head diameter of 0.6 in. and a tip diameter of 0.25 in. It has a force range of 0 to 5000 lb. This hammer has a calibrated sensitivity of 0.98 mV/lb. The hammer has 3 tips that can be attached to the built-in force transducer. Each tip varies in hardness. Two of the tips are made of plastic and the third is made of metal. Harder tips induce higher-frequency waves into the pile. The metal tip was used for the fixed-free pile testing since higher frequencies were desired. The pile response was measured by a Wilcoxon Research Model 732A piezoelectric accelerometer (receiver). This accelerometer has a traceable frequency response range of 10 Hz to 10 kHz. The calibration voltage sensitivity for this particular accelerometer is 10.2 mV/g. The accelerometer was attached to the pile with a magnet. The magnet is 0.75 in. in diameter and 0.5 in. thick with a bolt protruding from one circular side and a magnetized disk on the other. The accelerometer was threaded onto the bolt and mounted horizontally on the pile with the magnet. The hammer and the accelerometer response measurements were recorded by a Hewlett-Packard Model 3562A Dynamic Signal Analyzer. This analyzer has the ability to process the pile response in the time and frequency domains. The data is processed from the time to the frequency domain by the use of a Fast Fourier Transform. The signal analyzer has two external 3.25 in. floppy disk drives which enables the user to save the pile response measurements on disk for later manipulation.

Test Method

Pile A was the chosen for testing with a free end condition. The locations of the hammer and accelerometer were varied along the length of the pile at positions designated 1 through 9 as shown in Figure 4.6. The ninth position was not placed at the top of the pile since there would be almost no pile response there due to the fixed end condition at the top of the pile. A typical test measurement consisted of placing the accelerometer at a designated position (1 through 9) along the pile and inducing flexural waves at another designated position (1 through 9) with the hammer. The fixed-free pile tests were designated by the letter R with the hammer position and accelerometer positions being designated in that order by a numeral. For example, test R_{23} indicates a fixed-free pile test with the hammer located at position 2 and the accelerometer located at position 3. For each impact of the hammer, the FFT analyzer calculated and displayed the inertance frequency response function (FRF) between the hammer (input) and accelerometer (output):

$$\text{Inertance} = \frac{\ddot{U}(f)}{P(f)} \tag{4.1}$$

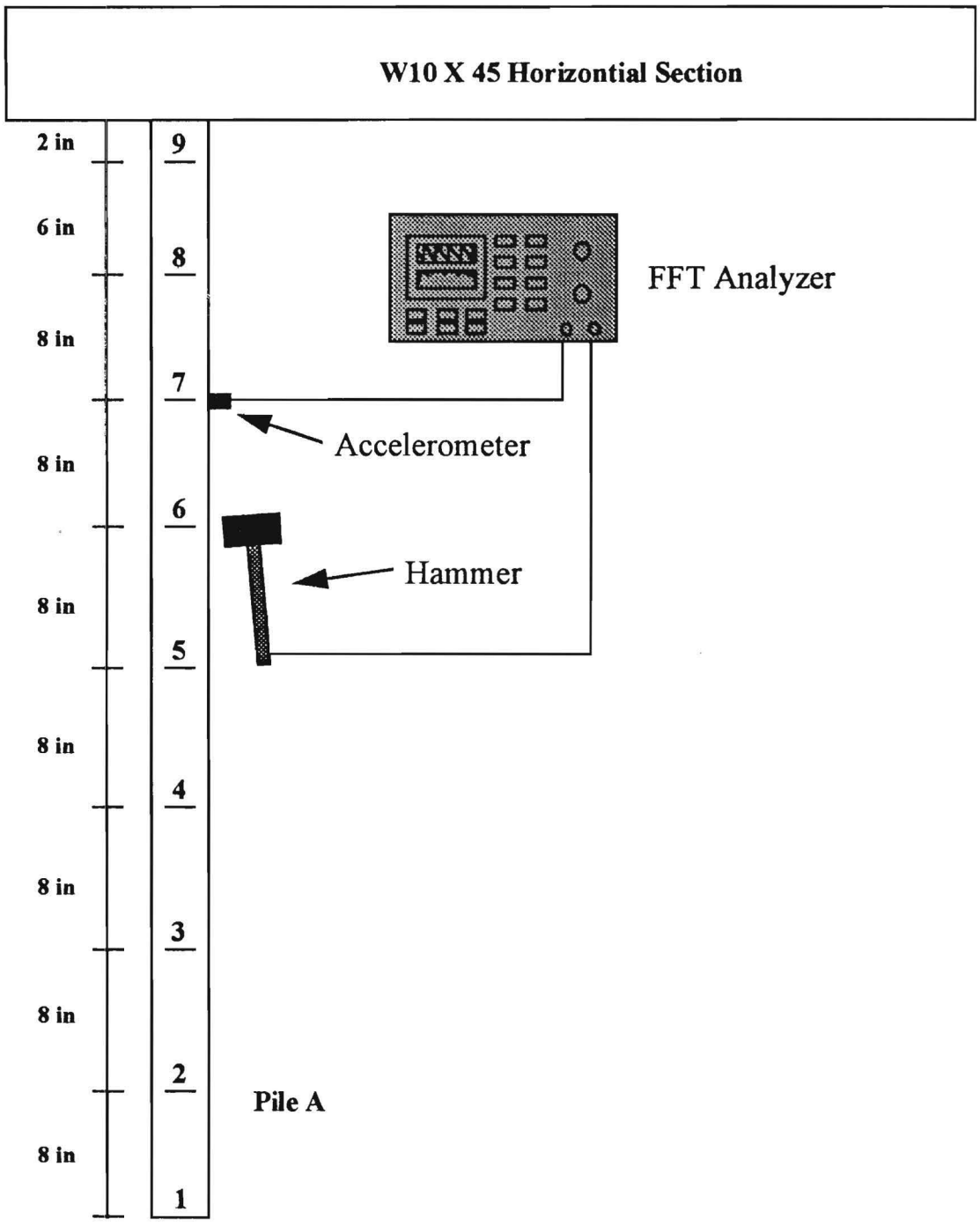

Figure 4.6 Test Configuration Used for Testing Pile A with Free End Condition

Five individual frequency response functions were averaged in the frequency domain to reduce the influence of random noise on the final measurement. Since the pile section (S3 x 5.7) is not symmetric, tests were performed in the direction of both the X-X axis and Y-Y axis. Figure 4.7 shows the orientation of the X-X and Y-Y axes with respect to the cross-section of the S3 x 5.7 pile.

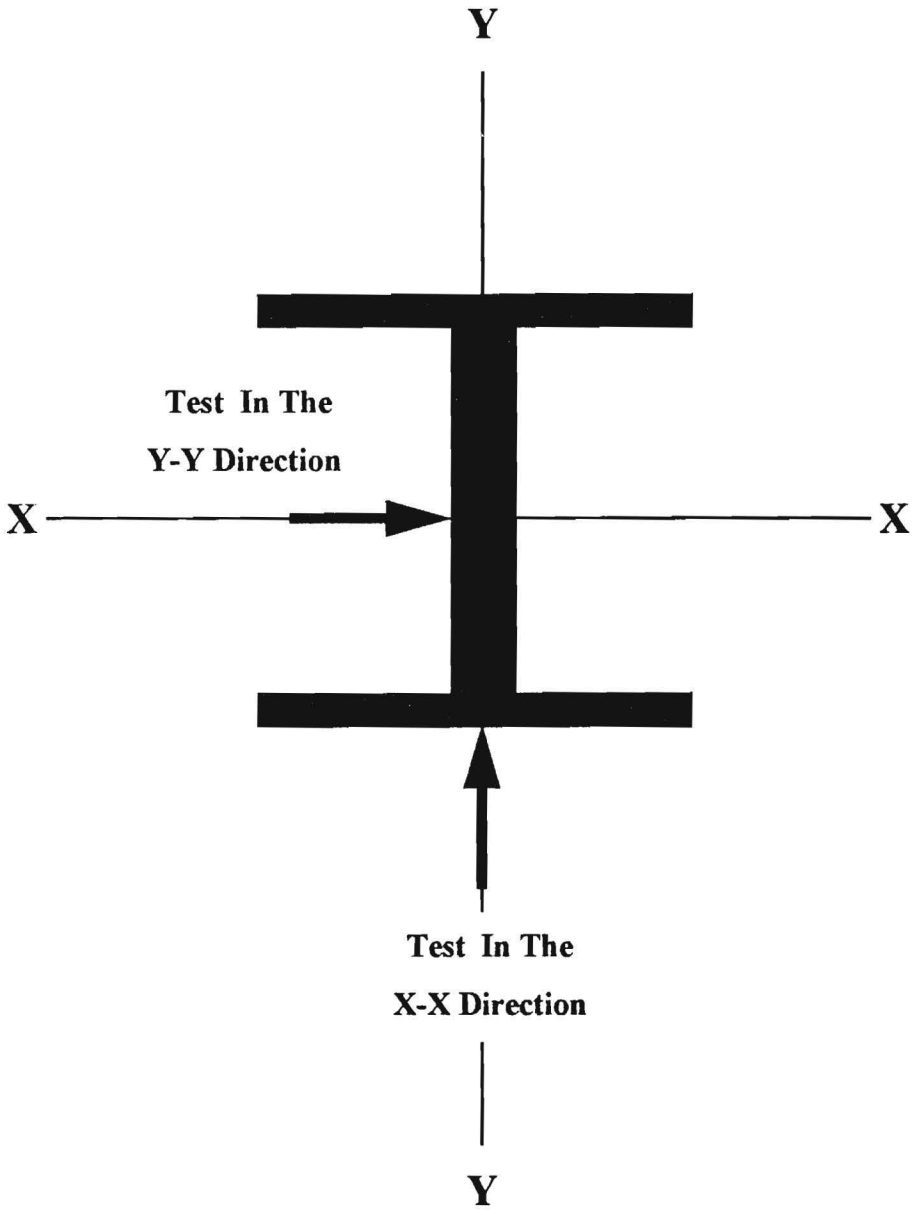

Figure 4.7 Definition of X-X and Y-Y Directions

Test Results

Figure 4.8 shows a typical frequency response function of Pile A with a free end condition. The source and receiver were both placed at Position 1 (R_{11}) and the pile was tested in the Y-Y direction. The magnitude plot is characterized by numerous sharp peaks corresponding to the natural frequencies of different modes of vibration of the pile. The first five flexural modes are labeled with numerals indicating the mode number. Three additional modes labeled as "Coupled" are spurious modes involving torsional and longitudinal motion. These modes arise because it is nearly impossible to strike the pile in such a way as to excite pure flexural modes.

Additional tests were performed with the source and receiver placed at different positions on the pile as described above. Figure 4.9 shows the frequency response function measured with the source at Position 2 and the receiver at Position 3 (R_{23}). Note that the amplitude of Modes 2 and 3 is greatly diminished in comparison with R_{11}. Modes 1, 4, and 5 as well as the coupled modes remain approximately the same as R_{11}. This difference is attributed to the mode shapes associated with each natural frequency. Figure 4.10 illustrates the mode shapes of the first five modes of vibration of a pile fixed at the upper end and free at the bottom. Note that Modes 2 and 3 have nodal points (points with zero deflection) at approximately the same positions as the source and receiver (63 in. and 54 in. from the top of the pile, respectively). Thus, Mode 2 is not strongly excited by the source placed at Position 2 (63 in. from the top of the pile). Similarly, the receiver at Position 3 (54 in. from the top of the pile) is not well placed to measure the response of the pile associated with Mode 3.

To provide the best opportunity for all of the modes to be excited and measured, measurements were performed at 45 different combinations of source and receiver positions along the length of the pile. A "matrix of frequency response measurements" was used to organize the test program. Each row of the matrix corresponds to a single source position and each column corresponds to one receiver position. Maxwell's reciprocal theorem states that "the displacement at point i due to a unit load at another point j is equal to the displacement at point j due to unit load at point i, provided that the displacements and forces 'correspond,' i.e., that they are measured in the same direction at each point" (Fung, 1964). Thus, the frequency response function R_{23} should be the same as R_{32} and, in general, the matrix of frequency response functions will be symmetric. Figure 4.11 shows the comparison of R_{23} and R_{32}. The two frequency response functions are approximately equal. Comparisons for other source and receiver positions yielded similar agreement. As a result, only the lower diagonal of the matrix of frequency response functions was measured to minimize testing time.

Figure 4.12 shows all 45 frequency response measurements for Pile A. Each "waterfall" plot in Figure 4.12 contains the frequency response functions measured at the 9 different receiver locations for a common source position. Plotting several frequency response functions in this way allows trends in natural frequencies, etc. to be more easily observed.

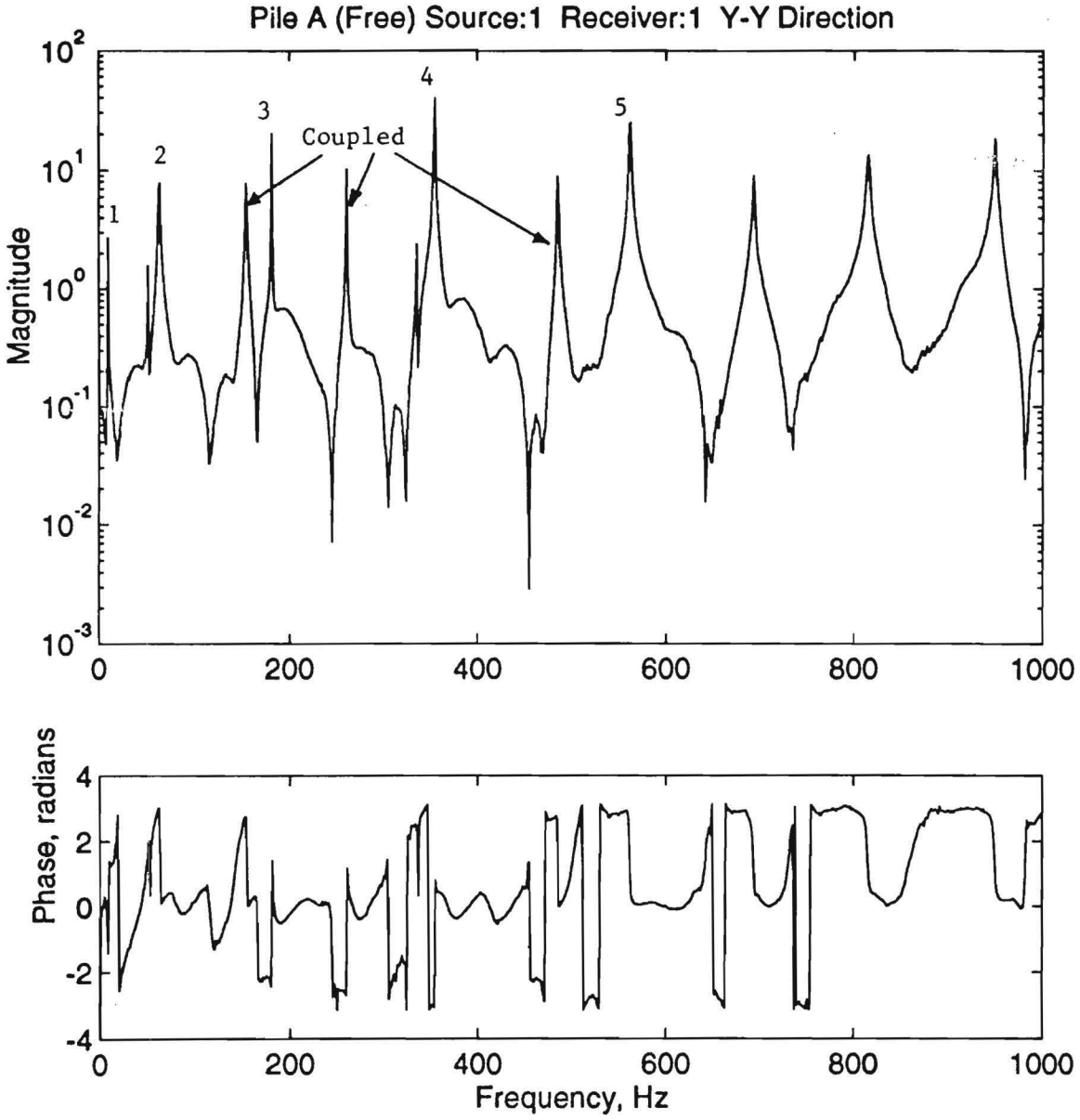

Figure 4.8 Frequency Response Function (R_{11}) for Pile A with Free End Condition

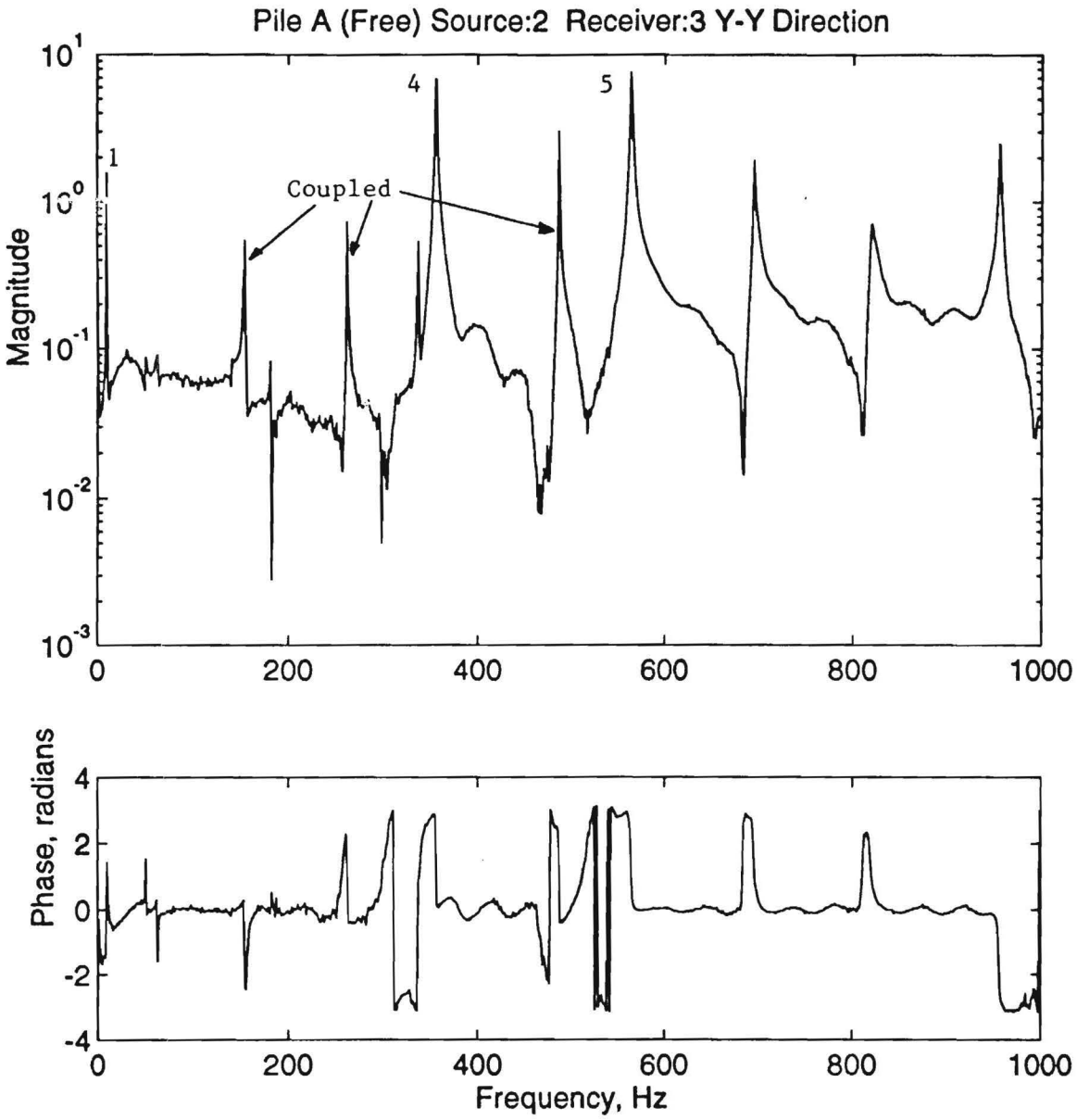

Figure 4.9 Frequency Response Function (R_{23}) for Pile A with Free End Condition

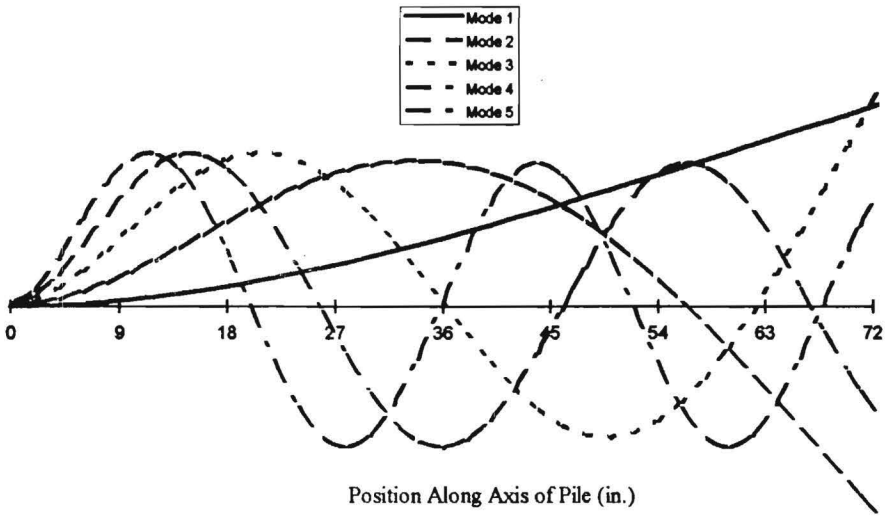

Figure 4.10 Mode Shapes of a Fixed-Free Pile

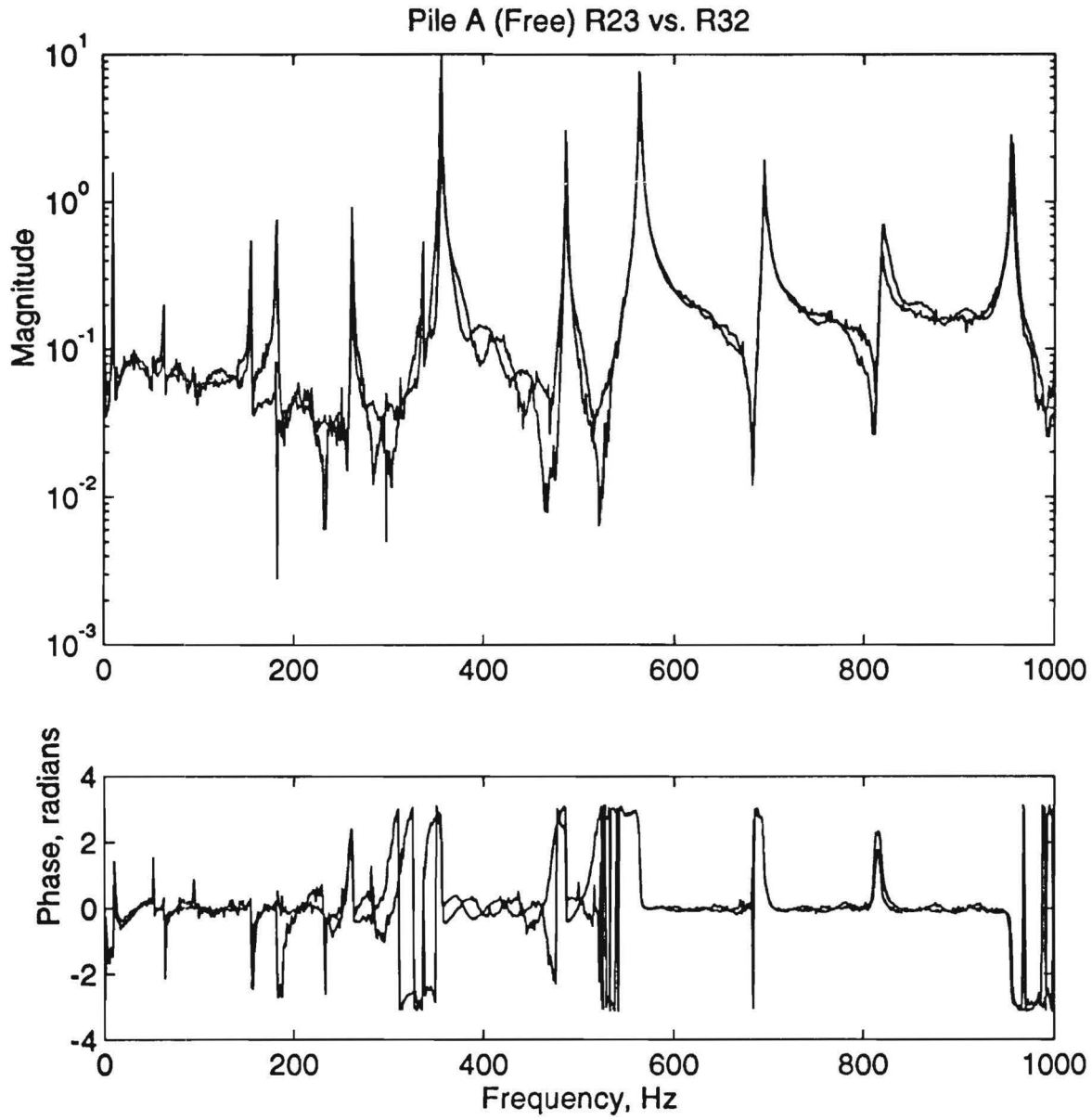

Figure 4.11 Comparison of Frequency Response Functions for Pile A with Free End Condition

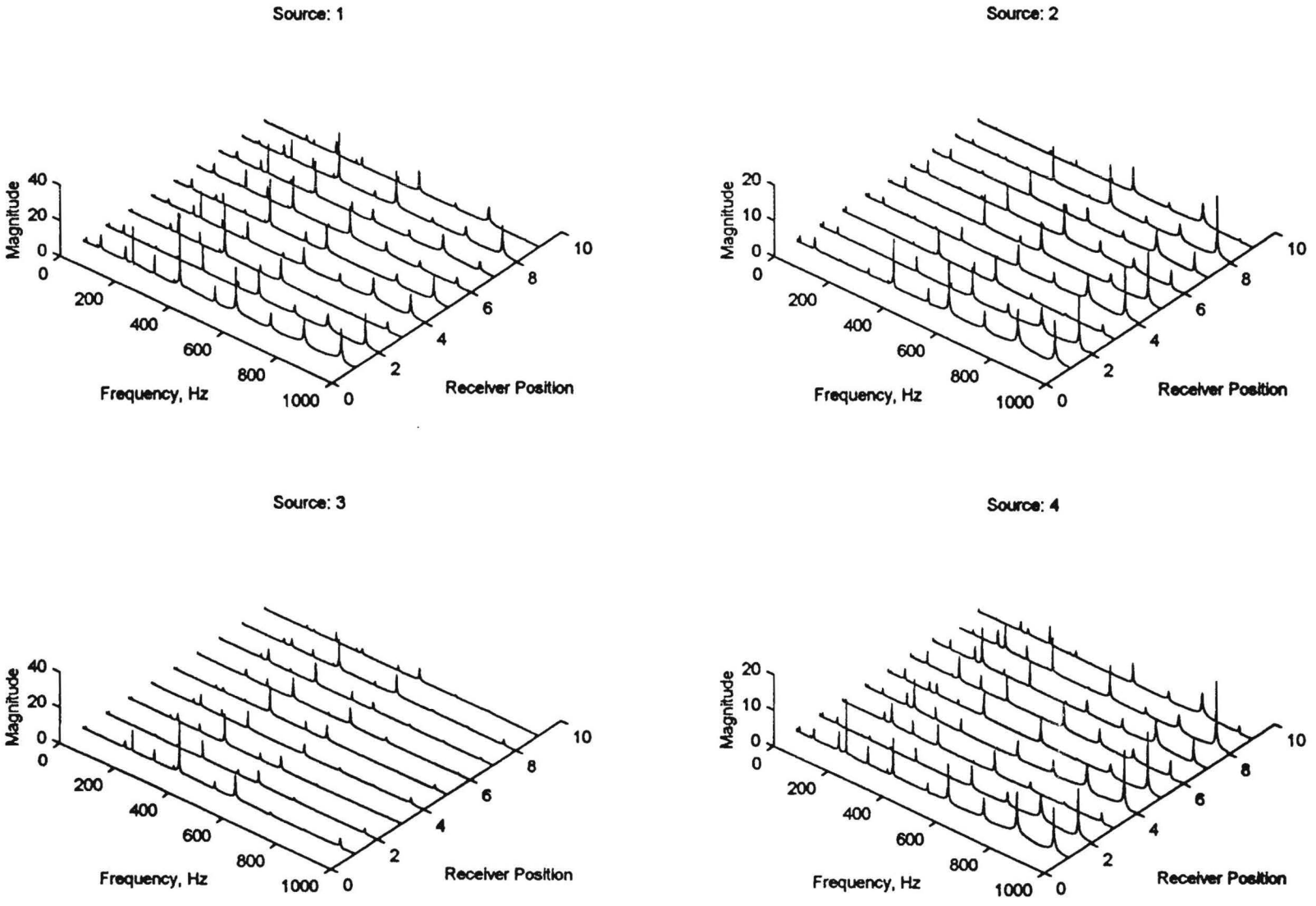

Figure 4.12 Waterfall Plots for Pile A with Free End Condition

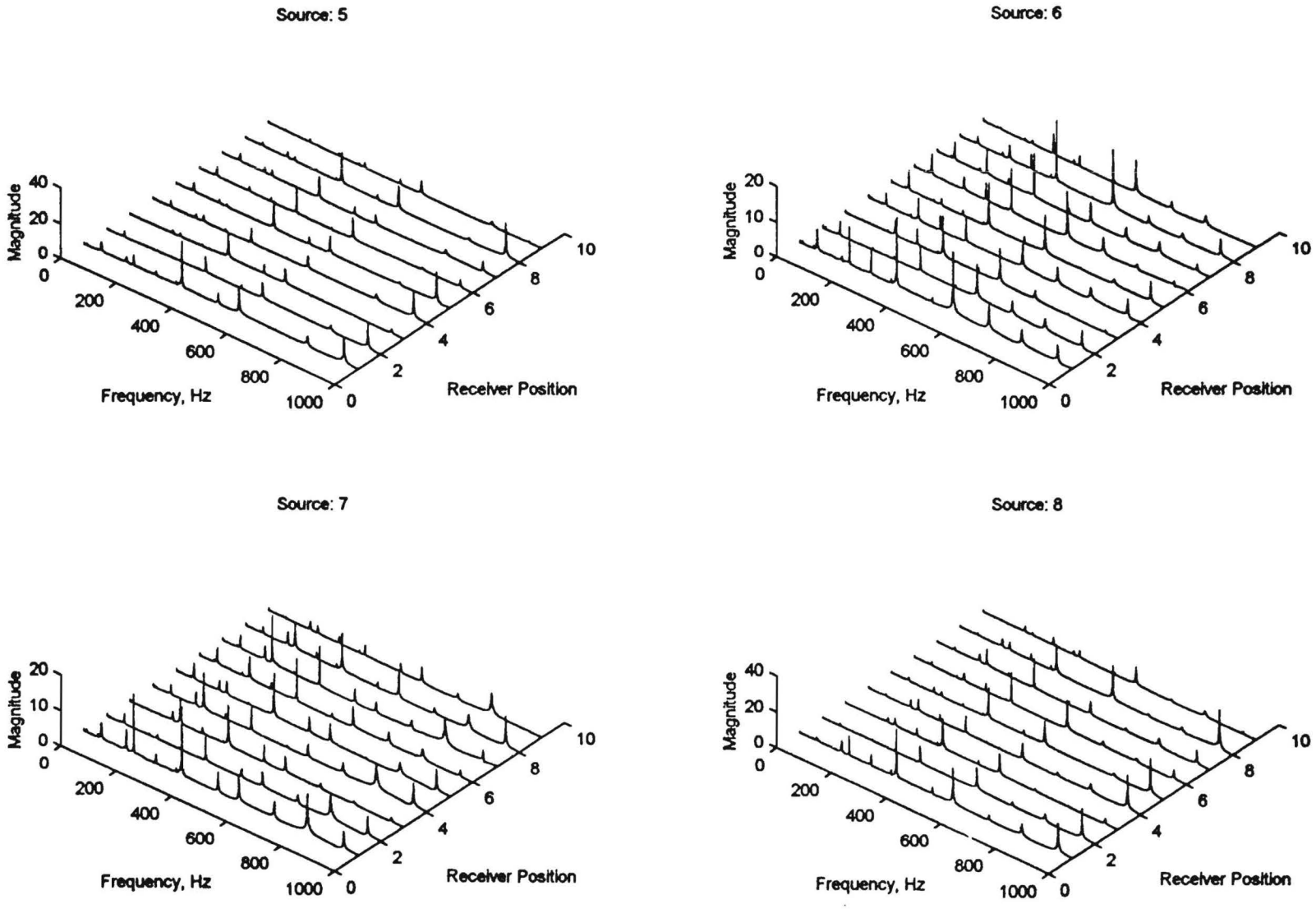

Figure 4.12 Waterfall Plots for Pile A with Free End Condition (continued)

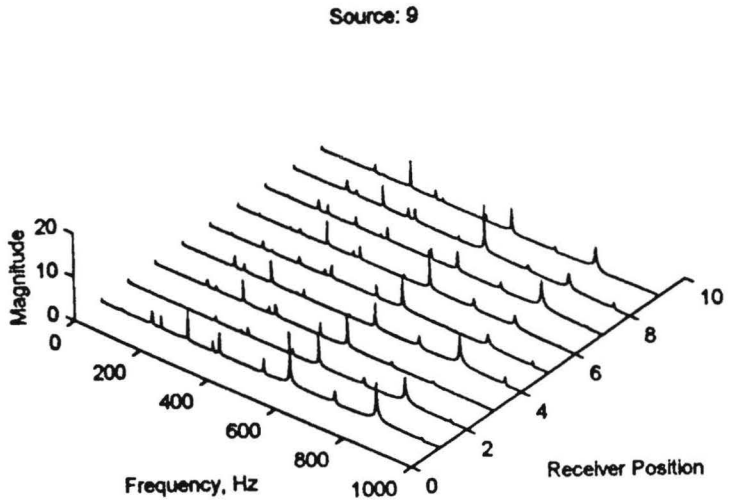

Figure 4.12 Waterfall Plots for Pile A with Free End Condition (continued)

Comparison of Experimental, Analytical, and Numerical Results on Fixed-Free Piles

Table 4.1 shows a comparison between the natural frequencies in both the X-X and Y-Y directions for the experimental, analytical, and numerical results. The analytical and numerical values were obtained using a fixed boundary condition at the upper end of the pile.

Table 4.1 Comparison of Experimental, Analytical, and Numerical Results on Fixed-Free Piles with Fixed End Condition

	Natural Frequency (Hz)		
Mode of Vibration	Experimental	Analytical	Numerical
Y-Y Direction			
1	10.0	11.2	11.2
2	63.3	70.0	70.1
3	181.3	196.0	196.4
4	356.0	384.1	384.9
5	564.0	634.9	636.2
X-X Direction			
1	22.5	26.3	26.34
2	155.7	165.1	165.1
3	390.0	461.2	462.2
4	760.0	903.9	905.7
5	1150.0	1494.2	1497.2

Both the analytical and numerical analyses yield natural frequencies that are larger than those observed experimentally. The difference becomes larger at higher frequencies (higher modes). The finite element model used must be refined somewhat to more closely approximate the natural frequencies of the experimental system. The fixed boundary condition at the top of the beam in the finite element model results in the system more stiff than its experimental counterpart. The finite element boundary condition was changed to two "pinned" connections in the locations of the welds. As a result, the rotational stiffness is a function of the elements themselves, rather than infinite as for the fixed connection. Translational

stiffness will remain infinite. Table 4.2 shows the comparison of the experimental and numerical solutions with the pinned end condition. (Note that the analytical solution could not be calculated for this more complex boundary condition.) The match between experimental and numerical values is improved, suggesting that the pinned connections model the actual end conditions more accurately. As such, pinned connections are used in all subsequent modeling of embedded piles.

Table 4.2 Comparison of Experimental, Analytical, and Numerical Results on Fixed-Free Piles with Pinned End Condition

	Natural Frequency (Hz)		
Mode of Vibration	Experimental	Numerical	Error
Y-Y Direction			
1	10.0	10.4	4%
2	63.3	66.1	4%
3	181.3	187.5	3%
4	356.0	363.9	2%
5	564.0	599.3	6%
X-X Direction			
1	22.5	23.8	5%
2	155.7	148.0	-5%
3	390.0	401.9	3%
4	760.0	750.6	-1%
5	1150.0	1168.7	2%

Tests on Embedded Piles

Following the tests performed on Pile A with a free end condition, the test facility was backfilled with sand to simulate embedded piles. The following sections describe the properties of the sand and the methods used to compact the soil around the piles. Note that for these tests "perfect insertion" was used (i.e., the sand was compacted around the pre-placed piles) rather than driving the piles as is usually the case.

Sand Fill

The sand that was used for fill in this testing is a Chattahoochee River sand. The sand was visually classified as a white-tan, medium to fine, poorly graded, micaceous sand (SP). The grain size distribution for the sand is presented in Figure 4.13. The maximum dry density of the sand was determined by ASTM D 4253-93. The average dry density of the six tests was 98.6 pcf. The minimum density of the sand was determined using ASTM D 4254 - 91. Three tests were performed using Methods A and B of this standard. The average minimum density from the six tests was 80.8 pcf.

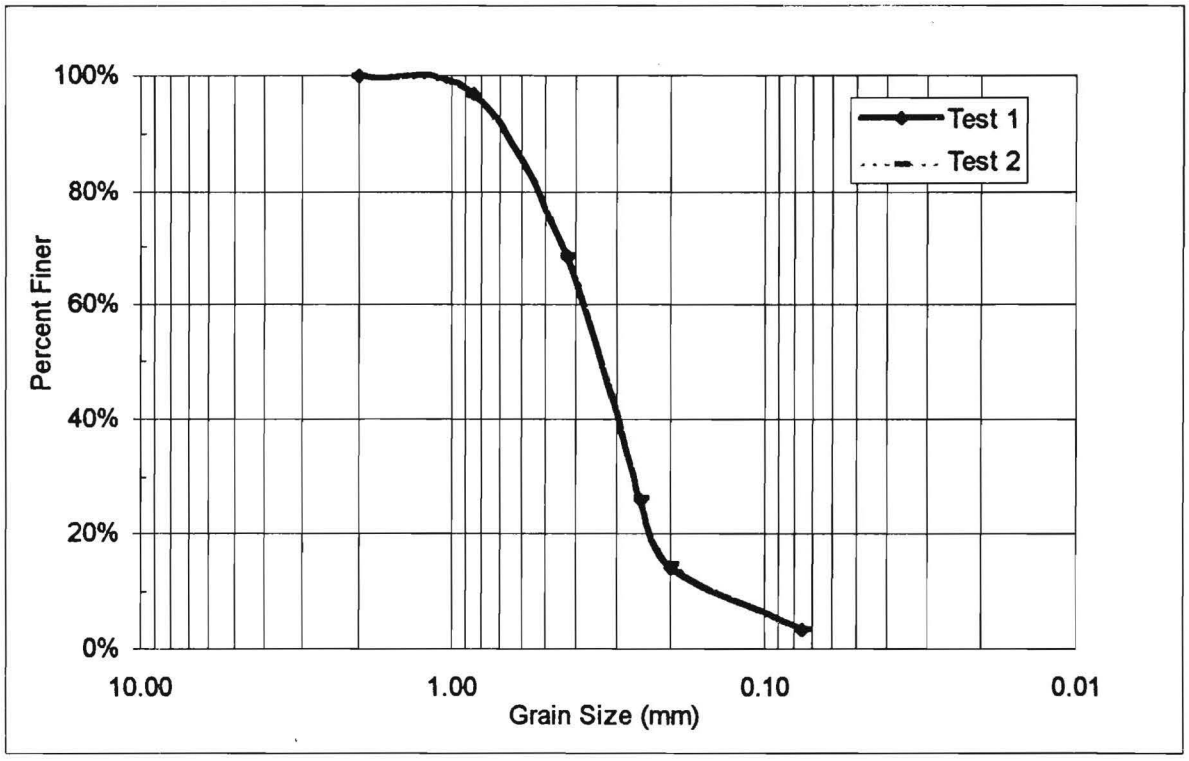

Figure 4.13 Grain Size Distribution for Chattahoochee River Sand

Sand Placement

The sand was placed in 6-in. thick lifts. The lifts were compacted with a Wacker Corporation vibratory plate compactor with a plate size of approximately 18-in. square. This size compactor enabled the operator to carefully maneuver it around each of the test pile sections so that the sand could be more uniformly compacted. This was especially important since the nature of the pile-sand interface influences the attenuation of the flexural waves. The lifts were compacted to greater than 95 percent of the maximum dry density of the sand. Density control tests were performed with a nuclear moisture-density gauge.

Test Configuration and Equipment

The test configuration and equipment were similar to those used for testing the fixed-free pile. Figure 4.14 shows the numbering scheme used to perform frequency response measurements. The source and receiver were placed at one of nine positions along the length of the pile. Tests were performed in both the X-X and Y-Y directions. As in the case of the fixed-free piles, a matrix of frequency response measurements was developed to organize the measurements.

Test Results

Figure 4.15 shows a typical frequency response measurement for an embedded pile. The measurement was performed in the Y-Y direction on Pile A with both the source and receiver at position 1. Like tests performed on the fixed-free piles, the frequency response is characterized by several peaks corresponding to different modes of vibration of the pile. At higher frequencies, the peaks are more rounded as a result of higher damping attributed to the surrounding soil. To excite and measure as many modes as possible, the frequency response measurements were repeated at 45 different combinations of source and receiver positions. Figure 4.16 shows the results of these measurements using the waterfall format introduced previously.

Similar sets of measurements were obtained on the other 9 small-scale piles. An example of the difference in frequency response measurements from the 10 small-scale piles is shown in Fig. 4.17. The figure contains the frequency response measurement in the Y-Y direction with the source and receiver at position 1 for all 10 piles. Qualitatively, the response of Piles A through F appears similar. The primary difference between these piles is the embedded length. Pile A has the least embedment (1 ft) and Piles E and F have the largest embedment (5 ft). Pile F also simulates an "end bearing" pile whereas Pile E is "floating." The frequencies at which the peak responses occur are similar (but not identical). Another difference is in the width of the peaks; the peaks appear to broaden as pile embedment increases. This is expected since greater embedment will result in additional damping of each mode of vibration. Piles G and H are encased. The casing clearly influences the frequency response. It is not known why the response of Pile H differs substantially from that of Pile G. Pile I and J differ in cross section (W4 x 13) compared to the other 8 piles (S3 x 5.7). Pile I is embedded 2 ft and Pile J is embedded 4 ft. Both frequency responses are qualitatively similar. It is important to note that comparisons involving other source and receiver locations or the X-X direction may yield different information than that drawn from Figure 4.17.

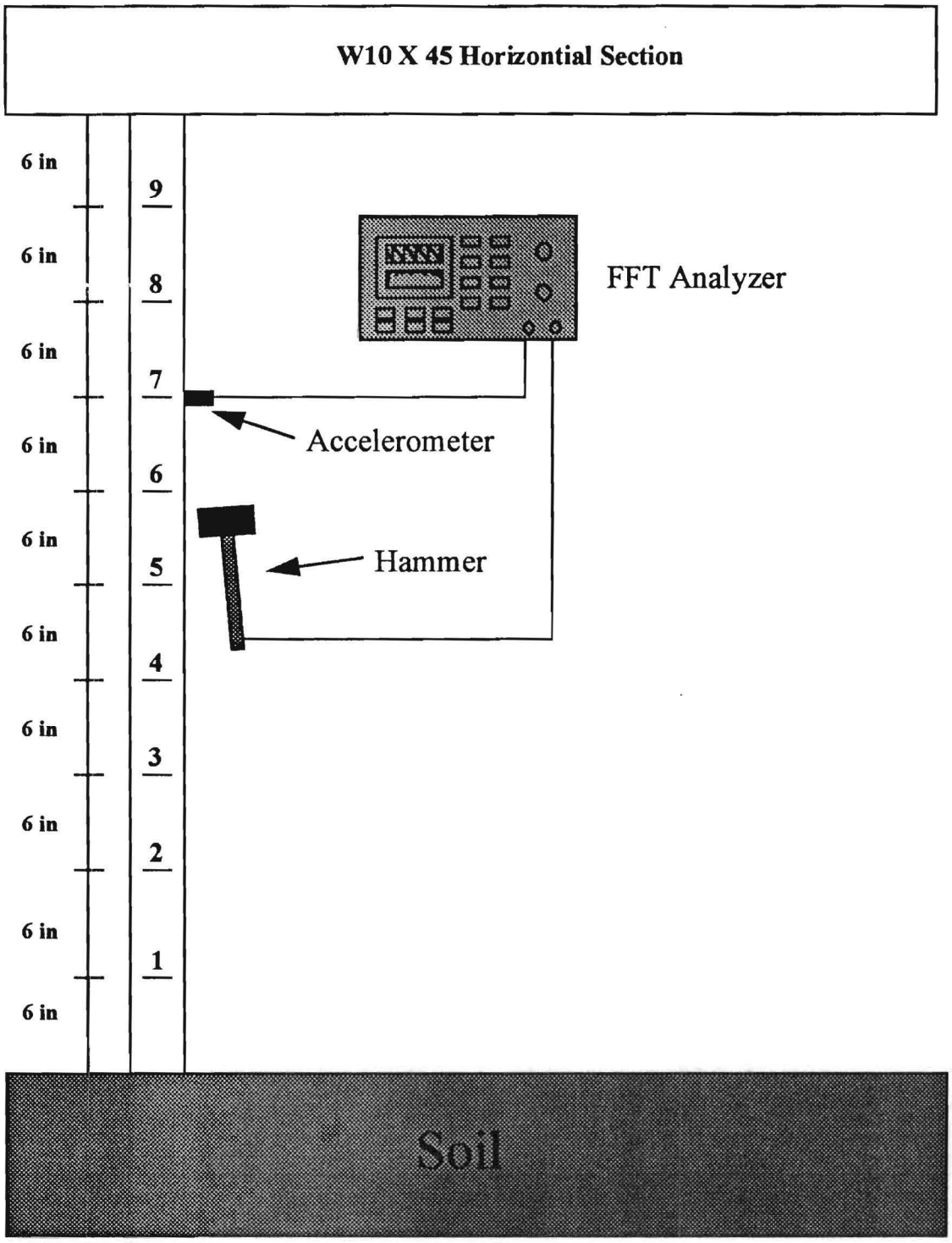

Figure 4.14 Test Configuration Used for Embedded Piles

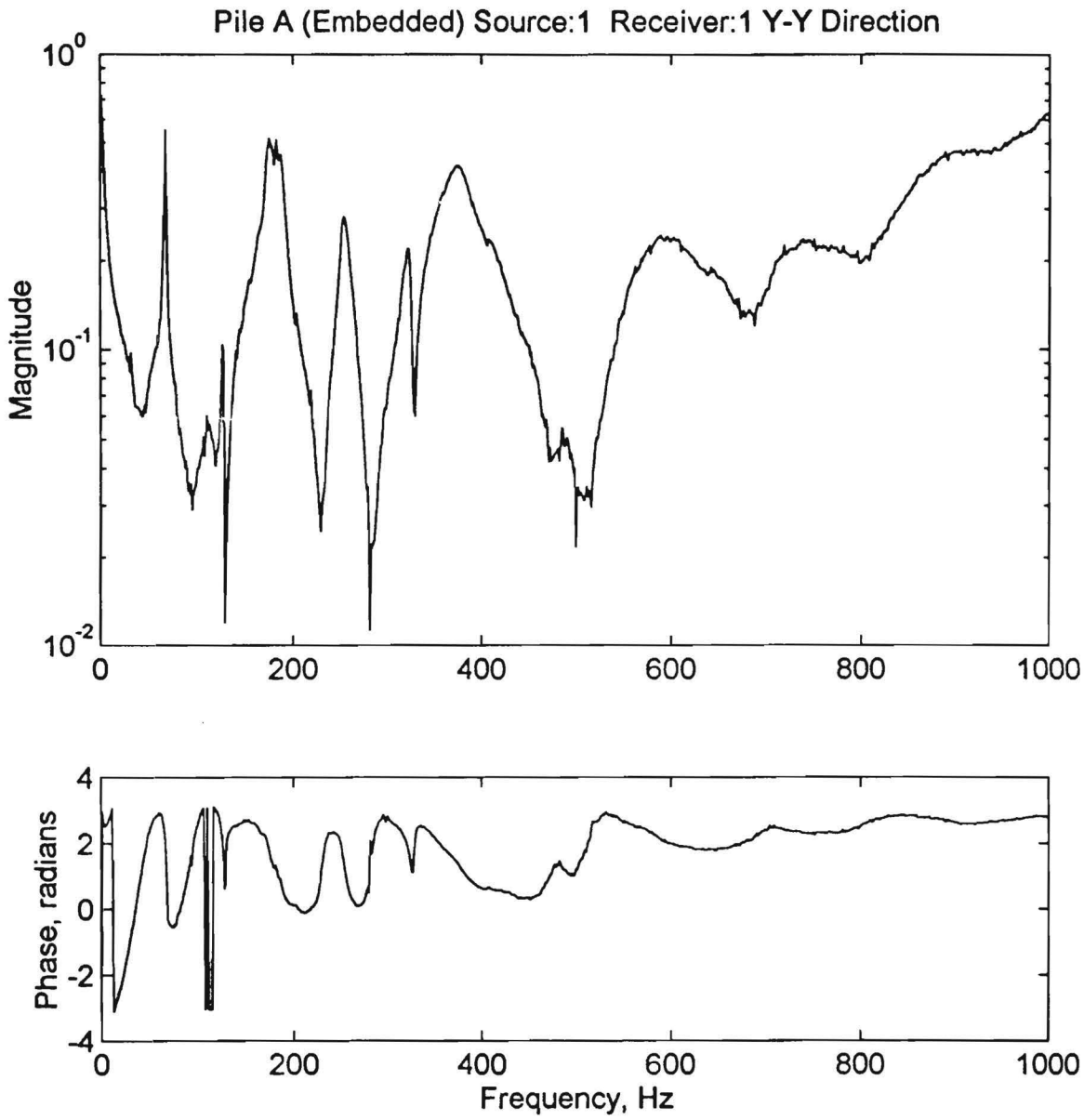

Figure 4.15 Frequency Response Function (R_{11}) for Pile A with Embedded End Condition

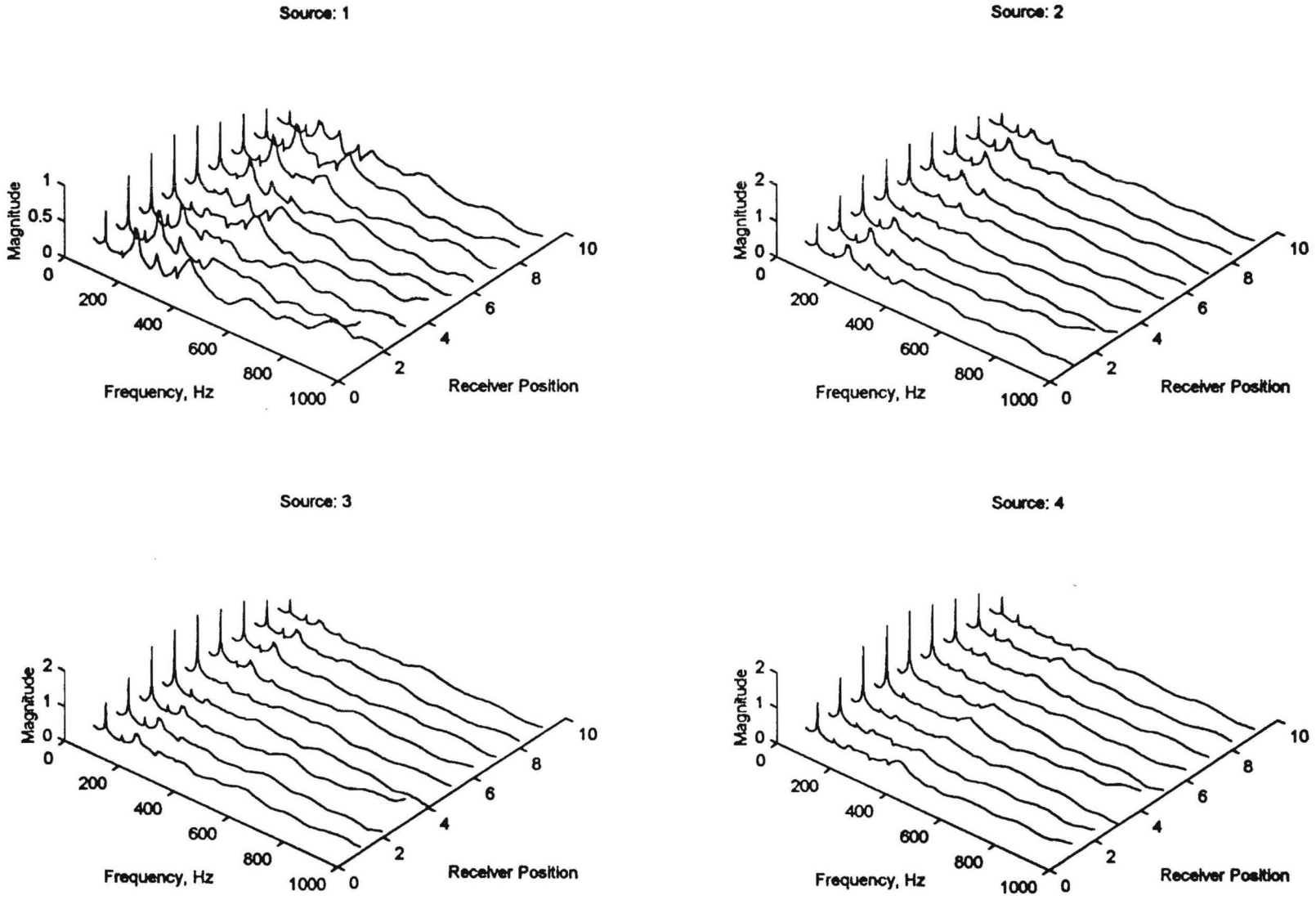

Figure 4.16 Waterfall Plots for Pile A with Embedded End Condition

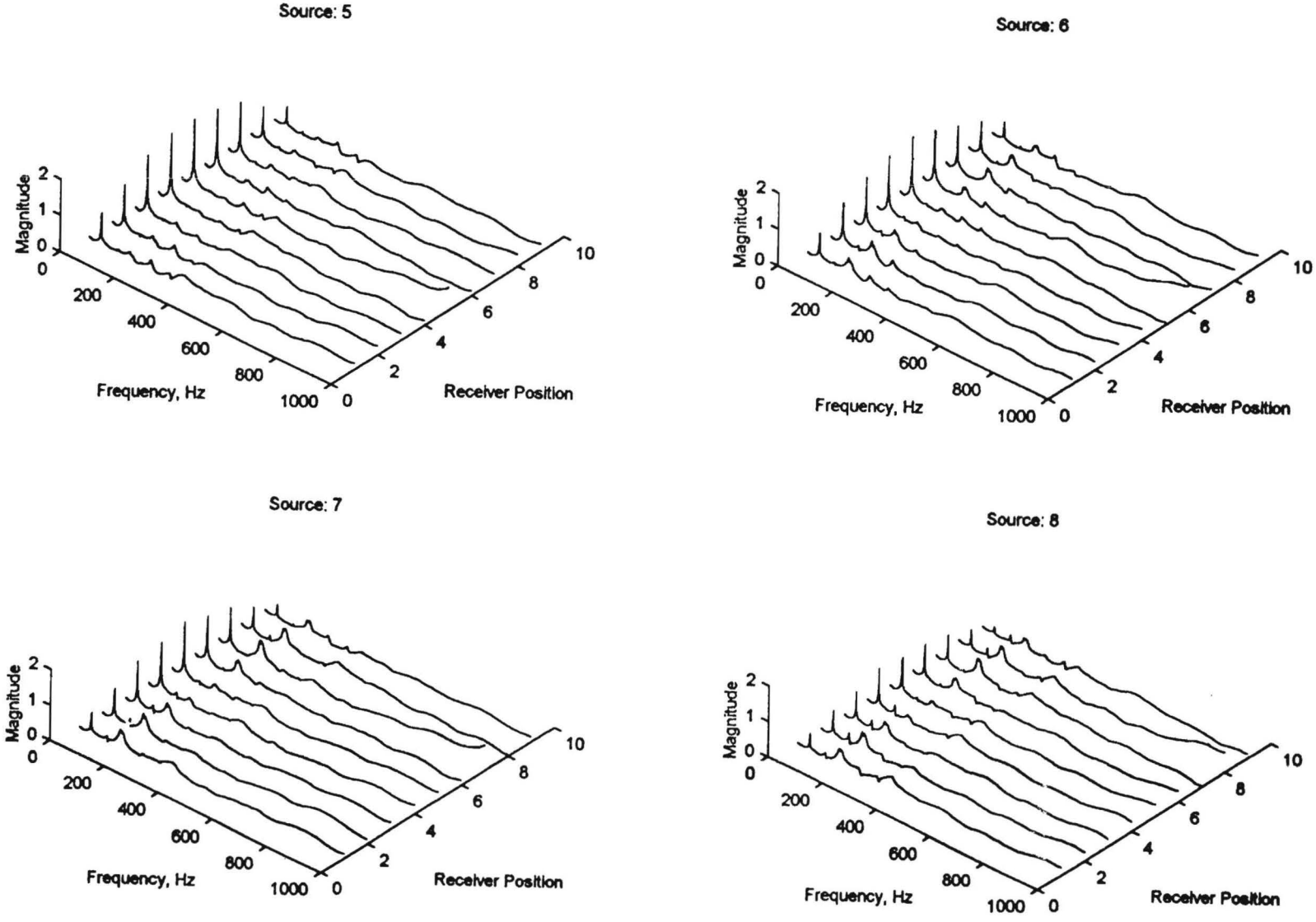

Figure 4.16 Waterfall Plots for Pile A with Embedded End Condition (continued)

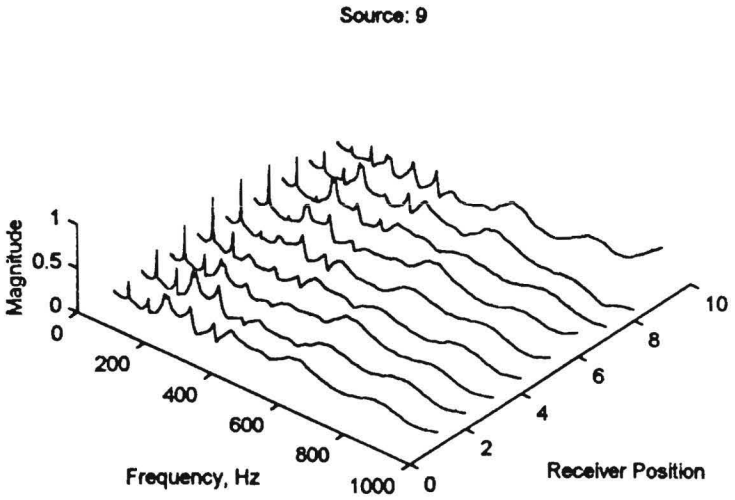

Figure 4.16 Waterfall Plots for Pile A with Embedded End Condition (continued)

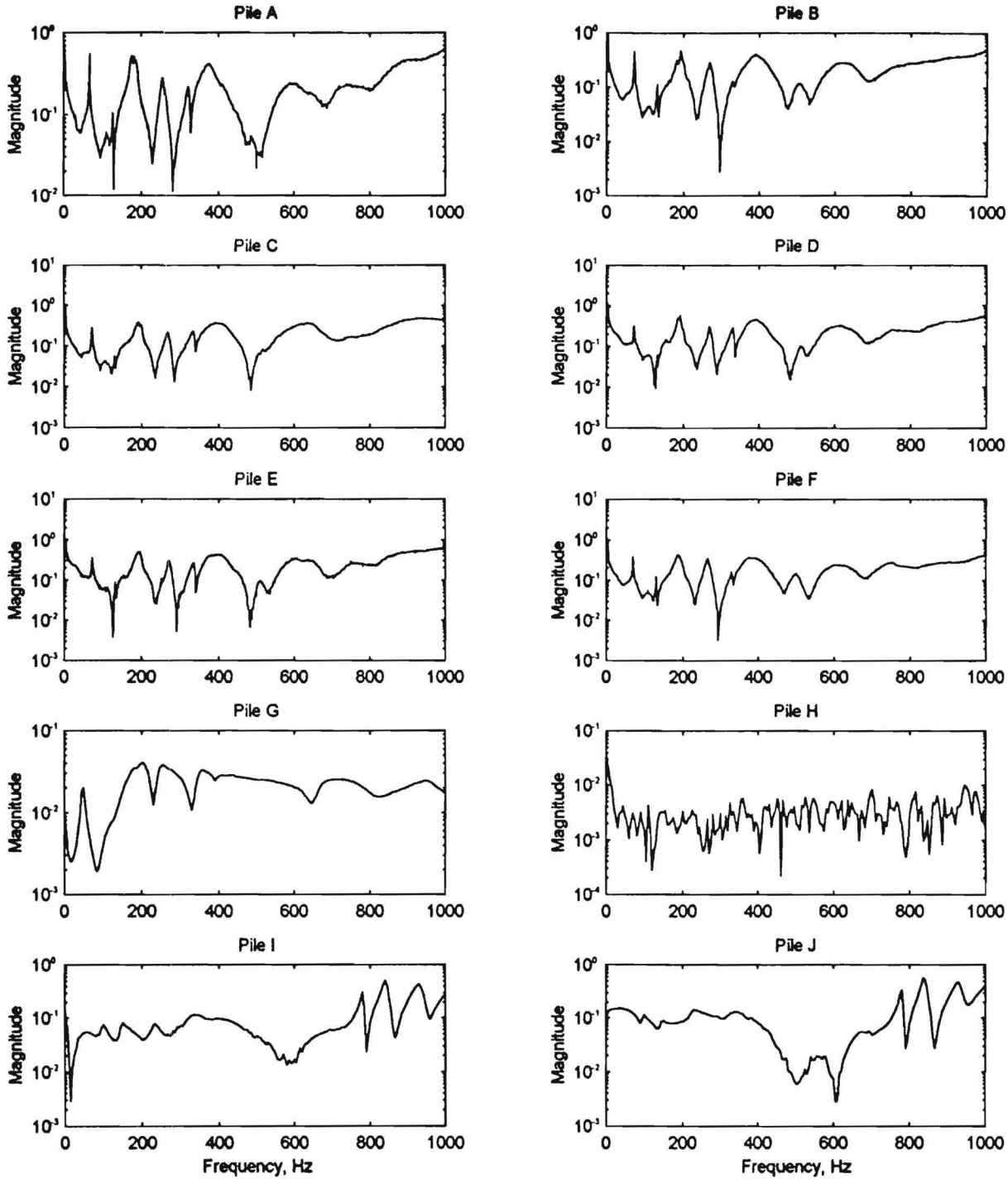

Figure 4.17 Comparison of Frequency Response Functions for Embedded Piles

Comparison of Experimental and Numerical Results on Embedded Piles

Finite element analyses were performed to model the response of embedded piles. The soil reactions in the finite element model are modeled through the use of Winkler springs (Novak et al., 1978). Figures 4.18 and 4.19 show several examples of the comparison between experimental and numerical frequency response functions. Three arbitrarily selected source-receiver combinations are presented for Pile A (Figure 4.18) and Pile E (Figure 4.19). Both figures are for measurements in the Y-Y direction. To facilitate comparison between the experimental and numerical data, the magnitude of each frequency response function was normalized to a maximum value of one. This normalization is necessary because of the different units used for the experimental (volts/volt) and numerical (in^2/sec/lb.) frequency response functions.

At frequencies less than approximately 300 to 400 Hz, the numerical frequency response functions match the predominant peaks in the experimental frequency response functions reasonably well. Many of the peaks which are present in the experimental data but not in the numerical data can be attributed to spurious modes of vibration resulting from longitudinal and torsional motion as discussed previously. In the finite element analyses, the piles were modeled as prismatic members with the same area moments of inertia as the corresponding S or W section. Thus, the finite element analyses are not able to model these other modes of vibration that occur in the actual pile. At frequencies greater than 300 to 400 Hz, the experimental frequency response functions yield larger magnitudes than the numerical frequency response functions.

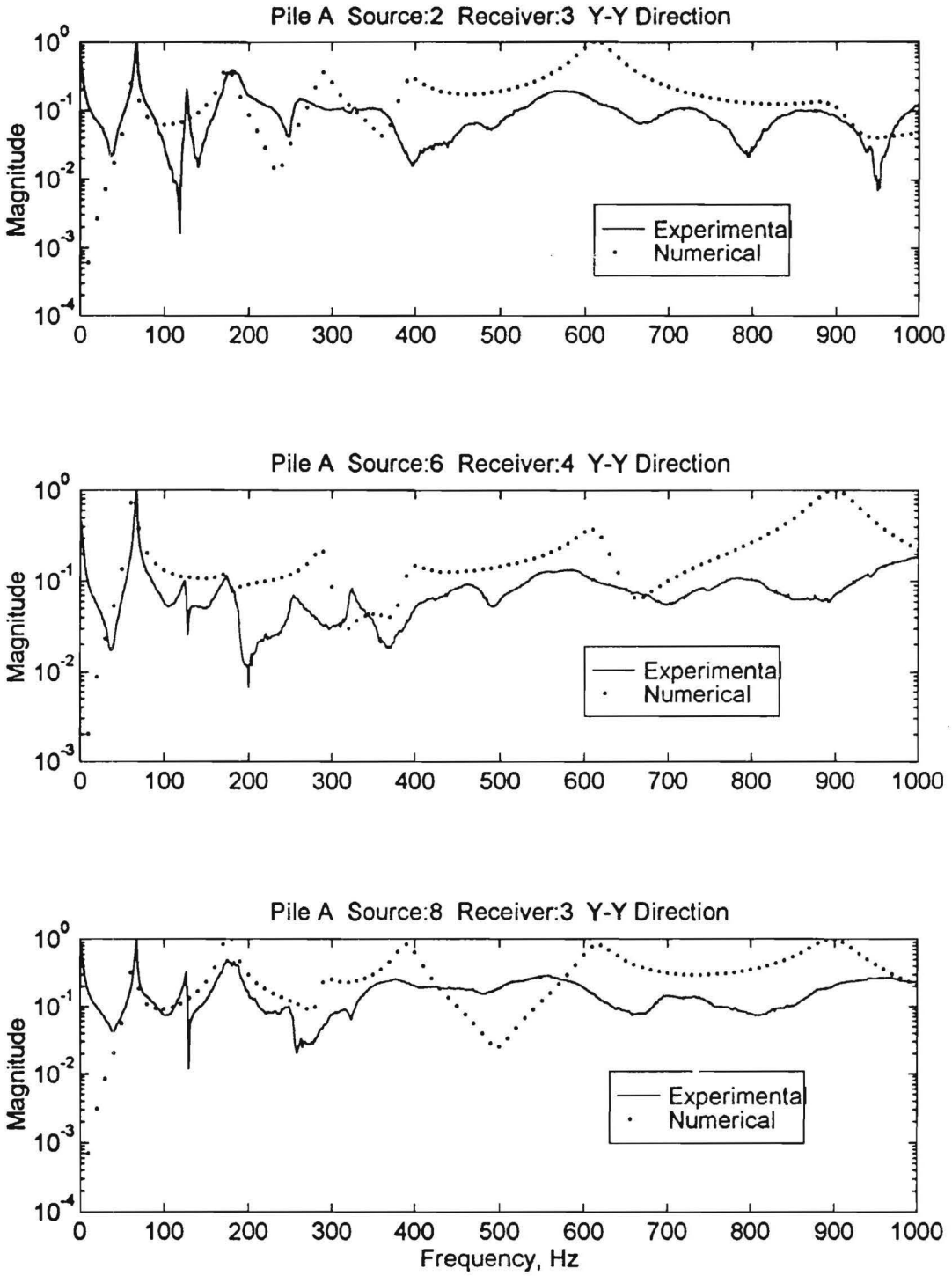

Figure 4.18 Comparison of Experimental and Numerical Frequency Response Functions for Pile A

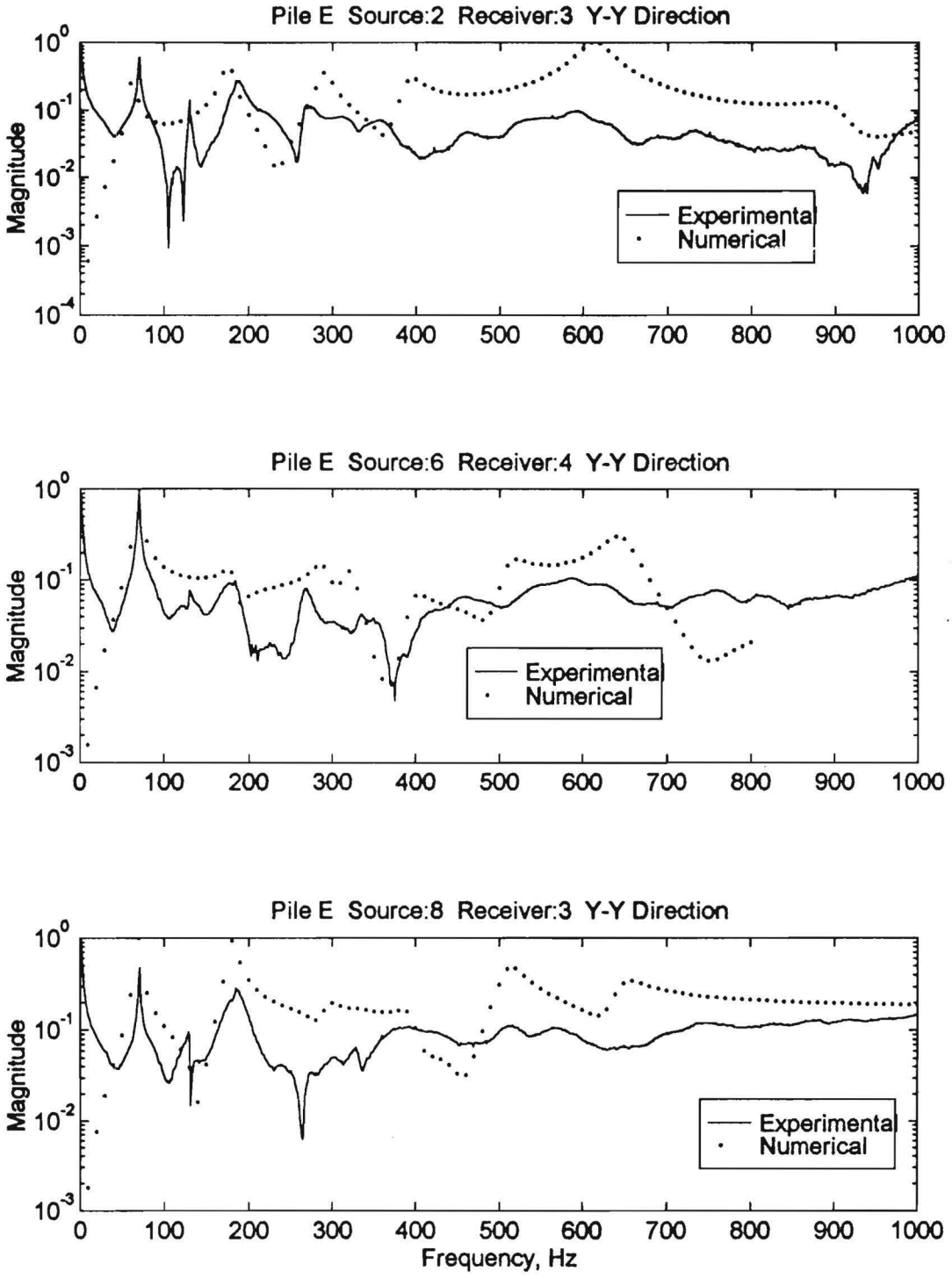

Figure 4.19 Comparison of Experimental and Numerical Frequency Response Functions for Pile E

5 Tests on Full-Scale Piles

Following the tests on the small-scale piles, a full-scale bridge was selected to perform additional nondestructive flexural wave tests. The purpose of the full-scale test was to evaluate the test method under more realistic field conditions.

Bridge Site

The bridge site is located on Merck Road over Camp Creek in southwest Fulton County, Georgia. As-built plans and pile tip elevations of the bridge were provided by the Georgia Department of Transportation. A photograph of the bridge is shown in Figure 5.1.

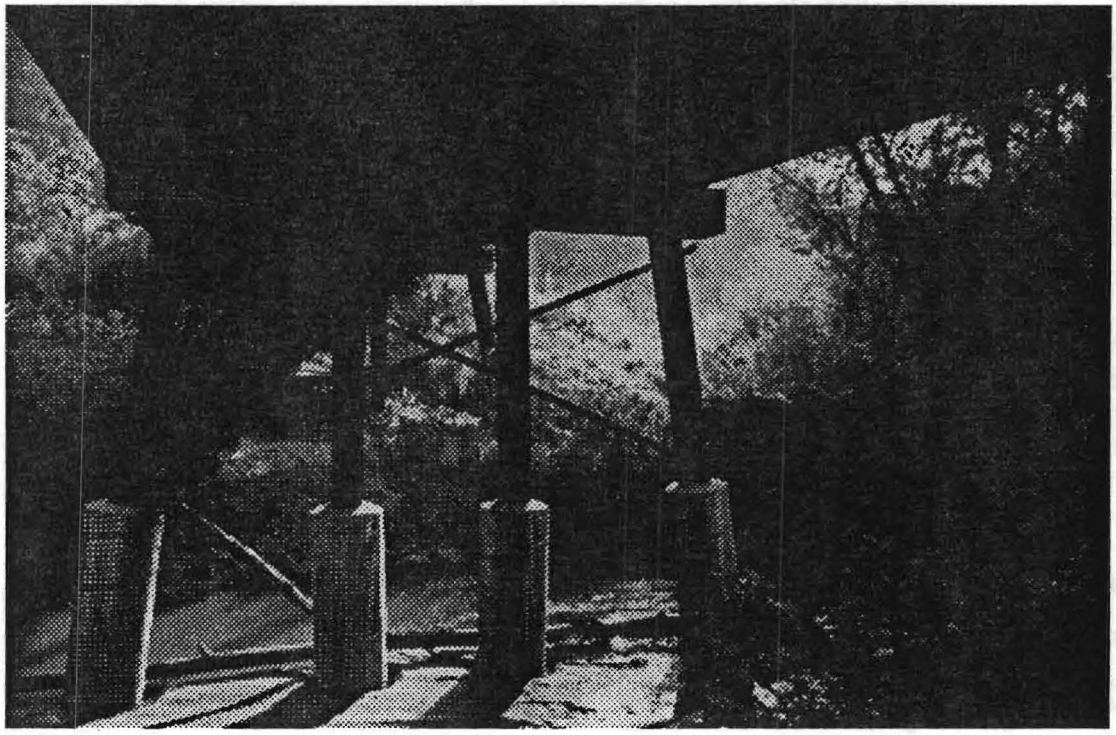

Figure 5.1 Bridge at Merck Road over Camp Creek

The bridge runs in a north-south direction and is supported by 6 bents with 4 piles per bent. The abutment bent piles are HP 10 x 57 sections and the intermediate bent piles are HP 14 x 73 sections. The bents are designated by numbers form 1 to 6 with Bent 1 starting numerically at the south abutment to Bent

6 at the north abutment. The bent piles are numbered from 1 to 4 from left to right as viewed by an observer facing north. Bent 4 is located in the channel of Camp Creek and the piles are encased in concrete (Bent 4 is shown in Figure 5.1). The concrete casements are made of 3-ft diameter corrugated steel pipe placed around the pile and filled with concrete. Bent 4 also had cross or sway bracing that connects the four piles to each other.

Test Setup

Field tests were performed on Pile 2 of both Bents 3 and 4. Bent 3 is on the bank of Camp Creek, and thus was not surrounded by water. Although Bent 4 was in the stream channel, there was such low flow on the day that testing was performed that the water level did not interfere with the tests.

The test configurations for the pile are shown in Figures 5.2 and 5.3. A photograph of the test equipment is shown in Figure 5.4. The pile response was measured with a Wilcoxon Research Model 728T piezoelectric accelerometer. The Model 728T is more sensitive than the Model 732A used in the scale model testing, and thus was able to record the smaller amplitude vibrations more reliably. This accelerometer has a traceable frequency response range of 1 Hz to 12 kHz. The calibration voltage sensitivity for this accelerometer is 517 mV/g. The accelerometer was attached to the pile using the same magnetic mounting base as described in Chapter 4. The hammer (source) used for the field testing was a PCB Piezotronics, Inc. Model GK291B50 modally tuned hammer with a built-in force transducer. The hammer is approximately the size of a large sledge hammer and weighs 12 lb. It has a force range of 0 to 5000 lb. This hammer has a calibrated sensitivity of 1 mV/lbf. The larger hammer also has 3 tips that can be attached to the built-in force transducer. The hard tip (#084A33) was used for all of the field measurements to excite higher natural frequencies. The field measurements were recorded by a Hewlett Packard Model 3560A Dynamic Signal Analyzer. The HP Model 3560A was used, instead of the HP Model 3562A, since it is battery operated and is much more portable than the HP Model 3562A. The HP 3560A was set up exactly as the HP 3562A was for the scale model testing as described in Chapter 4. The HP 3560A has built-in storage to which the measurements could be saved and transferred later to a personal computer.

Test Method

The test method used for the field testing was similar to that of the scale model tests. The positions of the source and receiver were varied on each pile depending on the length of exposed pile. Figure 5.2 shows that Pile 2 on Bent 3 had 10 ft of exposed pile length between the pile cap and the ground line. The source and receiver locations were placed at 1 ft increments and were labeled from 1 at the top to 10 near the ground line. Figure 5.3 shows the measurement locations for Pile 2 on Bent 4. The test measurements were performed up to 6 ft above the pile casement. The test were performed by standing on the pile casement and inducing the flexural waves into the steel pile. The tests were performed only up to 6 ft since accessibility was limited without a longer ladder or a truck with boom attachment.

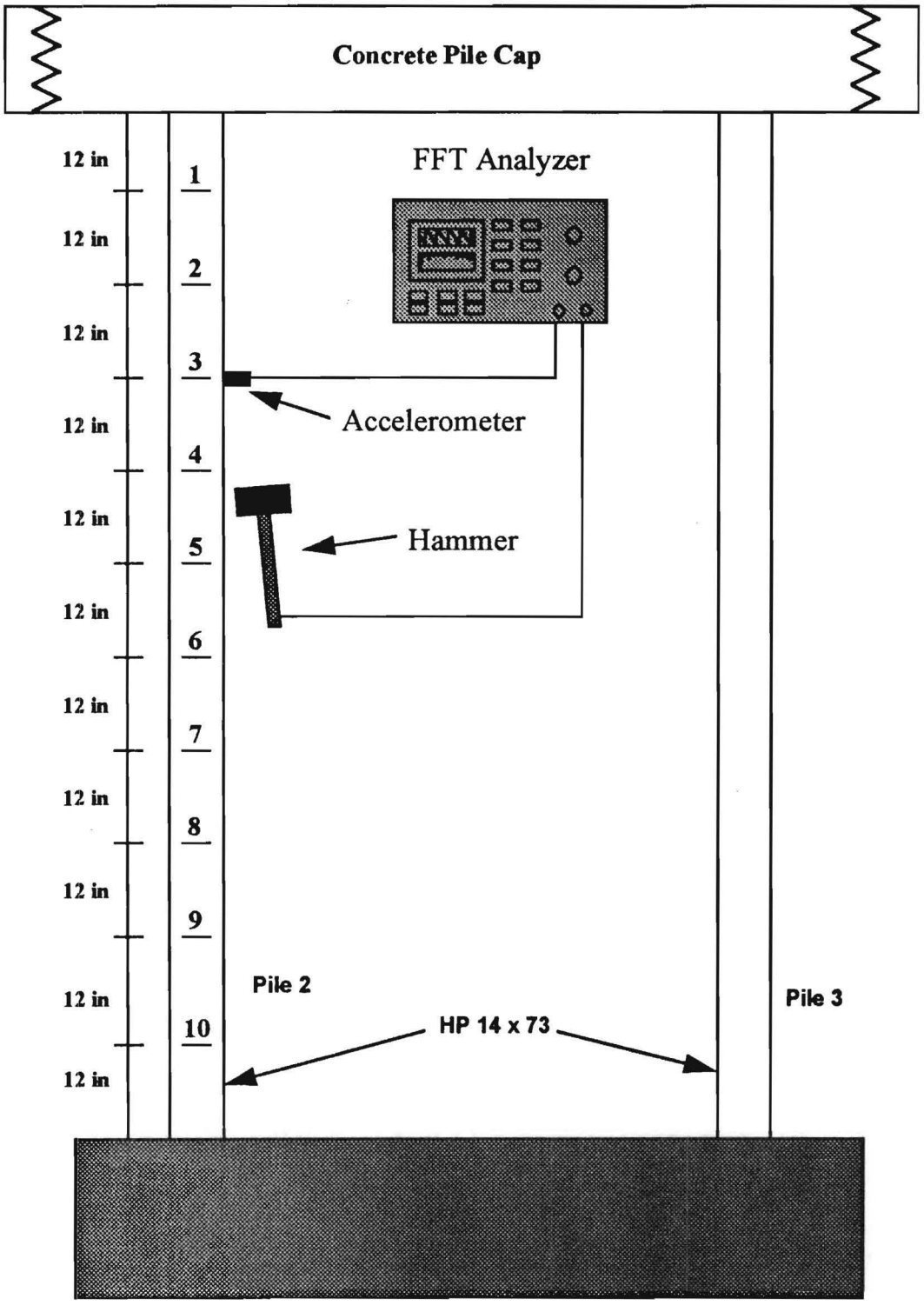

Figure 5.2 Field Test Configuration for Bent 3 - Pile 2

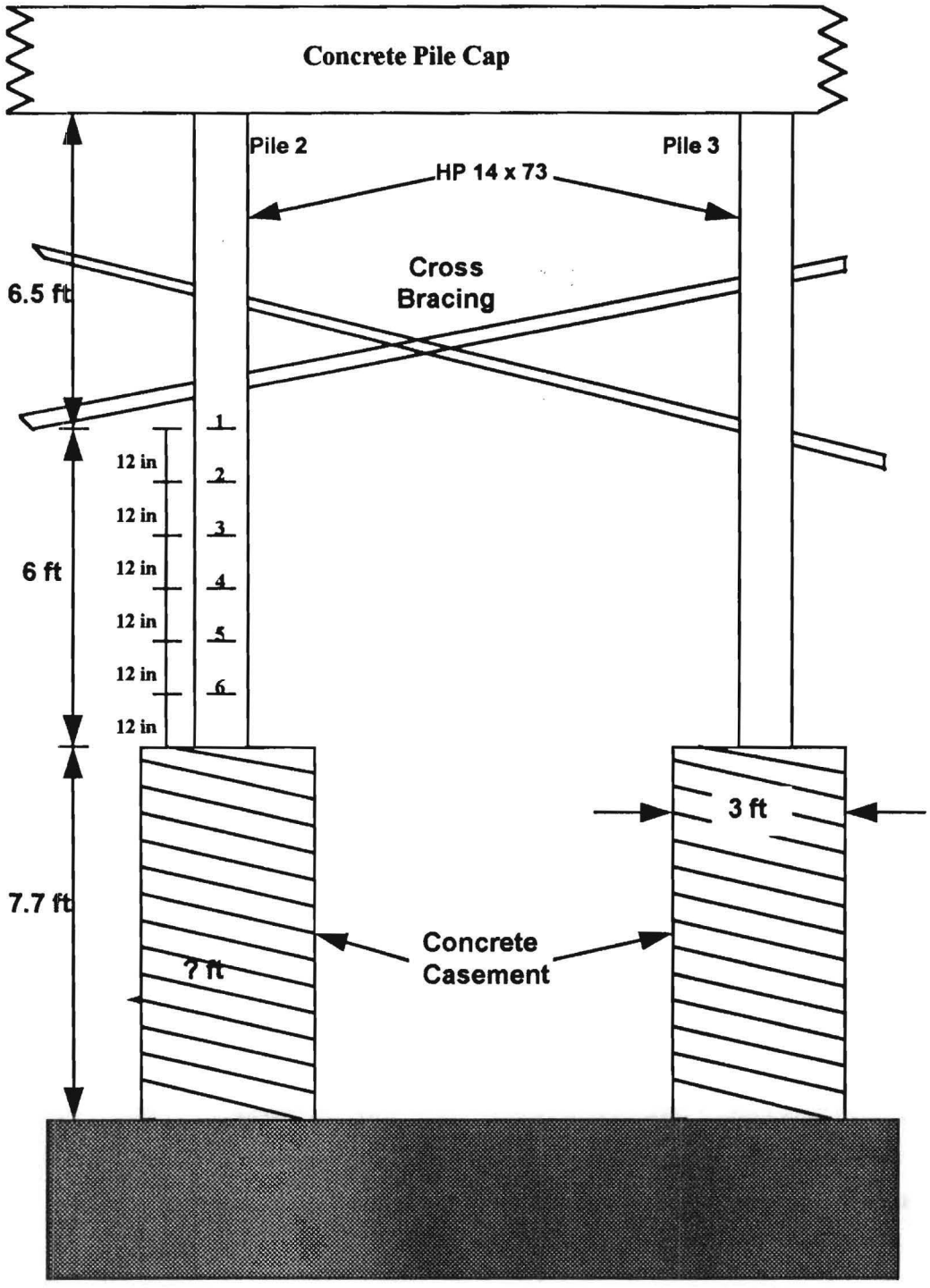

Figure 5.3 Field Test Configuration for Bent 4 - Pile 2

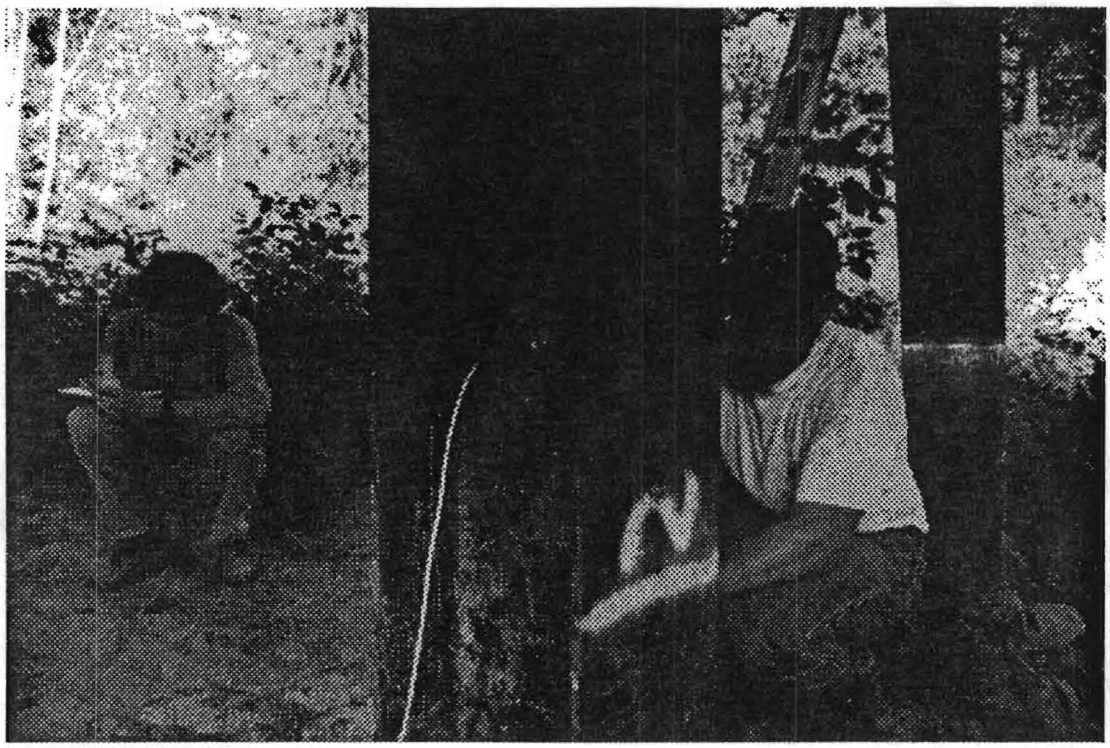

Figure 5.4 Photograph of Field Test

Pile 2 on Bent 3 was tested in both the X-X and the Y-Y directions . A limited number of source-receiver combinations were tested in each direction. In the Y-Y direction, the source and receiver were varied at the even number positions. In the X-X direction, the source was placed at the even positions and the receiver was placed at positions 8, 5 and 3. Pile 2 on Bent 4 was tested only in the Y-Y direction with the source placed at the 6 locations shown in Figure 5.3 The response of the pile was measured only at the even numbered positions. For each source-receiver combination, the frequency response function was measured using five averages.

Test Results

Figure 5.5 shows the frequency response function measured with the source at position 6 and the receiver at position 10 in the Y-Y direction on Pile 2 on Bent 3. This frequency response function is typical of those measured in the Y-Y direction on the non-cased bridge piles. The response is similar to the frequency response function measured on the non-cased small-scale pile in the laboratory; the plot is characterized by several broad peaks that reflect the high attenuation resulting from the soil surrounding the pile. Figure 5.6 shows a waterfall plot of the frequency response functions measured on Bent 3 - Pile 2. Figure 5.7 shows a typical frequency response function measured on the encased pile (Bent 4 - Pile 2).

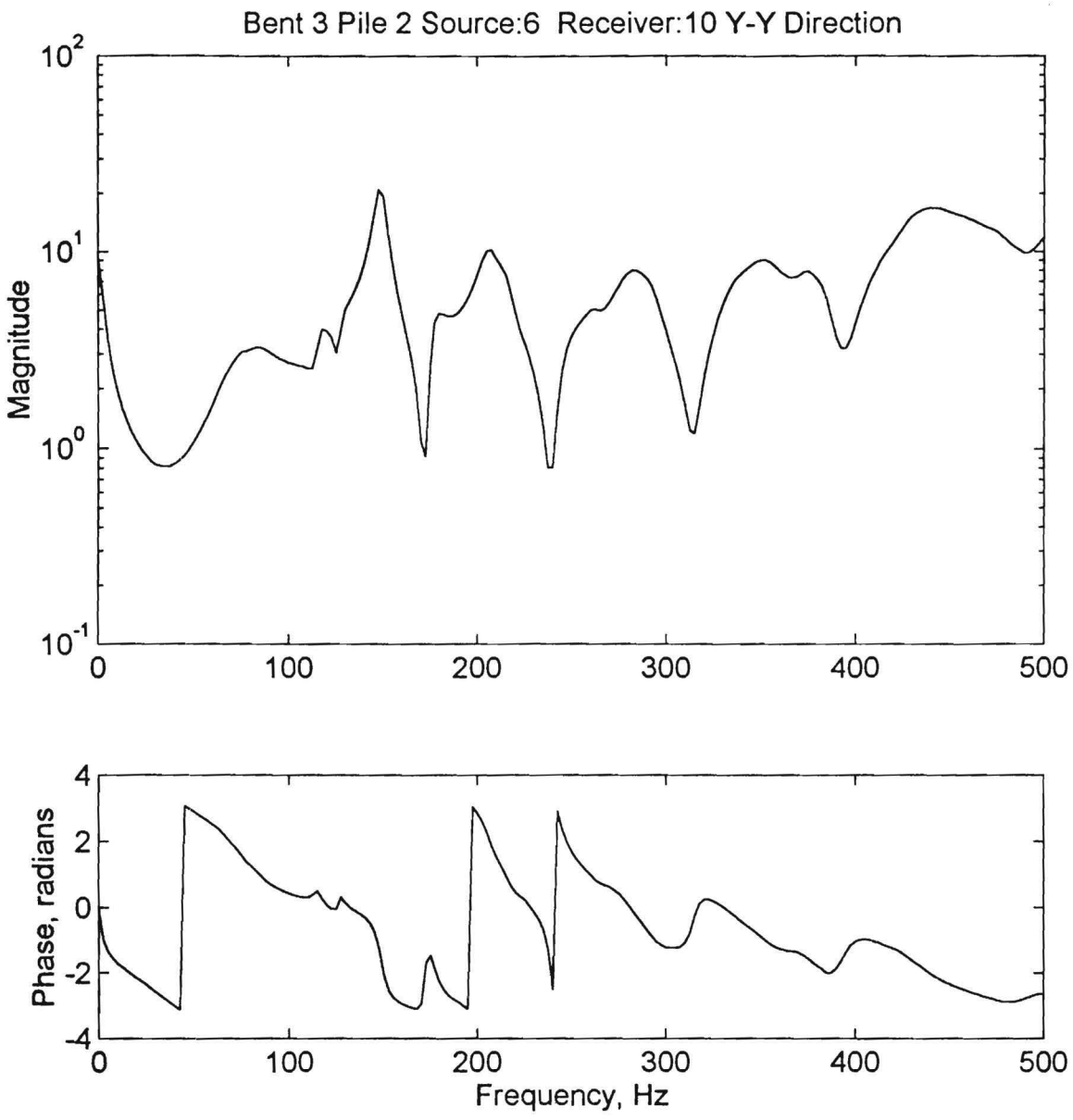

Figure 5.5 Typical Frequency Response Function for Bent 3 - Pile 2

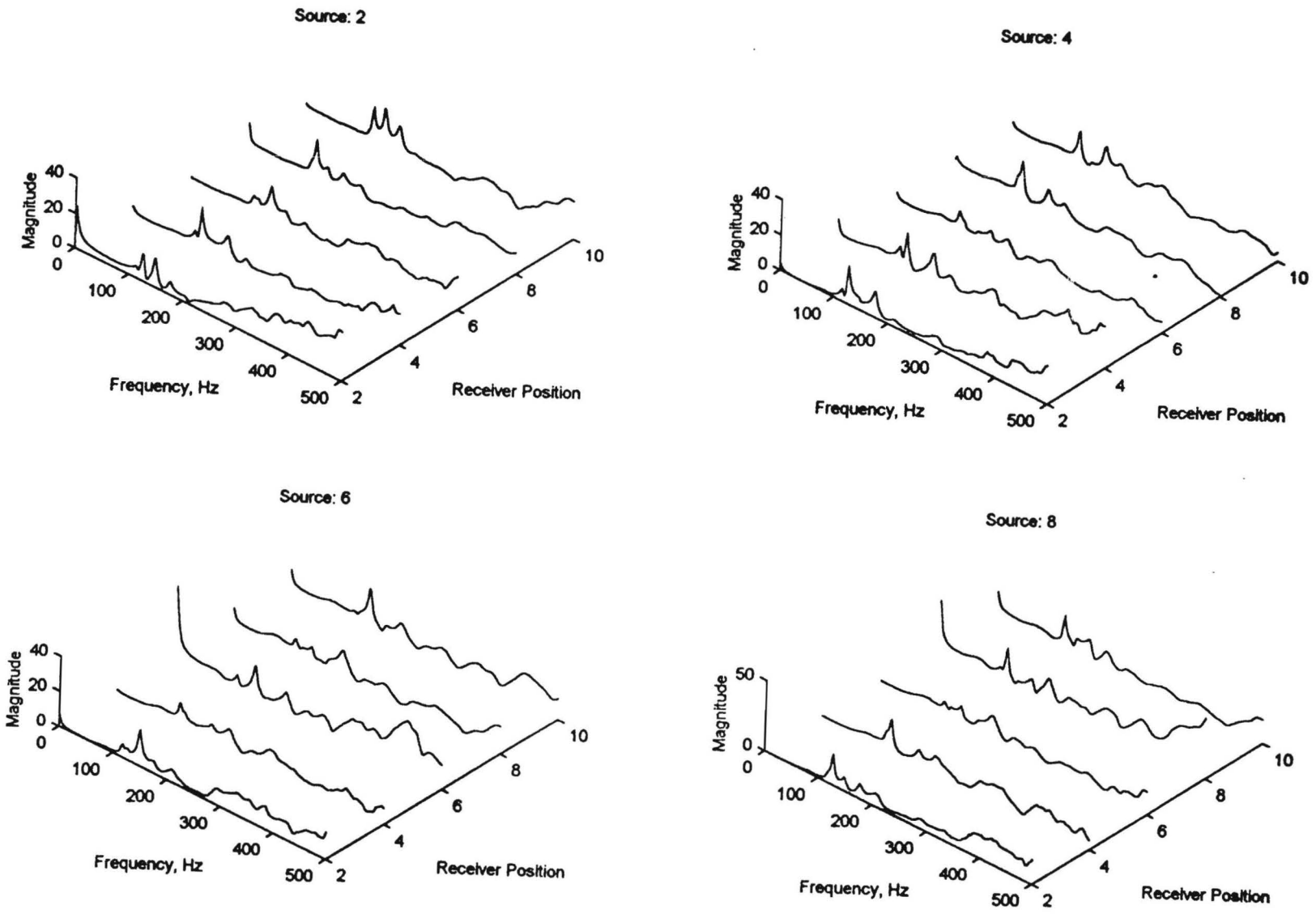

Figure 5.6 Waterfall Plots for Bent 3 - Pile 2

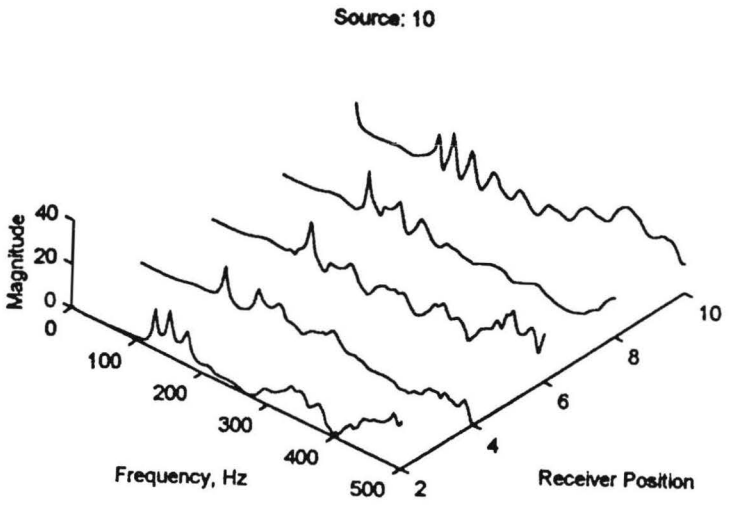

Figure 5.6 Waterfall Plots for Bent 3 - Pile 2 (continued)

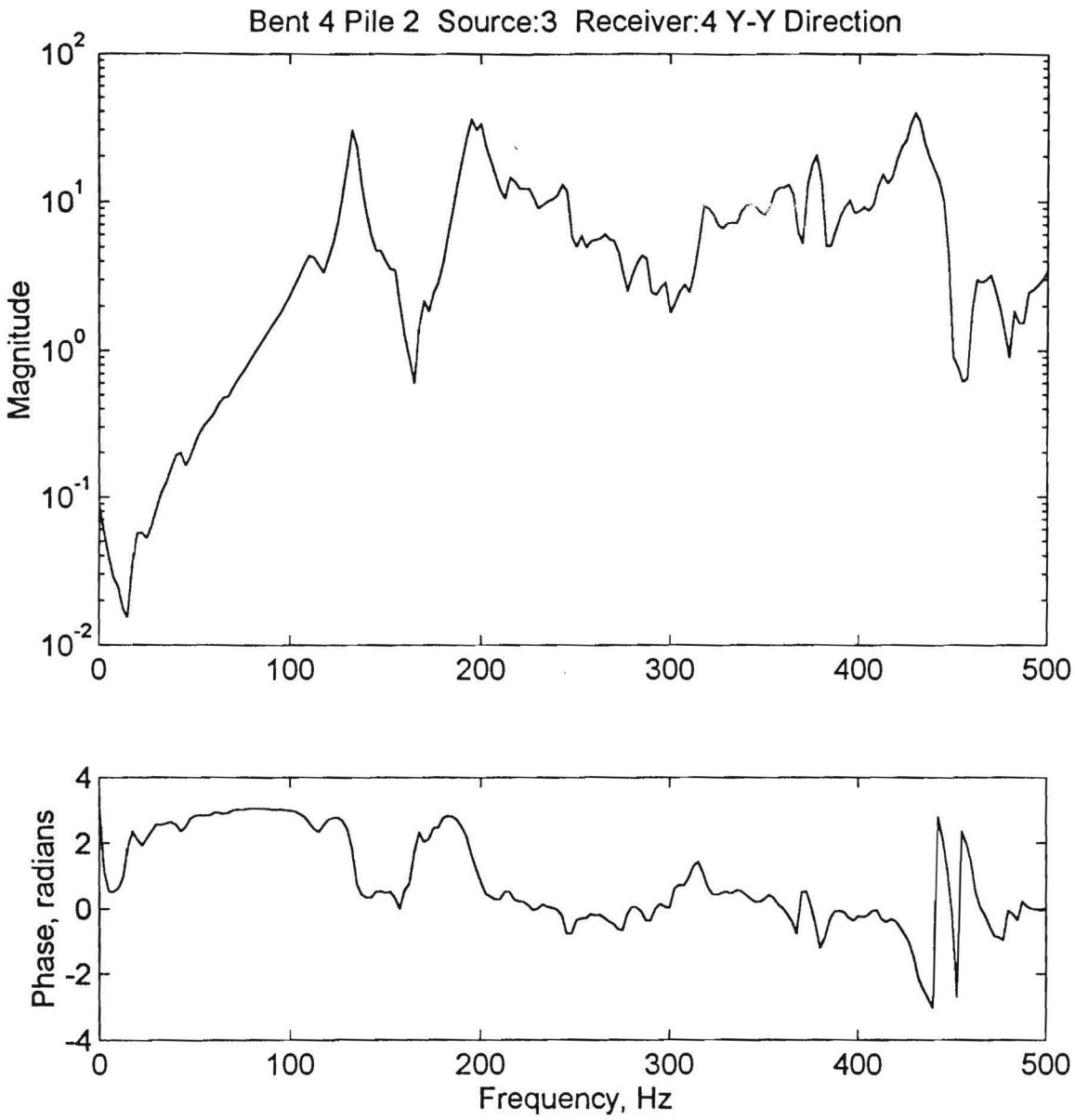

Figure 5.7 Typical Frequency Response Function for Bent 4 - Pile 2

6 Modal Analysis

Modal testing is not a new field, but its applications and potential have only recently been recognized and developed in civil engineering. The purpose of modal testing is to develop a mathematical model of the vibration characteristics of a structure through test data; this is in contrast to developing an analytical model. The purpose is to understand the pile's vibration behavior and study any variations in behavior for information concerning the pile's characteristics. Typically, these variations cannot be simply observed. Instead, one or more modal analysis techniques are used to quantify the variations. The purpose of this chapter is to discuss those being explored and the direction in which future studies should be directed.

The tool used here to perform modal analysis is the Modal Analysis application in the I-DEAS Test software package. The frequency response functions (FRFs) measured in the laboratory using a dynamic signal analyzer are stored on disk in a Hewlett Packard (HP) format. This can be converted to Function 58 format which is compatible with I-DEAS using the Standard Data Format Utilities from HP. Once the FRF's are in this format, I-DEAS can perform any operation on the functions.

Graphical Tools

The simplest application is using I-DEAS as a tool enabling graphical comparisons between experimental and numerical results. This allows a common format in which to compare the experimental FRF's with those generated through finite element analysis. Comparing peaks (i.e., natural frequencies) in the experimental and numerical frequency response functions provides a good indication of whether or not the geometry (including the embedment depth) of the numerical model matches the geometry of the experimental pile.

Figures 6.1 and 6.2 illustrate the comparison between experimental and numerical frequency response functions. Modes 1 through 4 correspond well. At higher frequencies, the modes of vibration become more complex, and more sophisticated techniques are required to model the response. The variations in the experimental response as compared to the numerical response, can be attributed to small structural details of the experimental pile which are not necessarily accounted for in the ideal finite element model.

Another tool that more clearly visualizes frequency response functions is known as the Mode Indicator Function (MIF). The Mode Indicator Function manipulates a set of functions using linear combinations to obtain a reduced set of functions. An important use of MIF's is to enhance true physical modes of a structure while reducing much of the noise typical of FRF data. A MIF provides a better global representation of the modal characteristics of a structure than does a single FRF. An individual mode may

be hidden in a single FRF, because it was not strongly excited or measured due to the particular source or receiver location. Figures 6.3 and 6.4 show the difference in clarity between an FRF and an MIF.

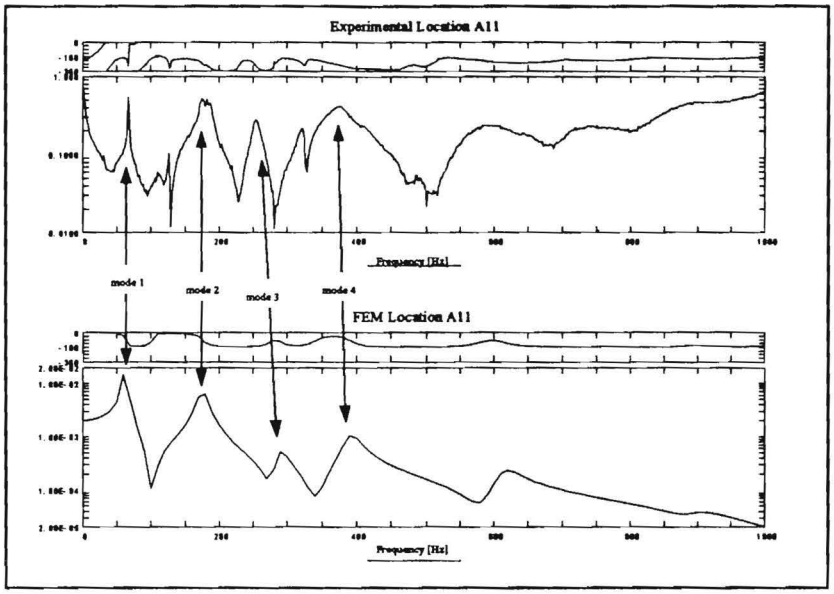

Figure 6. 1 Comparison of Frequency Response Functions for Pile A

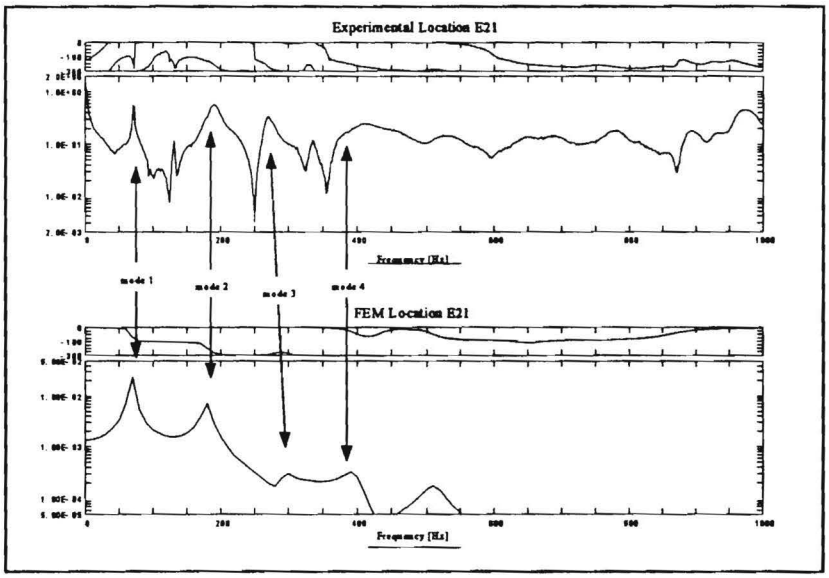

Figure 6. 2 Comparison of Frequency Response Functions for Pile E

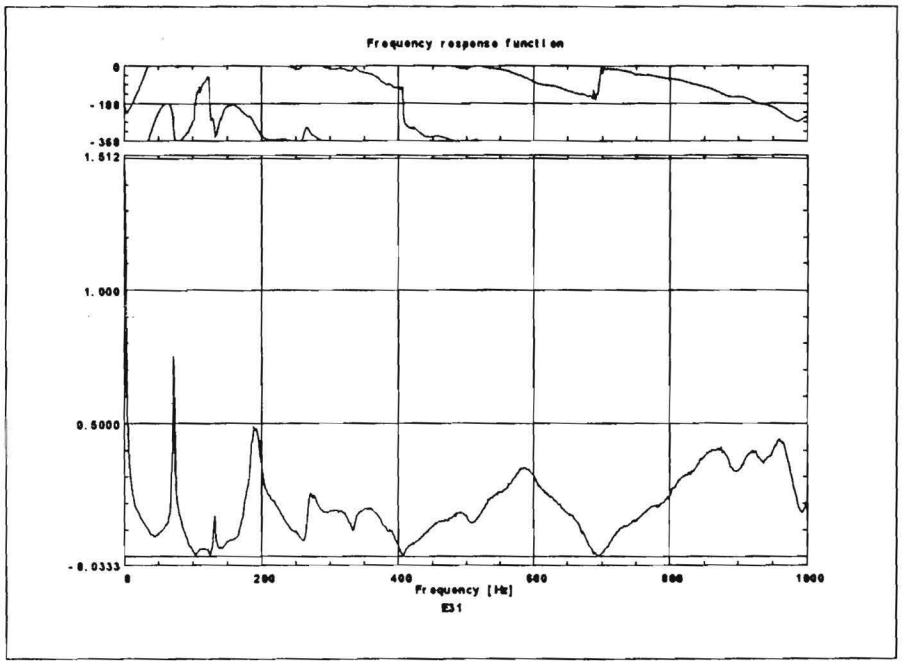

Figure 6.3 Frequency Response Function for Pile E

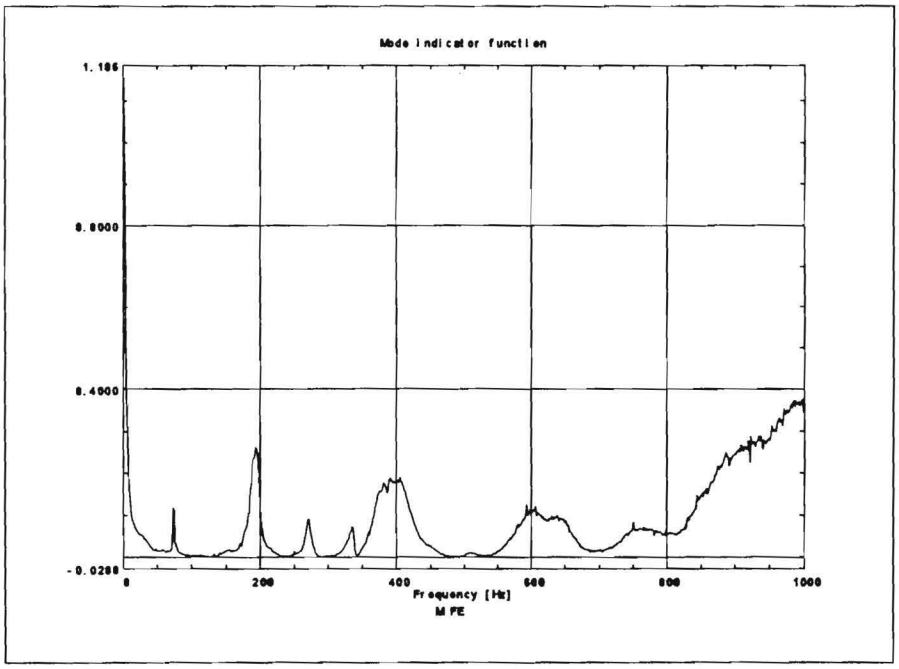

Figure 6.4 Mode Indicator Function for Pile E

Derivation of Mathematical Model

In the simplest sense, the development of the mathematical model representing the dynamic characteristics of a structure depends on curve fitting the experimental data. As with all mathematical modeling, the purpose is to determine the coefficients of a theoretical expression representing the measured data. These coefficients are directly related to the modal properties of the system, which give a quantitative representation of the stiffness, mass, and damping. This can be done at a number of levels, each with increasing complexity: first by looking at an individual peak of a single function, then at an entire function representing multiple resonances, and finally an entire set of FRF plots. When only one peak or resonance is considered, a single degree of freedom (SDOF) analysis is performed. When more than one peak is considered, a multi-degree of freedom (MDOF) analysis is required.

Each resonance frequency has an associated mode shape, or pattern of deflection created at the particular vibrating frequency. These shapes become more complicated as the frequency values rise. In real structures, modes and mode shapes do not occur in isolation. The actual vibrating shape, and hence the response function, is a superposition of a number of modes acting on the structure simultaneously.

A typical application of modal analysis is comparing measured vibration modes to those predicted by a finite element code. Modal analysis can also be used to study the effects of a structural modification on the dynamic behavior of a real structure after the modification has been implemented (construction is complete). This type of modal analysis requires the highest degree of accuracy in the modal extraction. In this study, the purpose of modal analysis is to determine the variations in the vibration response of piles as a function of embedded length. A high degree of accuracy must be obtained in estimating the modal parameters from the FRFs in order to develop accurate mathematical models. A variety of methods (multiple SDOF and MDOF) are available and each should be studied to determine which technique best isolates significant modes and then accurately extracts the modal parameters. Then a technique can be developed, based on the mathematical models, to determine embedded lengths.

7 Summary

Nondestructive tests on foundations were initially developed to provide a quality control test for cast-in-place deep foundations. In recent years, these nondestructive tests have been adapted to address the "unknown foundation" problem. Many of these tests rely on longitudinal waves that are difficult to generate if the bridge superstructure interferes with access to the top of the pile. The purpose of this study was to evaluate the use of flexural waves to determine pile tip elevations of unknown foundations. The basis of the approach taken in this study is the measurement of a large number of frequency response functions at various source and receiver positions along the exposed length of the pile. The natural frequencies and mode shapes obtained from the frequency response functions are functions of the embedded length of the pile. As such, the natural frequencies and mode shapes can be used to backcalculate the embedded length.

This study consisted of an experimental study on 10 small-scale piles, numerical calculations of pile response using the finite element method, and a trial test on a full-scale bridge. The 10 small-scale piles were selected so as to study the influence of embedment depth, tip condition (i.e., floating vs. end bearing), presence of concrete casing, and section geometry on the frequency response of the pile. Initially, tests on the small-scale piles were performed without any soil embedment. The purpose of these tests was to obtain experimental data which could be used to "calibrate" the finite element model of the pile. By adjusting the boundary condition at the upper end of the pile from a fixed boundary to one with two pinned connections, the experimental and numerical natural frequencies were made to match. These tests provided confidence in the ability to model the piles numerically.

Following this initial series of tests, the piles were embedded by placing and compacting sand around the piles. Nine different source and receiver positions were chosen on each of the 10 small-scale piles. Frequency response measurements were made using 45 different combinations of source and receiver positions to excite and record as many modes of propagation as possible within the pile. These measurements provide a comprehensive set of experimental frequency response data from which to develop an interpretive procedure to determine pile embedment depth.

The embedded piles were also modeled numerically using the finite element program I-DEAS. Comparisons between the experimental and numerical frequency response functions yielded satisfactory matches at frequencies less than approximately 300 to 400 Hz. The experimental data contained additional natural frequencies corresponding to spurious modes of vibration involving longitudinal and torsional motion. These modes were not contained in the numerical analyses because the pile was modeled numerically as a prismatic member (i.e. the actual S or W section shape was not modeled). The satisfactory match between experimental and numerical frequency response functions at lower frequencies provides a basis for iteratively matching experimental and numerical frequency response functions to determine the embedment depth.

Finite element analyses were also used in a parametric study of embedment depth. It was determined that the natural frequencies of the first three modes of vibration are sensitive to the embedment depth for embedment depths less than approximately 10 times the section depth. Similar results have been found in other studies (Yu and Roesset, 1995). The reason for this limitation is the attenuation of energy by the surrounding soil. For steel H sections, the limitation is more severe because of the large surface area available to dissipate energy.

A trial test was conducted on full-scale piles to evaluate the practical application of the approach. Two concerns that arose from the full-scale test are problems related to access to portions of the pile well above the ground line and short exposed lengths limiting the number of source and receiver positions that are available for use in making frequency response measurements.

Modal analysis techniques can be used to interpret experimentally obtained data. In this application, modal techniques have the potential to determine a single structural feature: embedded pile length. The use of the I-DEAS software package for this application was examined, and potential solutions were discussed. The exposed length, material properties and cross sectional geometry of a pile can all be measured directly; the only unknown (that affects the vibration behavior of a pile) is the embedded length. Modal analysis techniques have the potential to interpret field data to determine unknown embedment depth.

8 References

Davis, A.G. and Dunn, C.S. (1974). "From Theory to Field Experience with the Nondestructive Vibration Testing of Piles." *Proceedings*, Institution of Civil Engineers, Part 2, 57, 571-593.

Douglas, R.A., and Holt, J.D. (1993). "Determining Length of Install Timber Pilings by Dispersive Wave Propagation Methods." Center for Transportation Engineering Studies, North Carolina State University, June.

Fung, Y.C. (1964). *Foundations of Solid Mechanics*. Prentice-Hall, Englewood Cliffs, New Jersey, 525 pp.

Holt, J.D., and Douglas, R.A. (1994). "A Field Test Procedure for Finding the Overall Lengths of Installed Timber Piles by Dispersive Wave Propagation Methods." Technical Report No. NC/R&D/94-001, ITRE, North Carolina State University, March.

Malhotra, V.M., (1976), "Testing Hardened Concrete: Non-Destructive Methods," American Concrete Institute, Detroit, Michigan, Iowa State University Press, Ames, 87 pp.

Novak, M., Nogami, T., and Aboul-Ella, F. (1978). "Dynamic Soil Reactions for Plane Strain Case." *Journal of the Engineering Mechanics Division*, ASCE, Vol. 104, No. EM4, August, pp. 953-959.

O'Neill, M. W., (1992), "Construction Practices and Defects in Drilled Shafts," *Integrity Testing of Foundations 1991*, Transportation Research Record 1331, Transportation Research Board, Washington, DC, pp. 6-14.

Olson, L.D. and Wright, C.C. (1989). "Nondestructive Testing of Deep Foundations with Sonic Methods." *Foundation Engineering: Current Principles and Practices*. ASCE, Vol. 2, pp. 1173-1183.

Olson, L.D., Jalinoos, F., and Aouad, M.F. (1995). "Determination of Unknown Subsurface Bridge Foundations." Draft Final Report, NCHRP Project E 21-5, National Cooperative Highway Research Program, Transportation Research Board, National Research Council, Washington, D.C., April, 264 pp.

Paquet, J. (1968). "Étude Vibratoire Des Pieux En Béton Résponse Harmonique Et Impulsionelle: Application Au Controle (in French). *Annalles de l'Institut Technique du Batiment et des Travaux Publics*, No. 245, May, pp. 788-803.

Rix, G.J., Jacobs, L.J., and Reichert, C.D. (1993). "Evaluation of Nondestructive Test Methods for Length, Diameter, and Stiffness Measurements on Drilled Shafts." *Field Performance of Structures and Nondestructive Evaluation of Subsurface Infrastructure*. Transportation Research Record No. 1415, Transportation Research Board, pp. 69-77.

Stain, R.T. (1982). "Integrity Testing." *Civil Engineering*. April, 54-59.